Role of *N*-glycosylation for the function of E-cadherin in tissue morphogenesis

Dissertation

for the award of the degree

"Doctor rerum naturalium" (Dr.rer.nat.)

of the Georg-August-Universität Göttingen

within the doctoral program "Biology"

of the Georg-August University School of Science (GAUSS)

submitted by

Na Zhang

from Shanxi, China

Göttingen, 2022

Affidavit

I hereby declare that I wrote the Ph.D. thesis "Role of N-glycosylation for the function of E-cadherin in tissue morphogenesis" on my own with no other sources and aids than quoted.

Na Zhang

08.2022, Göttingen

Table of contents

Acknowledgment

First of all, I would like to thank my supervisor, Prof. Dr. Jörg Großhans, for giving me such a great opportunity to perform my Ph.D. studies in his lab. I am thankful that I can work on the E-cadherin dynamic project and also the aging (Narf) project. I am grateful for his support, and for always being there to answer questions. The way he deals with questions and his positive attitude always inspire me to move forward when challenges occur.

Furthermore, I would like to thank my thesis committee members, Prof. Dr. Gerd Vorbrueggen and Prof. Dr. Holger Bastians for their highly valuable suggestions during the committee meeting. When I was working on my first project, "The Role of Narf in Aging," some problems still occurred after one and a half years of my Ph.D., I appreciated their suggestion that I should start a new project so I could finish my Ph.D. on time.

Next, I would like to thank Dr. Deqing Kong, who started the E-cadherin N-glycosylation project, for showing me how to use the microscope and introducing me to the FRAP and laser ablation experiments, and for his strong support whenever I need. Moreover, I would also like to thank Dr. Deqing Kong, Ankit Roy Choudhury, and Roya Abbaszadeh for their helpful comments on my thesis. I also want to thank Dr. Deqing Kong and Dr. Long Li for their help in my daily life. And I want to thank Dr. Maria Kriebel for introducing the fly work and showing me the aging project when I joined the group. I also want to thank all the members of our lab, Dr. Shuling Yan, and Kaja Sommer, for this nice and cooperative working atmosphere. I am also grateful to Ljubinka Cigoga, Sabina Huhn, and Isolde Kranz for preparing the fly food, apple juice agar plates, and other general things.

A special thanks to Yu Zhang for his endless support and for always being there for me. He always helps me get out of a bad mood quickly. It is not easy for those of us who reside in two countries during this pandemic.

However, the greatest thank goes to my family. I would like to thank my parents and sisters for their endless support, open ears, and belief in me. I have not visited my family in the last three years during the corona pandemic. Thanks a lot for their understanding and my sisters, who do a lot for me.

1. Abstract

E-cadherin is central to the formation, stabilization, and maturation of adherens junctions, which serve to physically link epithelial cells and transmit mechanical pulling forces from the outside to the actomyosin cortex inside of cells. Besides this structural function, E-cadherin complexes mediate mechanical signaling. Mechanical pulling forces are translated into biochemical signals by proteins associated with E-cadherin with multiple mechanisms. E-cadherin complexes and clusters' activities and biochemical constitution are regulated on multiple levels, including post-translational modifications, interactions with the cortical actomyosin network, membrane trafficking, and cis/trans clustering. Here I will focus on the role of *N*-glycans in the function of E-cadherin, which has received little attention so far.

I utilized two experimental model systems. (1) The gene *xit* (*xiantuan*, Alg8 in *Saccharomyces cerevisiae*) encodes the glucosyl transferase, which adds the second but last glucose to the dolichol-oligosaccharide precursor during *N*-glycan synthesis in the endoplasmic reticulum. (2) At the endogenous genetic locus in *Drosophila*, site-specific Asn->Gln mutations in E-cadherin at *N*-glycosylation sites are introduced, preventing *N*-glycan transfer to these sites.

Besides the phenotypes in visible morphology during gastrulation, I analyzed the mobility of E-cadherin by fluorescence recovery after photobleaching (FRAP) and the mechanical properties of junctions by laser ablation and measurement of recoil. The visible spatial distribution and size of E-cadherin clusters were analyzed by high-resolution confocal microscopy. I detected consistent phenotypes in *xit* and hypoglycosylation mutants of E-cadherin: increased mobility, increased initial recoil velocity, and reduced clustering at junctions, which indicated that the *xit* phenotype is largely due to hypoglycosylation of E-cadherin in early embryos.

On the molecular level, analysis of the cadherin-catenin complex by coimmunoprecipitation (Co-IP) experiments and an E-cadherin-α-catenin fusion protein revealed an increased stoichiometry of α-catenin to E-cadherin in *xit* mutant,

suggesting that *xit* and hypoglycosylation impinge on interactions with cortical actomyosin.

To experimentally confirm and identify new sites of *N*-glycosylation, I conducted a mass spectrometric analysis of E-cadherin isolated from wild-type and *xit* mutants. To my surprise, I identified sites not predicted yet, sites whose *N*-glycosylation is dependent, and others not dependent on *xit*. These findings indicate that lacking terminal glucosyl residues on the dolichol-oligosaccharide precursor alters the specificity and not simply the activity of the oligosaccharide transferase.

In summary, I present evidence that *N*-glycans specifically modulate E-cadherin activity and function, and constitute a so far neglected molecular mechanism for modulation of E-cadherin function.

2. Introduction

2.1 Junction dynamics during tissue morphogenesis

Gastrulation is a process of early development in most animals where a single-layered cell mass (blastula) is transformed into a three germ-layered structure (gastrula), including ectoderm, endoderm, and mesoderm. Although gastrulation has some similarities, there is still a large variation among different animals. In *Drosophila melanogaster*, gastrulation starts with the embryo forming a ventral furrow and lasts only about 1 hour. At this stage, blastoderm cells form, nuclei elongate, and pole cells shift. During gastrulation, the mesoderm primordium is elongated and invaginated, consequently forming the three germ layers through cell migration and reorganization (Leptin, 1999). Later, the three layers differentiate into different tissues. For instance, the endodermal cell layer becomes the midgut epithelium (Reuter et al., 1993; Tepass and Hartenstein, 1994b) (**Figure 2.1**).

Germband extension is a vital morphological process that happens in multiple organisms, including invertebrates and vertebrates (Keller, 2006). It comes up shortly after gastrulation in *Drosophila melanogaster*. This process lasts roughly 1.5 hours, and afterward, the cell elongates two times along the anterior-posterior (A-P) axis while being shortened along the dorsal-ventral (D-V) axis (da Silva and Vincent, 2007; Irvine and Wieschaus, 1994). The germband extends from the posterior pole to the cephalic furrow along the AP axis (Gheisari et al., 2020) (**Figures 2.1 and 2.2**). Most of the morphological cell-cell extension occurs in the fast phase, which lasts about 25 minutes. The extension is terminated in the slow phase, taking around 70 minutes (da Silva and Vincent, 2007; Hartenstein and Campos-Ortega, 1985). At the end of the germband extension, the posterior germband extends to about 60% of the whole embryo length.

It is proposed that contraction of the actin network, cell division, and cell rearrangements drive the GBE process (Bertet et al., 2004; Irvine and Wieschaus, 1994;

Rice and Garen, 1975; Rickoll and Counce, 1980; Zallen and Wieschaus, 2004). Moreover, cell intercalation, one of the convergent extensions, including the rosette formation model, T1 transition model, and sliding vertex model (Bertet et al., 2004; Blankenship et al., 2006), is also considered to be significant in GBE, driven by junctional remodeling in an anterior-posterior independent manner (Bertet et al., 2004; Blankenship et al., 2006; Kong et al., 2017) (**Figure 2.2**). Cell intercalation is the epithelial remodeling process of neighboring cells (Walck-Shannon and Hardin, 2014). However, cell shape changes suggest extrinsic tensile forces are involved in GBE (Butler et al., 2009).
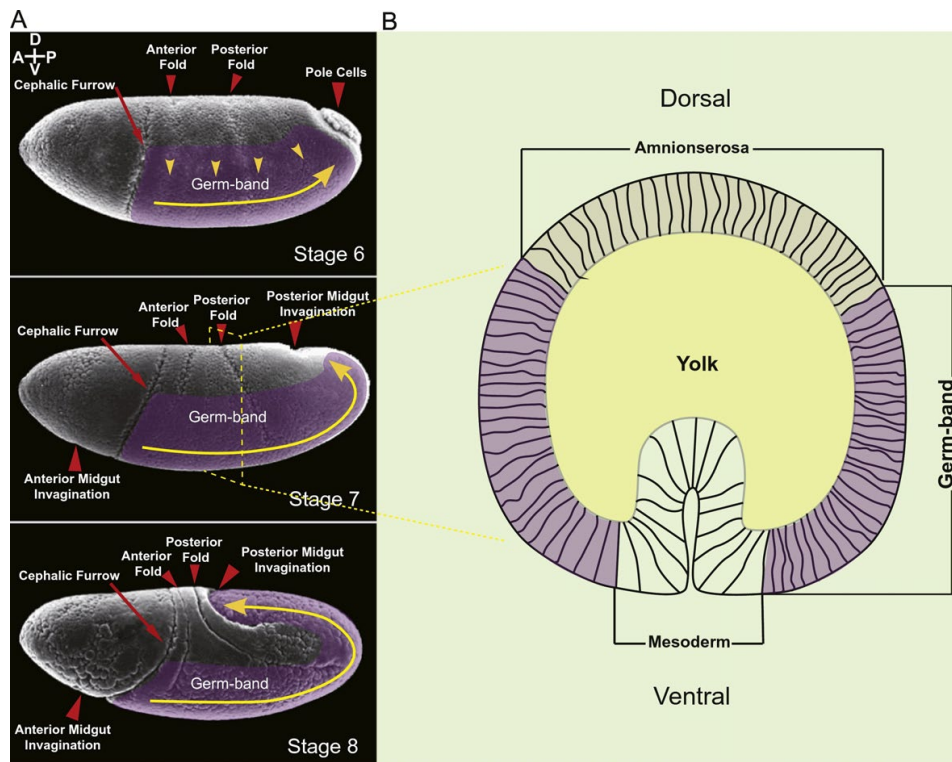
Figure 2.1: Gastrulation and germband extension in the *Drosophila* embryo. (A) Typical morphogenetic events at stages 6, 7, and 8 of *Drosophila* embryos in the lateral views by scanning electron microscopy photomicrographs, such as cephalic furrow (CF) and germband extension (GBE). The yellow line represents the germband extension process. (B) A cross-section of a stage 7 *Drosophila* embryo. The scheme was taken from (Kong et al., 2017), which was adapted from (dos Santos et al., 2015).

This thesis mainly focused on investigating the role of E-cadherin *N*-glycosylation during the germband extension and the function of E-cadherin in the early *Drosophila*

embryos. (Gastrulation and germband extension, stages 6,7,8)
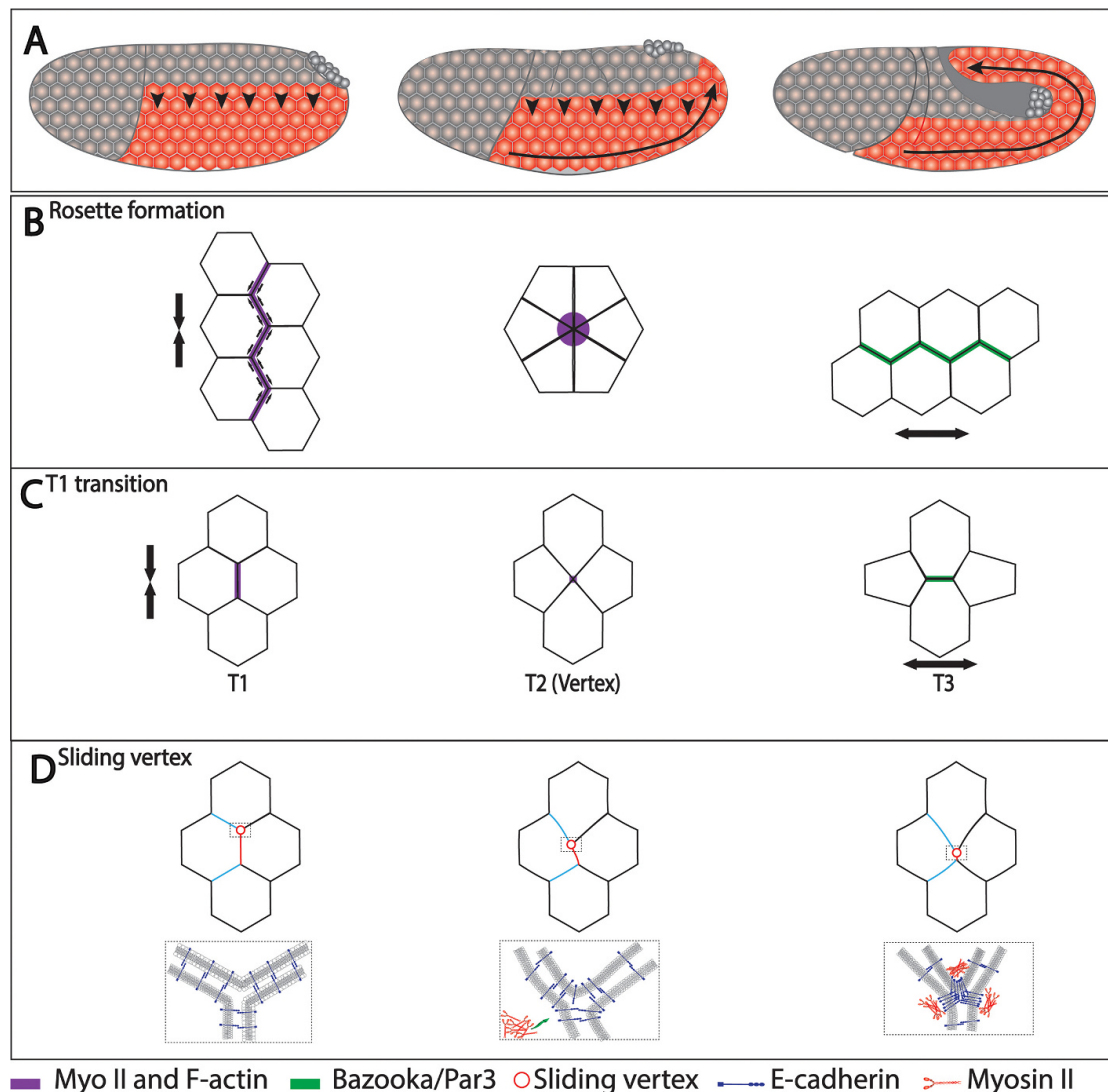
Figure 2.2: Three models for cell intercalation during germband extension. (A) Diagram of germband extension. (B) Rosette formation model. Six cells undergo nodal collapse and form a rosette by an active myosin II and F-actin contraction. (C) T1 transition model. The collapse of the junction leads to new vertex formation along the DV axis and junction expansion along the AP axis. (D) Sliding vertex model. Radial tension forms because of the fluctuation at the surface, which results in a novel vertex formed by fusing two neighboring cell vertices along the DV axis. The scheme was taken from (Leptin, 1999)

Stage 6 (onset of gastrulation) begins with the formation of a ventral furrow. Meanwhile, a cephalic furrow forms at around 65% of the embryo's length. The pole cells migrate towards the dorsal side of the embryos (Flymove). Overall, this stage features a fast process that only lasts for 10 minutes (**Figure 2.1**).

At stage 7, changes in cell shape on the dorsal side become more visible. It should be noted that gastrulation is finished at this stage. Stage 7 typically starts once the cell plate has achieved a horizontal position on the dorsal egg surface and concludes once the anterior wall of the proctodeal invagination begins to shift cephalad (Flymove). This stage also stays around for approximately 10 minutes (**Figure 2.1**).
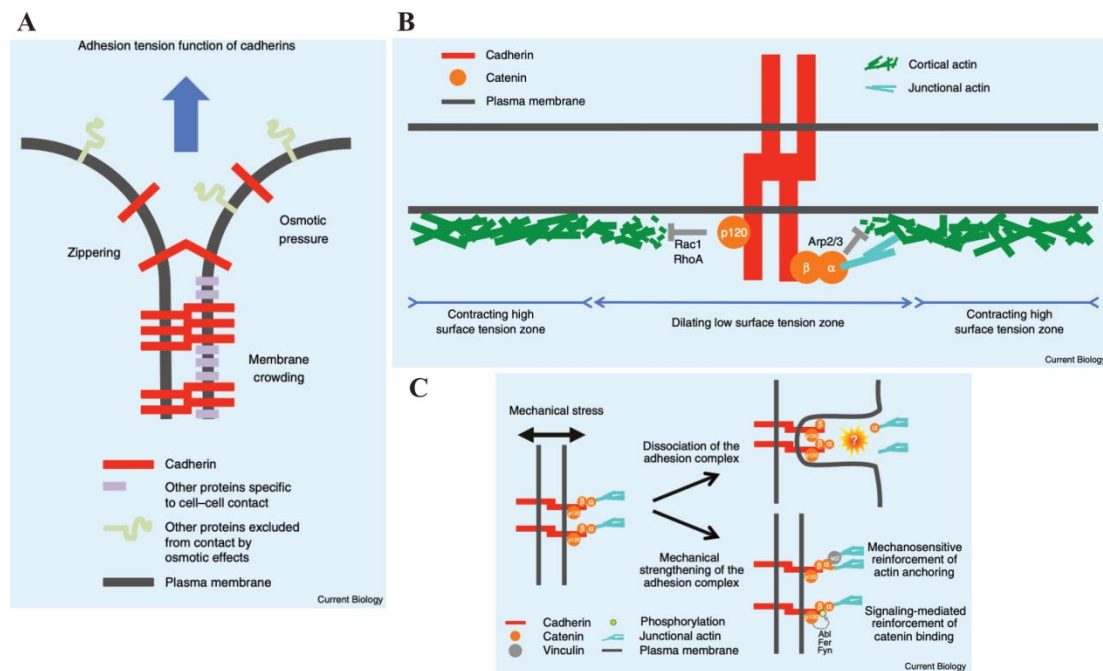
Figure 2.3: Three functions of cadherin in cell-cell contact. (A) Adhesion tension. Cadherin trans-clusters, cadherin complexes, and other proteins regulate the cadherins' adhesion tension function. (B) Adhesion signaling. Cadherins regulate cell-cell contact by mediating catenin recruitment and actin polymerization. (C) Adhesion coupling. Cadherins stabilize cell-cell contact by resisting the pulling force caused by the actomyosin cytoskeleton and regulating the tension along the junctions. The scheme was taken from (Maître and Heisenberg, 2013).

At stage 8, the germband continues to extend on the embryonic dorsal side, eventually reaching 60% of the embryo's total length. At last, stage 8 ends with mesodermal part segmentation (Flymove). Notably, this phase lasts for about half an hour (**Figure 2.1, 2.2**).

2.2 E-cadherin

Cadherins are transmembrane glycoproteins that facilitate cell-cell adhesion in a

Ca^+-dependent pattern (Maître and Heisenberg, 2013; Van Roy and Berx, 2008).

E-cadherin was first described as an 84-kDa glycoprotein (gp80) by Jacob and co-workers on mouse embryonic carcinoma cells in 1980 (Boller et al., 1985; Hyafil et al., 1981; Hyafil et al., 1980). They generated a gp84 monoclonal antibody and realized that gp84 could be converted into a stable 120-kDa isoform, which is called uvomorulin (Hyafil et al., 1981). Later, a mouse gene was cloned and the uvomorulin antibody was subsequently purified (Schuh et al., 1986). Afterward, Yoshida-Noro and Takeichi gave more generic names-cadherins for this cell-cell adhesion molecular (Yoshida-Noro et al., 1984). E-cadherins, are mainly expressed in epithelial cell lines and tissues. Therefore, the prefix "E" was given. Subsequently, E-cadherin cDNA was cloned and differential expression of cadherins was shown to mediate the selective adhesion of cells (Nose et al., 1988). E-cadherin is considered to serve as the prototype of all other catenins. Moreover, scientists found that catenins interact with the E-cadherin cytoplasmic domain, and E-cadherin could inhibit cancer cell invasion (Ozawa et al., 1989; Vleminckx et al., 1991). Subsequently, Kukuruzinska's group found that the molecular structure and stability of the E-cadherin junction are impacted by *N*-glycosylation (Liwosz et al., 2006).

Identification of E-cad in *Drosophila*: shotgun, Arm, and a-catenin

Cadherins are highly important for the tissue morphogenesis process via regulating cell-cell contact formation and stability in various organs (Gumbiner, 2005; Halbleib and Nelson, 2006; Lien et al., 2006; Van Roy and Berx, 2008). Generally, cadherins consist of classical, desmosomal, protocadherins, and unconventional cadherins (Angst et al., 2001; Hulpiau and Van Roy, 2009). Among them, classical cadherins are named by where they are found. For example, cadherin-1 (E-cadherin) is found in epithelial tissue and cadherin-2 (N-cadherin) is found in neurons, respectively. This thesis will focus mainly on the role of E-cadherin post-translational modification-*N*-glycosylation in its function.

The cadherin superfamilies are functional in many biological processes, including

cell communication, cell polarity, signal transduction, neurotransmission, and development (Arboleda-Estudillo et al., 2010; Bosveld et al., 2012; Chihara and Nance, 2012; Hayashi and Carthew, 2004; Martin et al., 2010; Wang et al., 2012). Among these, cadherins have mainly three functions in the development and maintenance of cell-cell contact (Maître and Heisenberg, 2013). The first function is to lessen adhesion tension at the cell-cell contact; the second function is to lower cortex tension by regulating the actomyosin cytoskeleton; these two functions result in decreasing interfacial tension; the last function of cadherin is to stabilize the cell-cell contact by resisting mechanical forces (Bosveld et al., 2012) (**Figure 2.3**).

The classic cadherin cytoplasmic domain binds to p120-catenin near the plasma membrane, p120-catenin connects to β-catenin, and β-catenin binds to α-catenin to link the cadherin-catenin complex to the actin cytoskeleton (Cavey and Lecuit, 2009; Meng and Takeichi, 2009). In 2008, Lecuit's group found homophilic E-cadherin clusters are very stable compared with the unclustered E-cadherin (Cavey et al., 2008). Later, the actin dynamic was discovered to correlate with local E-cad recruitment and its immobilization in 2014 (Engl et al., 2014). Overall, E-cadherin is functional in embryogenesis and cell adhesion (tumor metastasis when loss of cadherin function) and is linked to the cancer process.

The classic E-cadherin in vertebrates and invertebrates is the type I and type IV cadherins, respectively. Although they are similar in adhesion function, they have different domain organizations (Oda and Takeichi, 2011). In mice, mature E-cadherin consists of 728 amino acids (Nagafuchi et al., 1987). In mammals, mature E-cadherin consists of a single transmembrane domain, a cytoplasmic domain, and an ectodomain with five tandemly repeated domains, which are cadherin repeats from EC1 to EC4, while EC5 is composed of four conserved cysteines (Nollet et al., 2000; Van Roy and Berx, 2008) (**Figure 2.4**). *Cis* and *trans* interactions of E-cadherin in the extracellular domain are essential for the establishment of adhesion junctions (Shi et al., 2010), where *cis* interactions take place in the proteins within the same membrane, while *trans* interactions take place in opposite membranes (Indra et al., 2018; Yap et al., 1997)

(**Figure 2.7**). Homophilic binding of E-cadherin is the basis of E-cad's function in adhesion. The E-cadherin cytoplasmic domain binds to p120-catenin directly, p120-catenin interacts with β-catenin, β-catenin binds to α-catenin, and α-catenin undergoes a conformational alternation, which can recruit vinculin, bind to F-actin, and finally link the cadherin-catenin complex to the actin cytoskeleton (Abe and Takeichi, 2008), which is crucial for cell-cell adhesion (Drees et al., 2005; Jamora and Fuchs, 2002) (**Figure 2.5**). Additionally, α-catenin can interact directly with F-actin.
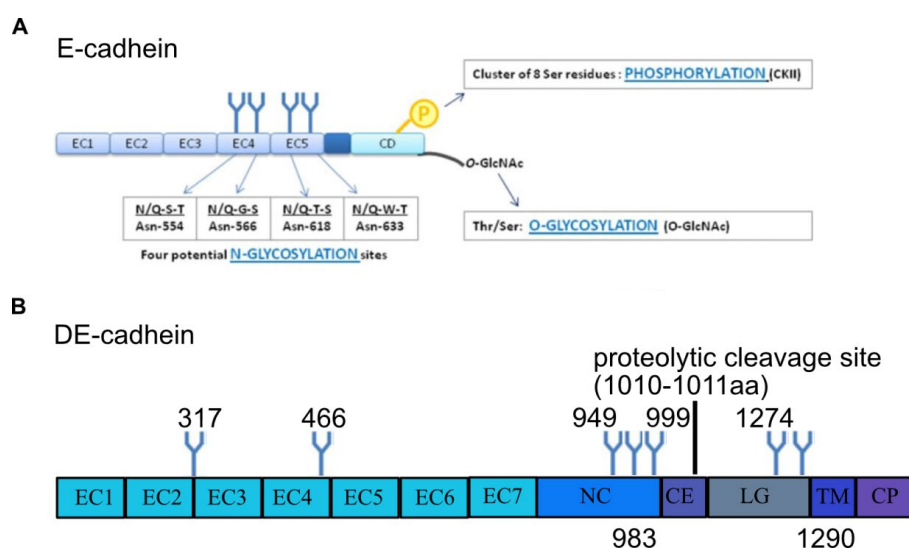
Figure 2.4: E-cadherin domains and posttranslational modifications (*N*-glycosylation) in humans and *Drosophila*. (A) Human E-cadherin contains 5 extracellular domains (EC), and there are two *N*-glycosylation sites in EC4 and EC5, respectively. In terms of the cytoplasmic domain (CD), it contains an O-glycosylation site and a phosphorylation site. The *Drosophila* E-cadherin includes 7 EC domains: a nonchordate-specific classical cadherin domain (NC), a cysteine-rich EGF-like domain (CE), a laminin globular domain (LG), a transmembrane domain (TM), and a cytoplasmic domain (CP), a proteolytic cleavage site at amino acid 1010–1011 (Figure 2.4B). In total, there are 11 potential *N*-glycosylated sites in DE-cadherin and 7 of them have been verified by mass spectrometric experiment. The scheme was modified from (Pinho et al., 2011; Zielinska et al., 2012).

The *Drosophila* homology of E-cadherin was first identified in invertebrates by the Harada group in 1994 (Oda et al., 1994; Tepass et al., 1996; Uemura et al., 1996). DE-cadherin is encoded by *shotgun* (Tepass et al., 1996) and consists of 1507 amino acids, but the *N*-terminal region (1-69aa) is removed after maturation (Oda and Tsukita,

1999). DE-cadherin composes of an extracellular cadherin domain, a transmembrane domain (TM), a cysteine-rich EGF-like domain (CE), a laminin globular domain (LG), and a cytoplasmic domain (CP), a proteolytic cleavage site at amino acid 1010-1011 (**Figure 2.4**). The extracellular DE-cadherin domain is different compared to vertebrates; it contains 7 consecutive extracellular cadherin domains (**Figures 2.4 and 2.5**). DE-cadherin plays a pivotal role in the stability of adhesion and the process of cell-cell contacts by interacting with β-catenin (*Drosophila* homology of Armadillo (Peifer and Wleschaus, 1990)), α-catenin, p120-catenin, and vinculin (Hazan et al., 1997; Imamura et al., 1999), and thus linking the cadherin-catenin complex to the actin-myosin network. In addition, p120-catenin interacts directly with the E-cadherin juxtamembrane domain and serves as a modulator of the E-cadherin mediated cadherin-catenin complex (Peifer and Yap, 2003) (**Figure 2.5**).

As tumors with dysfunction of E-cadherin cannot be accounted for by the genetic/epigenetic mechanisms, post-translational changes of E-cadherin are supposed to influence the protein's function (Pinho et al., 2011). The main post-translational modifications of E-cadherin include phosphorylation, O-glycosylation, and *N*-glycosylation. Among them, glycosylation is particularly important, and roughly 50% of proteins are glycosylated in a eukaryote. Moreover, glycosylation includes *N*-linked glycosylation, O-linked glycosylation, phosphoserine glycosylation, C-mannosylation, and glypiation.

Additionally, phosphorylation and O-glycosylation of E-cadherin localize to the cytoplasmic domain of the protein. E-cadherin phosphorylation increases its affinity to β-catenin and promotes cell-cell contact (Chen et al., 2016). O-glycosylation of E-cadherin decreases the binding of p120ctn and leads to reduced intercellular adhesion (Pinho et al., 2011). In brief, the post-translational modifications of E-cadherin can affect its functionality.
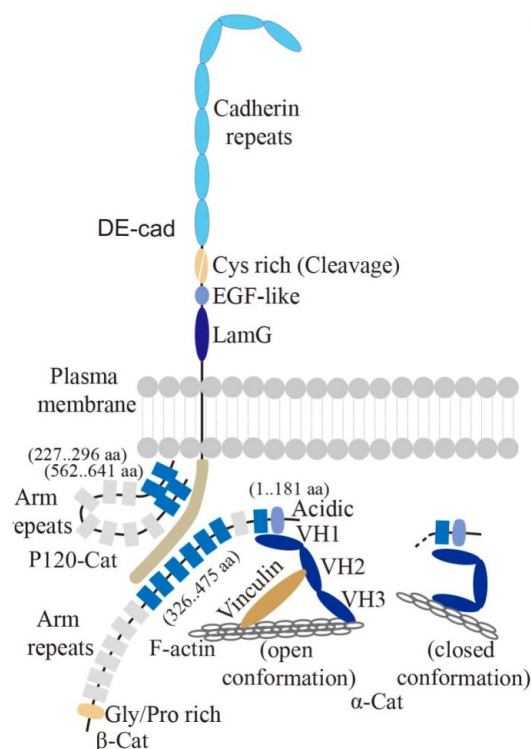
Figure 2.5: DE-cadherin-catenin complex (E-cadherin interaction partners). The DE-cadherin extracellular domain regulates cell-cell adhesion and forms the cadherin-catenin complex through cytoplasmic domains and links the cadherin-catenin complex to the actin-based cytoskeleton. The DE-cadherin cytoplasmic domain binds to p120-catenin directly, p120-catenin connects with β-actin, β-actin binds to α-catenin, and α-catenin interacts with F-actin to link the cadherin complex to the actin cytoskeleton. α-catenin contains three vinculin homology domains (VH1-3). VH1 is a β-catenin binding domain at the *N*-terminal and VH3 is an F-actin binding domain at the *C*-terminal. The central VH2 domain is regulated by force and, in turn, plays a role in junction remodeling. The scheme was taken from (Kong and Großhans, 2020).

2.3 *N*-glycosylation

It is known that *N*-glycosylation plays a vital role in biological functions, including stabilizing the proteins against denaturation and proteolysis, making the protein more soluble, controlling immunological responses, and assisting the orientation of the protein, and ER quality control (Helenius and Aebi, 2004).

The majority of the matured proteins are synthesized and folded in the ER, where they can get their functionalities and constantly maintain proper physiological

homeostasis. However, protein folding is a delicate and error-prone process. Therefore, ER contains an ER quality control (ERQC) system that can help protein folding, modify secreted and membrane proteins, and degrade misfolded protein products *via* ER-associated degradation (ERAD) or autophagic degradation systems (Araki and Nagata, 2011; McCaffrey and Braakman, 2016) (**Figure 2.6**). Correctly folded proteins can pass through the ERQC systems and secrete them to their native sites with the help of chaperones and oxidoreductase family members (Adams et al., 2019; Ellgaard and Helenius, 2003). Misfolded glycoproteins are detected and degraded by the ERAD system (Adams et al., 2019; Araki and Nagata, 2011; McCaffrey and Braakman, 2016).

ERQC system consists of five steps, including cotranslational translation, posttranslational membrane insertion, calnexin (CNX) and calreticulin (CRT) cycle, ER exit, and ER-associated degradation (ERAD) (Adams et al., 2019; Araki and Nagata, 2011; McCaffrey and Braakman, 2016) (**Figure 2.6**). Newly synthesized protein translocation starts after the release of the SRP (signal recognition particle) and SRP receptor (Araki and Nagata, 2011). Oligosaccharide transport is facilitated by the oligosaccharyltransferase (OST) complex, and glucosidases I and II can remove the two outmost glucose (Araki and Nagata, 2011). Later, the carboxy-terminal single transmembrane domain (TMD) of tail-anchored (TA) proteins, which are known as post-translationally inserted proteins, are recognized and inserted into the ER membrane (Araki and Nagata, 2011; Mateja et al., 2009; Wang et al., 2008). Importantly, the CNX/CRT cycle promotes the glycoproteins' folding in the ER, and glucosidase II removes the last glucose site of the glycoproteins, thus blocking the interactions between glycoproteins and calnexin and calreticulin. Consequently, correctly folded proteins can exit the ER. By contrast, non-native glycoproteins get one glucose site back on the glycan and go to the CNX/CRT cycle again. Only the permanently misfolded proteins will be degraded by the ERAD system, which is medicated by the cytosolic peptide *N*-glycanase (PNGase or NGLY1). (Adams et al., 2019; Araki and Nagata, 2011; Ellgaard and Helenius, 2003; Kuribara and Totani, 2021; McCaffrey and Braakman, 2016). If the *N*-glycan does not contain any glucosyl

residues, the newly synthesized proteins will not go to the calnexin/calreticulin cycle, which assists in the glycoproteins folding and degrading in the ER. In a word, *N*-glycans not only promote folding directly but also indirectly promote the interactions between glycoproteins and glucosidases, lectins, glucosyltransferases, and so on (Ellgaard and Helenius, 2003).
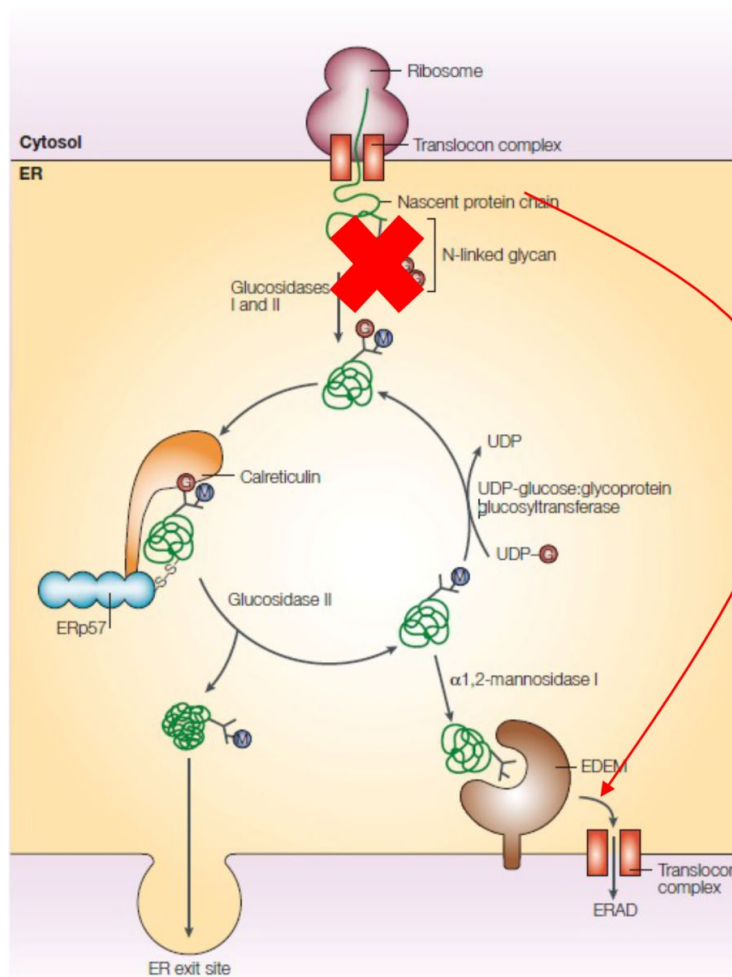
Figure 2.6: Roles of *N*-linked glycans in ER quality control. In the ER, correctly folded proteins can pass the ER quality control system and exit the ER with the help of glucosidases and glucosyltransferases. In contrast, non-native glycoproteins go to the CNX/CRT cycle where they can get additional glucose residues, and permanently misfolded proteins will be degraded by the ERAD system. If the *N*-glycan does not contain any glucosyl residues, the proteins will be degraded directly, so no proteins can exit the ER. The scheme was modified from (Ellgaard and Helenius, 2003).

ERQC can be divided into primary quality control and secondary quality control (Ellgaard and Helenius, 2003). Primary QC works for all proteins while second QC is reserved for certain classes of proteins that can interact with the folded cargo proteins

(Ellgaard and Helenius, 2003). The CNX/CRT cycle is one of the typically primary QC, and ER retention and export belong to secondary QC.

N-glycosylation is a highly conserved biological process through evolution. *N*-glycosylation is the process by which *N*-acetylglucosamine (GlcNAc) is attached to the nitrogen atom of asparagine (Asn) residue in a consensus sequence Asn-X-Ser/Thr (Threonine) (Kornfeld and Kornfeld, 1985). The formation of *N*-linked glycans consists of two processes, including the synthesis of an oligosaccharide precursor (dolichol-linked precursor) and the following processing activities by multiple ER and Golgi glycosyltransferases and glycosidases. In yeast, the addition of the first, second, and terminal glucose residues is encoded by the genes ALG6, ALG8, and ALG10, respectively. And dolichol-glucose, which is produced by ALG5, is the source of glucose. (Helenius and Aebi, 2004). These four enzymes are essential for the completion of protein *N*-glycosylation but are not important for cell growth. In *Drosophila*, mutants of wollknäuel (*wol*), garnystan (*gny*), and *xiantuan* (*xit*) are the homologs of ALG5, ALG6, and ALG8, and these mutants are lethal and lead to specific morphogenetic defects (Burda and Aebi, 1998; Reiss et al., 1996; Stagljar et al., 1994; Zhang et al., 2014) (**Figure 2.7**).

Recently, our group found there was a mobility shift between WT and *wol*, *gny*, and *xit* mutants. However, when treated with glycosidase F, which can remove all the *N*-linked glycans, this band shift is gone. This strongly suggests that E-cadherin is hypo-glycosylated in *wol*, *gny,* and *xit* mutants (Zhang et al., 2014). Hypo-glycosylated E-cadherin (mutant V13) promotes intercellular adhesion in human CHO cells and epidermoid carcinoma A253 cells (Jamal et al., 2009). Additionally, it was discovered that enhanced recruitment of γ-catenin and vinculin to adherens junctions (AJs), which is crucial for the stabilization of AJs, is a characteristic of hypo-glycosylated E-cadherin (Liwosz et al., 2006; Palovuori and Eskelinen, 2000).

E-cadherin *N*-glycosylation sites are conserved throughout the species and localized in the extracellular domain. Canine and human E-cadherin contain four N-glycosylation sites. Canines have one site in their extracellular domain 4 and two in

their extracellular domain 5, an additional *N*-glycosylation site was reported in a carcinoma cell line in its EC5 domain. The EC4 and EC5 of human E-cadherin have two *N*-glycosylation sites, respectively. There are 11 potential *N*-glycosylation sites in *Drosophila*, and 7 of them have been verified by mass spectrometric experiments (Zielinska et al., 2012) (**Figure 2.4**).
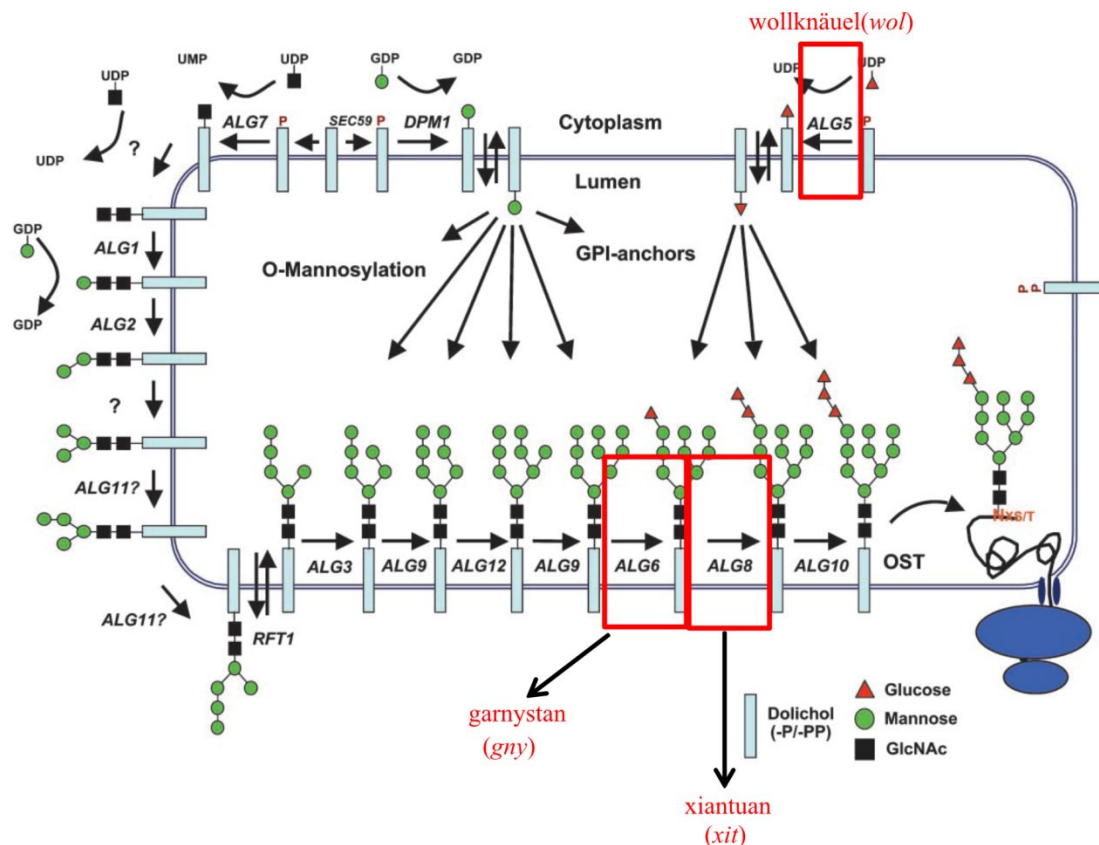
Figure 2.7: Synthesis of *N*-linked glycans and *Drosophila* mutants in the *N*-glycosylation pathway. Synthesis of the *N*-linked glycan starts on the cytoplasmic side of the ER. There is a dolichol-linked precursor on the ER membrane, then several mannose residues and glucose residues are attached to the precursor, and once this process is completed, this tag can be transferred to a protein. ALG6, ALG8, and ALG10 encode the enzyme which catalyzes the addition of the first, second, and last glucose in yeast. ALG5 is important for the synthesis of precursor glucose and may have a role in transferring activated glucose to the ER lumen. In *Drosophila*, mutants of wol, gny, and *xit* are the homologs of ALG5, ALG6, and ALG8, which are essential for *N*-glycan synthesis. The scheme was modified from (Helenius and Aebi, 2004).

2.3.1 Roles of *N*-glycosylated E-cadherin

N-glycosylation of E-cadherin is one of the most prominent posttranslational

modifications. There are three essential glycosyltransferases committed to the *N*-glycan biosynthesis process: *N*-acetylglucosaminyltransferase III (GnT-III), N-acetylglucosaminyltransferase V (GnT-V), and fucosyltransferase (FUT8), which catalyze the structures of bisecting GlcNAc (β1,4 GlcNAc), β1,6 GlcNAc branched GlcNAc, and α1,6 fucose *N*-glycan, respectively (Brockhausen et al., 1988; Narasimhan, 1982; Pinho et al., 2011; Uozumi et al., 1996). GnT-V can promote tumor metastasis while GnT-III plays a crucial role in tumor suppression. Gastric cancer mutant Asn-554 shows a protective role in gastric cancer by preventing E-cadherin dysfunction (Carvalho et al., 2016). The 633 locus is critically important for the trafficking, expression, and folding of E-cadherin. (Zhou et al., 2008). In mice, a mutant of the gene Mgat-I, which encodes the enzyme *N*-acetylglucosaminyltransferase I (GlcNAc-TI), shows an embryonic lethal (Ioffe and Stanley, 1994). In addition, E-cadherin *N*-glycosylation plays a modulating role in tumor progression (Pinho et al., 2009). In a word, E-cadherin *N*-glycosylation influences the stability and structure of AJs, cell adhesion, migration, and tumor invasion.

2.4 E-cadherin in junction remodeling and mechanotransduction

E-cadherin is essential for tissue morphogenesis by forming clusters, thereby supporting intercellular adhesion and transmitting tension (Quang et al., 2013; Takeichi, 1991; Zhu et al., 2003). The distribution of E-cadherin is uneven at the adherens junctions and instead forms clusters, which can transmit cell tension. E-cadherin forms *cis*- (lateral) and *trans*-associated molecules in the extracellular domain (Hong et al., 2010; Patel et al., 2006). E-cadherin helps cell-cell contact formation and transmits tensile forces during the cell remodeling process (Lecuit et al., 2011; Wang et al., 2012).

It is known that E-cadherin *trans*-clusters were first observed in mammalian epithelial cell lines (Kametani and Takeichi, 2007) and the same dimer was also found in *Drosophila* (Harris and Peifer, 2004; Müller and Wieschaus, 1996). E-cadherin clustering was first observed as a spot-like junction in *Drosophila* embryos (Tepass and Hartenstein, 1994a). These spots become denser during *Drosophila* embryogenesis

(Cavey et al., 2008). However, E-cadherin clustering has been well studied by the super-resolution microscope recently, particularly the fluorescence photoactivated localization microscopy (F-PALM) and stochastic optical reconstruction microscopy (STORM), which can reach 50–60 nm diameters (Quang et al., 2013; Wu et al., 2015). Later, the clustering of E-cadherin was suggested to have two length scales; nanoclusters (around 50 nm diameters) and microclusters (1-2 μm diameters) (Yap et al., 2015). By affecting E-cadherin *trans* and *cis* interactions, where *trans* interactions occur between neighboring cadherins and extracellular domain 1, while *cis* interactions normally occur in the EC1 and EC2 (Harrison et al., 2011), E-cadherin size and clustering processes are mediated (**Figure 2.8**).

On the other hand, E-cadherin is physically associated with F-actin, which is dependent on α-catenin. E-cadherin clustering is mediated by interacting with the cadherin-catenin complex and actin-associated proteins. Additionally, E-cadherin helps actin assembly and recruits active myosin II (Gomez et al., 2015), which promotes junction tension and has a role in junctional actin organization (Ratheesh and Yap, 2012; Wu et al., 2015; Yap et al., 2015). In addition, compared to unclustered E-cadherin, clustered E-cadherin is more stable. (Cavey et al., 2008). E-cadherin cluster number, size, and mobility are regulated by the actomyosin network (Engl et al., 2014; Quang et al., 2013), and cortical actomyosin promotes the E-cadherin clustering process and strengthens the adhesion caused by force (Shewan et al., 2005; Smutny et al., 2010). In addition, actomyosin itself is sensitive to force. In this way, E-cadherin molecules can bind and be tethered by actin, and thus, more E-cadherin molecules bind to the cadherin-catenin complex, and the affinity is increased (Cavey et al., 2008).

Recently, Schwartz's group first reported experimental evidence that cadherin *cis* and *trans* interactions are mutually cooperatively by super-resolution microscopy with intermolecular single-molecule Förster resonance energy transfer (Thompson et al., 2021). They found that cis interactions increase trans-binding stability by 30 times, and in turn, trans interactions increase the stability of cis clusters, which is independent of cytoplasmic interactions (Thompson et al., 2021). In 2021, Leckband's group finds that

p120-catenin binding is important for the cis interactions of E-cadherin and that uncoupling p120ctn disrupts the cis and trans interactions with adhesions (Vu et al., 2021). However, actin plays a two-tiered role in E-cadherin stabilization and immobilization. On the one hand, small and stable actin is enriched in the homophilic E-cadherin clusters, while on the other hand, the actomyosin network controls the lateral E-cadherin mobility by a tethering mechanism (Cavey et al., 2008) (**Figure 2.9**), which means homophilic E-cadherin cluster immobilization is essential for adhesion stabilization (Cavey and Lecuit, 2009).
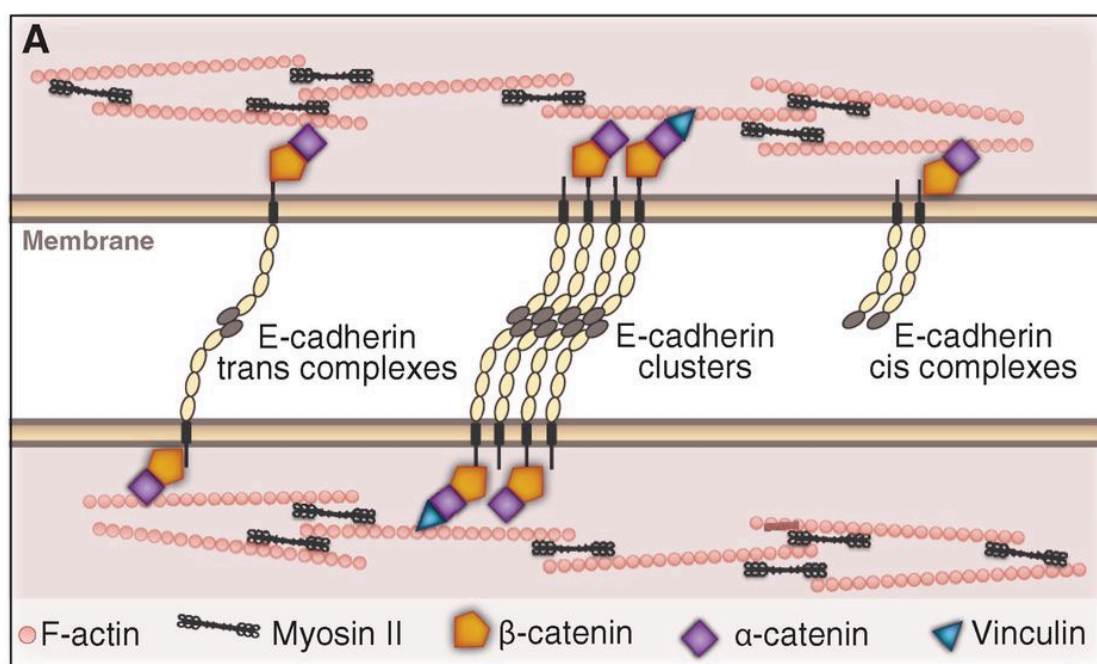
Figure 2.8: E-cadherin *cis* and *trans* clusters. E-cadherin forms cis and trans complexes and controls adhesion and transmits force at cell junctions. E-cadherin stabilizes adhesion by forming clusters and increasing the interaction with actin filaments through β-catenin, α-catenin, p120-catenin, and vinculin. The scheme was taken from (Guillot and Lecuit, 2013b).

In addition, endocytosis modulates both E-cadherin cluster size and density, which was observed in cell cultures and also *in vivo* (de Beco et al., 2009; Levayer et al., 2011; Song et al., 2013). In *Drosophila*, Shibire (*Shi*) mutant, homology of Dynami, which medicates endocytosis, shows larger clusters and the distribution of E-cadherin is more abundant (Quang et al., 2013), which in turn supports the proposal that E-cad *cis* clusters promote its endocytosis (Levayer et al., 2011; Quang et al., 2013). Therefore, it

was proposed that E-cadherin clustering promotes endocytosis and thus in turn regulates the size and number of clusters (Yap et al., 2015).

Taken together, interactions with the E-cadherin ectodomain, interactions with the cadherin-catenin complex (actomyosin network), interactions with the transmembrane domain, and E-cadherin endocytosis medicate the E-cadherin clustering process (Yap et al., 2015). However, there is no clear definition of E-cadherin clustering and immobilization. Further factors underlying the E-cadherin clustering process still need to be investigated.
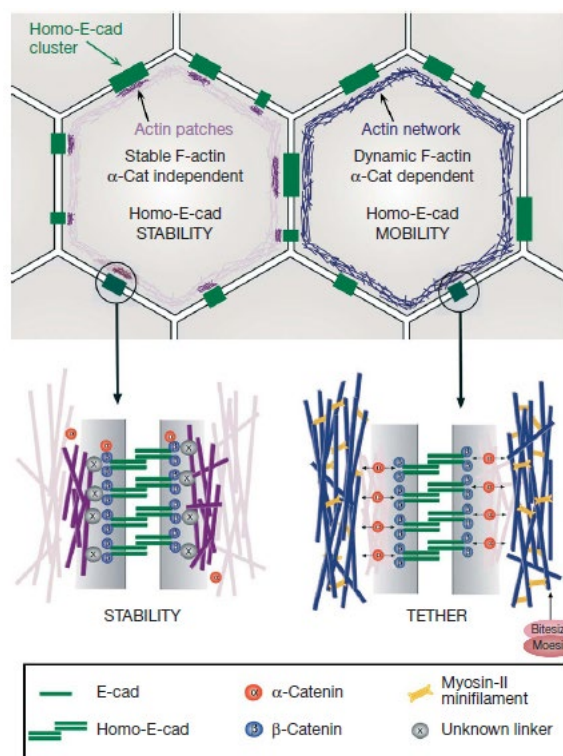
Figure 2.9:Model of two-tiered regulation of homo-E-cad stability and mobility.

A stable, tiny actin patch enriches and probably stabilizes homo-E-cad in SAJs, which is independent of α-catenin (left). A dynamic, contractile network is mediated by moesin and thus limits E-cadherin lateral mobility through α-catenin (right). The scheme is from (Cavey et al., 2008).

Since the discovery of cadherins, scientists have found that they play pivotal roles not only in adhesion but also in epithelial morphogenesis and development, including establishing and maintaining apicobasal cell polarity, cell movement, cell recognition, and sorting (Halbleib and Nelson, 2006). Cadherin subtype switching is the typical

feature of cadherin morphogenetic functions during development. Cadherin switching means the conversion from E-cadherin to N-cadherin or the expression level of E-cadherin does not alter, but the increase of N-cadherin does (Wheelock et al., 2008). When cells lose their epithelial features, they can move or migrate more easily, leading to epithelial-mesenchymal transition (EMT), a typical feature of tumor progression. In *Drosophila*, a conversion from DE-cadherin to DN-cadherin was observed in the mesoderm during gastrulation (Oda et al., 1998). In addition, by interacting with an actin filament and myosin II, DE-cad plays a crucial role in *Drosophila* gastrulation and germband extension, a process of junction remodeling and expansion of cell-cell adhesions (Bertet et al., 2004). Complete knock-out of mouse E-cadherin leads to embryonic lethality with a cell junctional defect and dysfunction of cytoskeleton organization (Larue et al., 1994). DE-cadherin is expressed in almost all epithelial cells and is crucial for apicobasal polarity. DE-cadherin moves to the apical domain and forms adherens junctions during gastrulation (Harris and Peifer, 2004).

It has been found that DE-cadherin is not uniformly distributed during germband extension in *Drosophila* but forms *cis* and *trans* clusters, which are observed by a super-resolution microscope, and E-cadherin clustering is important for stabilizing adhesion and force transmission (Cavey et al., 2008; Hoffman and Yap, 2015; Quang et al., 2013). Moreover, DE-cadherin plays a significant role in *Drosophila* oogenesis, which regulates the cell sorting process by mediating germline and helping follicle cells reach the correct oocyte location (Godt and Tepass, 1998). In addition, E-cadherin can be attracted to the cell surface upon cell-cell contact. However, the chelation of extracellular calcium leads to E-cadherin fragmentation. It has been shown that the expression of classical cadherin reaches its highest level in distinct tissues during development (Halbleib and Nelson, 2006). Furthermore, germband extension is not complete and cell intercalation is delayed in *xit* and E-cadherin hypo-*N*-glucosylated mutants (Zhang et al., 2014). In addition, E-cadherin recycling and endocytosis are also important for the development and regulation of adhesion and stabilizing of the epithelia.

Taken together, despite the role of E-cadherin in adhesive junctions and force transmission having been investigated, more in-depth studies are still in demand.

Force is generated by the actomyosin network and transmitted by adhesion complexes (Heisenberg and Bellaïche, 2013). Therefore, force serves an indispensable role in the development of utilizing changing cell morphology, size, number, position, and gene expression (Heisenberg and Bellaïche, 2013). Since the nineteenth century, scientists have been devoted to studying embryonic morphogenesis. Recently, with the establishment and applications of advanced biophysical tools, such as micropipettes, laser cutting (Kiehart et al., 2000; Marinari et al., 2012), and molecular sensors (Grashoff et al., 2010), considerable progress has been achieved in the quantitative dynamic of cell-cell contact (Krzic et al., 2012). On the other hand, with the help of multiple physical models, simulating and predicting developmental processes with a certain mechanistic model has been realized (Heisenberg and Bellaïche, 2013; Morelli et al., 2012).

Moreover, force is driven by actin-myosin contractility as well as cell-cell adhesion. And actin-myosin networks are also crucial for transmitting force. It is known that clusters are the basic units of the adhesion complex that transmit force (Lecuit et al., 2011). Force generation and transmission are both self-organizing processes (Heisenberg and Bellaïche, 2013; Lecuit et al., 2011). Changes in cellular processes lead to cell migration and cell rearrangement. And these changes affect neighboring cell-cell contact and trigger tissue morphology alternation. Meanwhile, force is transmitted from a single cell to the adjacent cells. Consequently, cells regulate force generation by mediating actin filament assembly and actin-myosin contractility (Lecuit et al., 2011). The ARP2/3 complex and formins are two of the most well-studied actin filament regulators. ARP2/3 activation promotes the formation of branched actin to generate protrusive force (Lecuit et al., 2011; Mogilner and Oster, 2003; Shaevitz and Fletcher, 2007). However, formin activation encourages the formation and elongation of unbranched actin filaments or organizes myosin II and cross-linkers into contractile networks (Lecuit et al., 2011). Moreover, branched and

unbranched actins can act synergistically (Lecuit et al., 2011). Additionally, branched actin networks are stiff enough to resist compression and unbranched actin networks are too soft against the force, but they can facilitate the reassembly and reorganization of the actin network in turn, which serves as a cross-linking (Lecuit et al., 2011).

In epithelial cells, the force is transmitted by adhesion structures across the cell membrane to neighboring cells and the extracellular matrix (ECM). Among adhesion complexes, clusters are the basic units (Lecuit et al., 2011). Moreover, cadherins and integrins regulate cell-cell and cell-ECM adhesion, respectively. They can bind to actin, form clusters, and interact with actomyosin networks. E-cadherin, as the main component of the adhesion, binds to actin filaments via α-catenin, β-actin, and vinculin (adaptor proteins). Likewise, integrins bind to actin filaments by actin cytoskeleton proteins. Therefore, adhesion complexes undergo pulling forces through actomyosin contractility, leading to α-catenin conformation change and promoting the coupling of actomyosin networks and cell-cell adhesion (Heisenberg and Bellaïche, 2013; Lecuit et al., 2011).

Furthermore, mechanotransduction between adjacent cells or tissues is important for cell-cell contractility and dynamics. Myosin II regulates mechanical tension by stabilizing the association of actin and myosin (Cremo and Geeves, 1998; Heisenberg and Bellaïche, 2013; Kovács et al., 2007). Meanwhile, an increment of the cadherin-catenin complex can strengthen actin-myosin accumulation and contractility (Heisenberg and Bellaïche, 2013; Kovács et al., 2007; Liu et al., 2010). For example, cell intercalation plays an essential role in *Drosophila* germband extension in a myosin II-dependent manner (Zallen and Wieschaus, 2004).

2.5 Concluding remarks

In conclusion, E-cadherin plays an essential role in epithelial morphogenesis by regulating cell and tissue rearrangements through different regulatory mechanisms (Lecuit and Yap, 2015). During epithelial morphogenesis, cellular contractility is a

cardinal regulator. So far, our understanding of tissue morphogenesis has undergone a transformation from adhesion between adjacent cells contributing to tissue rearrangement (Foty and Steinberg, 2005; Takeichi, 1991) to actomyosin contractility-driven tissue remodeling (Guillot and Lecuit, 2013b; Heisenberg and Bellaïche, 2013; Lecuit and Yap, 2015). In addition, E-cadherin forms *cis* and *trans* complexes and controls adhesion, and transmits force at cell junctions (Guillot and Lecuit, 2013b). Normally, *trans* interactions occur between neighboring cadherins and extracellular domain 1, while *cis* interactions normally occur in the EC1 and EC2 [92], therefore, E-cadherin stabilizes adhesions by forming clusters and binds to the actomyosin skeleton. On the other hand, actomyosin itself is sensitive to force. In this way, E-cadherin molecules can bind and be tethered by actin, and thus, more E-cadherin molecules bind to the cadherin-catenin complex and the affinity is increased (Cavey et al., 2008). Moreover, E-cadherin *cis* and *trans* interactions mutually influence each other and increase their stabilization (Thompson et al., 2021). Even though interactions with the E-cadherin ectodomain, interactions with the cadherin-catenin complex, interactions with the transmembrane domain, and E-cadherin endocytosis medicate the E-cadherin clustering process (Yap et al., 2015), a more in-depth study of E-cadherin clustering needs to be performed. We all know that *N*-glycosylation is essential for stabilizing proteins, increasing their solubility, controlling immunological responses, assisting the orientation of proteins relative to a membrane, and the ER quality control (Helenius and Aebi, 2004). Moreover, E-cadherin *N*-glycosylation influences the organization and stabilization of AJs, cell adhesion, migration, and tumor aggression. However, there is no report that E-cadherin post-translational modifications could affect the E-cadherin clustering process *in vivo* so far. Our lab found that *xit* is an enzyme that encodes the terminal glucose residues. E-cadherin is one of its substrates. *xit* mutant is hypo-*N*-glycosylated in E-cadherin and shows a developmental defect. However, even though the E-cadherin total protein level is not changed in the *xit* mutant, the distribution is more uniform, which means, that *xit* may affect the clustering of E-cadherin (Zhang et al., 2014). This may be the first time

to show a posttranslational modification of E-cadherin affects the force transmission and the E-cadherin clustering process. In this thesis, I will investigate in-depth whether and how E-cadherin *N*-glycosylation can influence the clustering process of E-cadherin and thus influence morphogenesis.

The germband extension is a very fast process, but it plays a significant role in the development and tissue morphogenesis. The number of E-cadherin increases by about 50% during gastrulation in *Drosophila* embryos by a quantitative imaging system (from stage 7b to stage 9) (Quang et al., 2013). The reason why the E-cadherin number sharply increased in 1.5 hours and what is the development role of E-cadherin in gastrulation still need to be investigated.

2.6 The aims of the study

1. I aimed to define to what degree the phenotypes of *xit* mutants are due to hypoglycosylated E-cadherin.

2. I aimed to identify specific mechanisms of E-cadherin function that depend on *N*-glycosylation.

3. Results

Parts of the results were built on previous work by my colleague, Dr. Kong. Some of the figures were kindly provided by Dr. Kong.

3.1 Biochemical mapping of the *N*-glycosylation sites of E-cadherin: Experiment and prediction, coverage, and *xit* dependence

xit was identified when the X chromosome screen was performed to find novel mutants that impact oogenesis (Vogt et al., 2006). Later, our lab revealed that *xit* specifically affects the germband extension and regulates the efficient expression and *N*-glycosylation of E-cadherin in *Drosophila* (Zhang et al., 2014). In addition, E-cadherin RNAi embryos exhibited impaired germband extension (Zhang et al., 2014). The mutants in *wollknäuel* (*wol*) and *garnystan* (*gny*), homologs of ALG5 and ALG6, respectively, also showed an incomplete germband extension. *xit* encodes a glucosyltransferase in the endoplasmic reticulum (Zhang et al., 2014). Moreover, ALG8, the homolog of *xit* in *Saccharomyces cerevisiae* (Stagljar et al., 1994), transfers the second glucose residue into the dolichol glycan during the synthesis of *N*-linked glycans. Our lab reported that *xit* reduced the junctional E-cadherin but not the overall protein level (Zhang et al., 2014). In addition, *xit* had a reduced molecular weight compared to the wild-type in DE-cadherin (Zhang et al., 2014). However, when treated with glycosidase F (peptide-*N*-glycosidase F), this band shift is eliminated (Zhang et al., 2014), which means the smaller molecular weight of DE-cadherin was caused by hypo-*N*-glycosylation. The total E-cadherin protein level did not change, suggesting that despite the hypo-glycosylation, E -cadherin is not subject to ERAD.

To identify which E-cadherin *N*-glycosylation sites are affected in *xit*, I performed a mass spectrometry experiment with Co-IP samples. As an additional control, I also did a PNGase F treatment and performed a Co-IP experiment with m3 (E-cadherin with
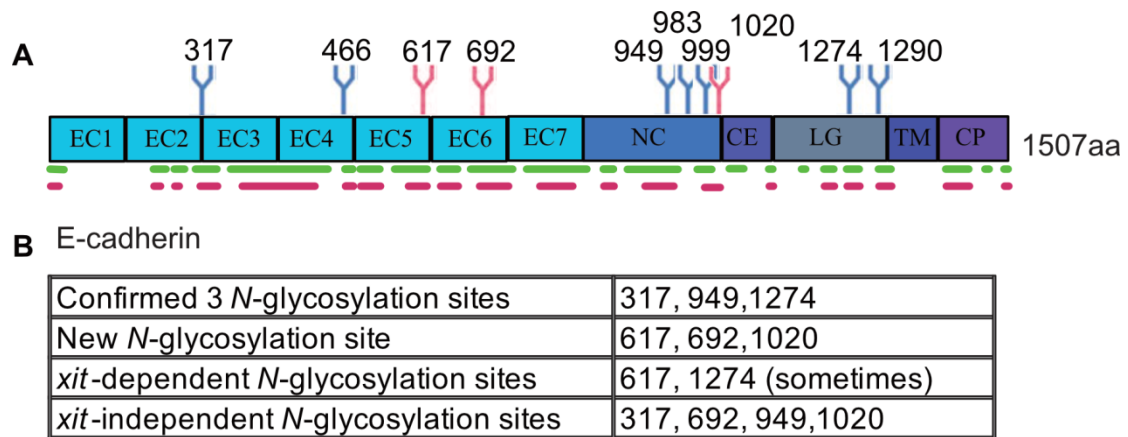
3 *N*-glycosylated point mutations) and m4 (E-cadherin with 4 *N*-glycosylated point mutations) (**Figure 3.1**). PNGase F (peptide-*N*-glycosidase F), which can remove almost all *N*-linked glycans, results in the conversion of Asn to Asp and thus leads to a mass unit change for each *N*-glycosylation site (Datta et al., 2015). The MS was done by the University of Marburg's core facility for Mass Spectrometry and elemental analysis. The MS samples and the blotting samples were completely consistent. Figure 3.1 shows that Co-IP worked. Firstly, the E-cadherin protein was enriched in the bound portion with and without PNGase F treatment (**Figure 3.1**). Secondly, there was a mobility shift in the bound portion after PNGase F treatment, indicating that the additional control worked (**Figure 3.1**). There was a reduced molecular weight in *xit* in both the *N*- (Zhang et al., 2014) and the *C*-terminal of E-cadherin compared to the wild-type (**Figure 3.1**), suggesting *xit* affected both the *N*-terminal and *C*-terminal of E-cadherin *N*-glycosylation (**Figure 3.1**).
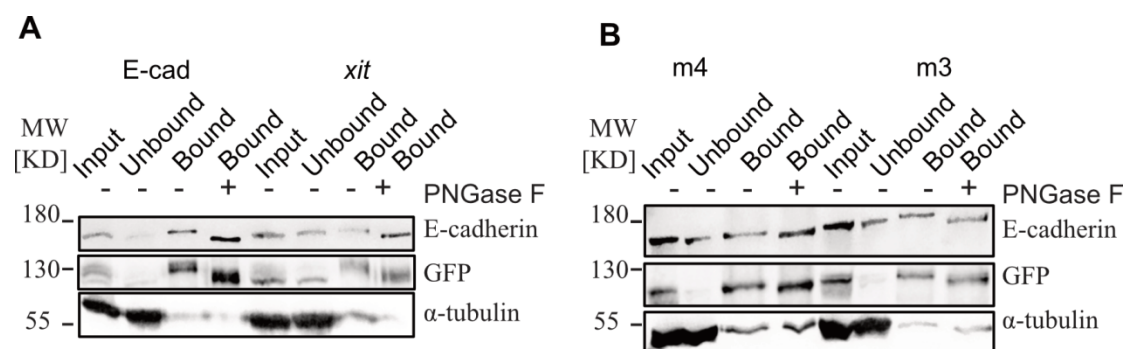
Figure 3.1: Co-IP experiments with PNGase F treatment. (A) Co-IP experiment by GFP trap agarose in E-cadherin GFP knock-in and *xit* three to six-hour embryos with and without PNGase F treatment. (B) Co-IP experiment using GFP trap agarose in m3 and m4 three to six-hour embryos, both with and without PNGase F treatment.

According to UniProt/Q24298, DE-cadherin has 11 potential *N*-glycosylation sites, seven of these sites have been verified (Zielinska et al., 2012), and they are all marked in blue in Figure 3.2A. The coverage ratio of the MS experiments for the E-cadherin GFP knock-in sample was around 60%, and the matching rate was about 50% in *xit* (**Figure 3.2A**). Through the MS analysis, I confirmed 4 E-cadherin *N*-glycosylation sites, 317, 949, and 1274 (**Figure 3.2**), which had already been

identified (Zielinska et al., 2012). Moreover, I found three other new E-cadherin *N*-glycosylation sites, 617, 692 and 1020 (**Figure 3.2**), which were highlighted in red in Figure 3.2A. In addition, *xit* specifically affected the E-cadherin sites 617 and 1274 *N*-glycosylation (**Figure 3.2B**). However, multiple tests have shown that E-cadherin1274 point *N*-glycosylation was occasionally *xit*-dependent (**Figure 3.2B**). In wild-type (E-cadherin GFP knock-in) embryos, the amino acid changed from asparagine (N) to glutamine (Q). However, these two sites were *xit*-dependent because this conversion could not be detected in *xit* (**Figure 3.2B**).

B E-cadherin

Confirmed 3 *N*-glycosylation sites	317, 949,1274
New *N*-glycosylation site	617, 692,1020
xit-dependent *N*-glycosylation sites	617, 1274 (sometimes)
xit-independent *N*-glycosylation sites	317, 692, 949,1020

Figure 3.2: *xit* specifically affects the E-cadherin sites 617 and 1274 *N*-glycosylation during germband extension. (A) The schematic diagram shows the position of E-cadherin peptides covered in the MS analysis. The green lines indicate E-cadherin GFP knock-in and the red lines represent the *xit* mutant (± PNGase). The blue symbols show the E-cadherin *N*-glycosylation sites identified by others, while the red symbols show the sites that I identified and confirmed. (B) Summary of the MS experiment's E-cadherin *N*-glycosylation sites.

Furthermore, there was no difference in E-cadherin GFP knock-in and *xit* in sites 317, 692, 949, and 1020, suggesting that E-cadherin *N*-glycosylation of these positions was independent of *xit* (**Figure 3.2B**). There are only two potential *N*-glycosylation sites at the *C*-terminals of DE-cadherin. As there was a mobility shift in the *xit* mutant compared to the wild-type (**Figure 3.1A**), one of these two sites must be involved in the *xit* genotype. Unfortunately, the MS results did not cover site 1290 (**Figure 3.2B**).

3.2 Hypoglycosylation of E-cadherin

To further identify the role of E-cadherin in tissue morphogenesis, we used two experimental model systems. One was the *xit* mutant, which showed a stronger phenotype, and the other was site-specific E-cadherin *N*-glycosylation mutations with different combinations introduced at the endogenous genetic locus (**Figure 3.3**). The E-cadherin peptide of the MS analysis only covered 50–60% of the protein, and some *N*-glycosylation sites were not covered by the MS results, so we generated the endogenous *N*-glycosylated mutations of E-cadherin based on the report by others (Zielinska et al., 2012). Meanwhile, we will also introduce E-cadherin point mutations that depend on *xit*.

There are 11 potential *N*-glycosylation sites in DE-cadherin, and a mass spectrometric experiment has confirmed 7 of these (Zielinska et al., 2012). Based on the information, Dr. Kong generated endogenous E-cadherin GFP with mutations in knock-in flies by replacing asparagine with glutamine residues (**Figure 3.3B, Figure 3.4**). The MS experiment in the *xit* mutant led to the discovery of new sites. A new transgene carrying the new sites (617 and 1274) will be generated.
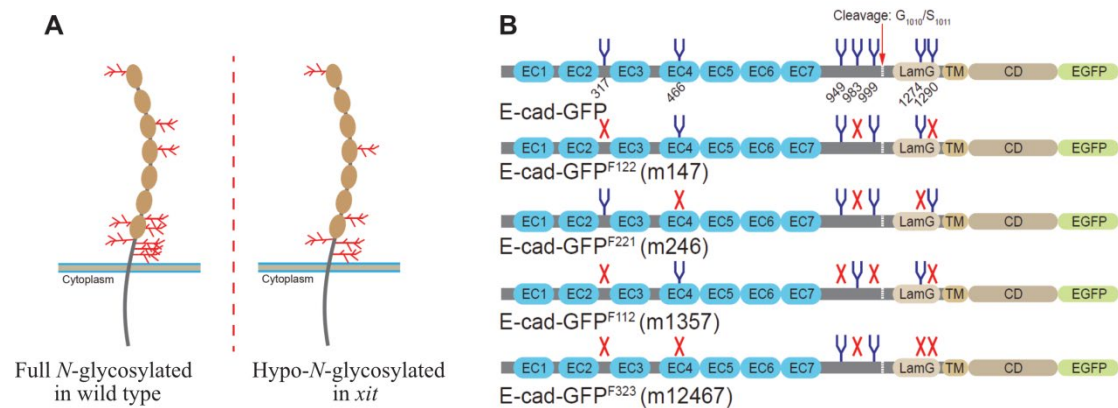
Figure 3.3: Two experimental systems for the function of E-cadherin *N*-glycosylation during tissue morphogenesis. (A) Schematic overviews of normal *N*-glycosylation in DE-cadherin and hypo-*N*-glycosylation in glucosyltransferase *xiantuan* (*xit*) mutant. (B) Site-specific *N*-glycosylation mutations in DE-cadherin substitute glutamine residues for asparagine residues in each *N*-glycosylation consensus sequence (NXS/T) with various combinations. The schemes are kindly provided by Dr. Kong. In this thesis, m3 refers to m246 unless noted with m147.

3.2.1 Generation of *N*-glycosylation alleles

The transgenes were then confirmed using western blot and sequencing (**Figure 3.5, 3.6**). In contrast to transgenes with up to 4 mutated *N*-glycosylation sites, the m5 is semi-lethal and sterile. In the m5 stock, only a few homozygous flies (less than 5%) are found, indicating that most of the homozygous do not survive until the eclosure of adults. The few homozygous females do not lay eggs. To circumvent the developmental lethality, m5 was recombined with the Frt2R, and eggs from ovoD-selected germline clones were analyzed. The cuticle preparation of m5 allows us to distinguish between two groups of larvae on the slides: some were brown, indicating that they were embryonic lethal, while others were normal. Additionally, we could distinguish the zygotic homozygous (m5 $m^{-/-}z^{-/-}$) from the zygotic heterozygous (m5 $m^{-/-}z^{-/+}$), which had a stronger phenotype. We discovered that some of the head and thorax segments were missing, suggesting the denticle patterns in m5 $m^{-/-}z^{-/-}$ have changed. (**Figure 3.7**). We also planned to generate the E-cadherin with 7 *N*-glycosylated point mutations. However, we did not get the transgene, suggesting there may be a dominant-negative effect.

DE-cad is proteolytically processed during biogenesis between the amino acids 1010 and 1011 (Zielinska et al., 2012), so the E-cadherin antibody could detect the *N*-terminal of DE-cadherin, and the GFP antibody could recognize the *C*-terminal of DE-cadherin as the DE-cadherin was fused with GFP. As a result, depending on the location of the mutations, there is a clear band shift between the wild-type and mutants in the *N*-terminal or *C*-terminal of E-cadherin (**Figure 3.6**).
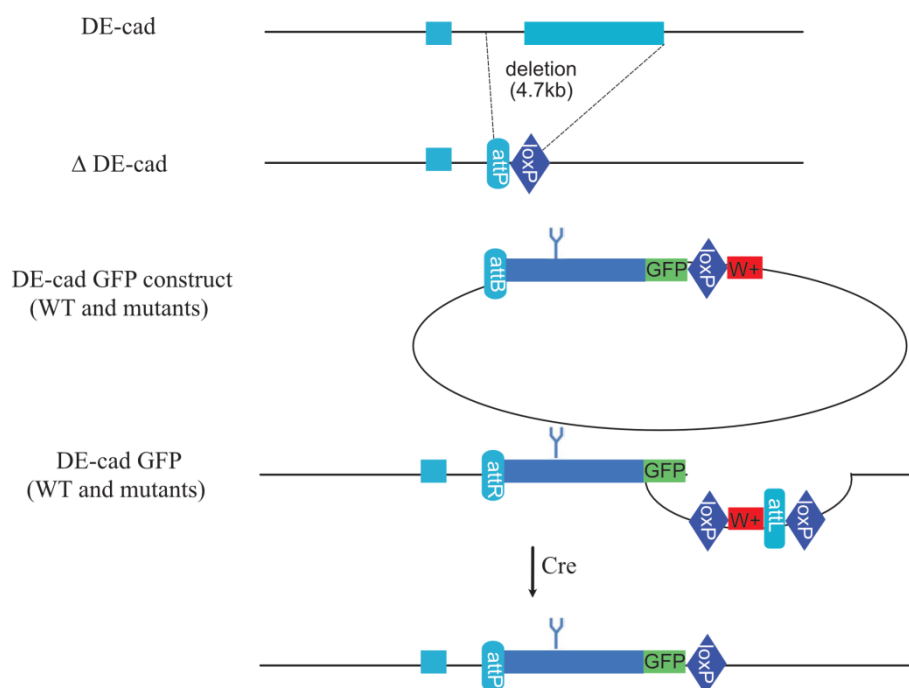
Figure 3.4: Transgenesis of the E-cad locus. Schemes for the generation of E-cadherin GFP *N*-glycosylation mutants. The DE-cadherin genomic DNA was removed and the DE-cad knockout line was generated. The DE-cad GFP knockin and hypo-*N*-glycosylation mutants were generated by injection. And the redundant sequence between two loxP sites was removed by the Cre-loxP recombination.
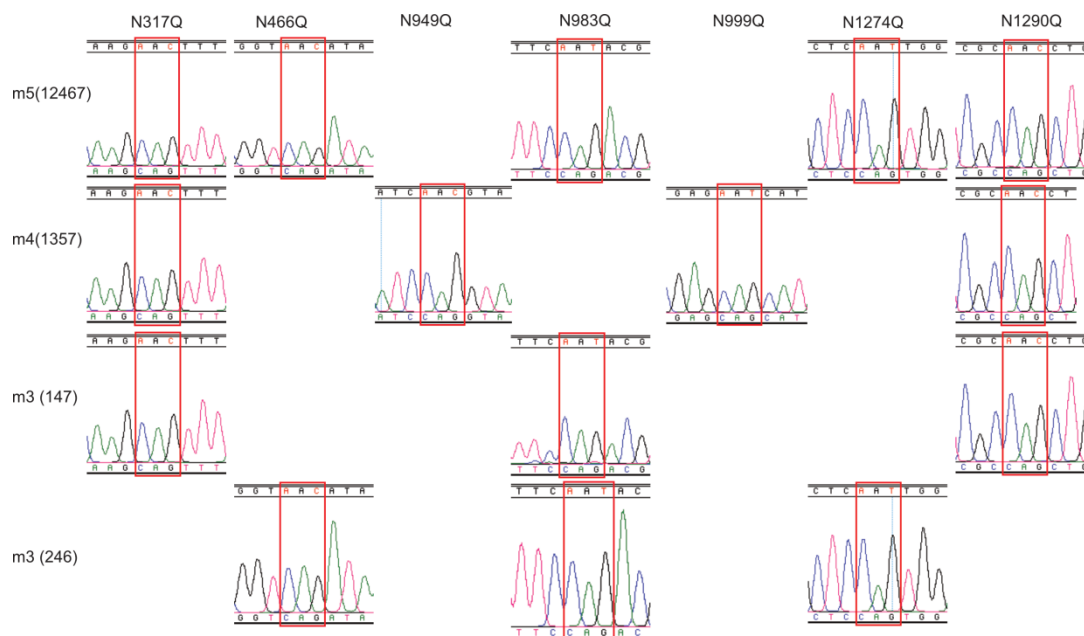
Figure 3.5: Sequences of E-cadherin *N*-glycosylation mutants. The sequencing was done by Dr. Kong. N (asparagine) was replaced by Q (glutamine) in DE-cadherin.
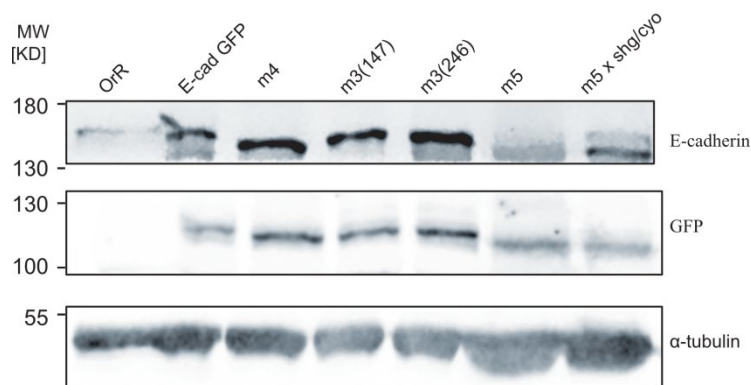
Figure 3.6: WB of E-cadherin in wild-type and *N*-glycosylation mutants. Total embryo lysis of indicated genotypes with E-cadherin, GFP, and α-tubulin antibodies by western blot.
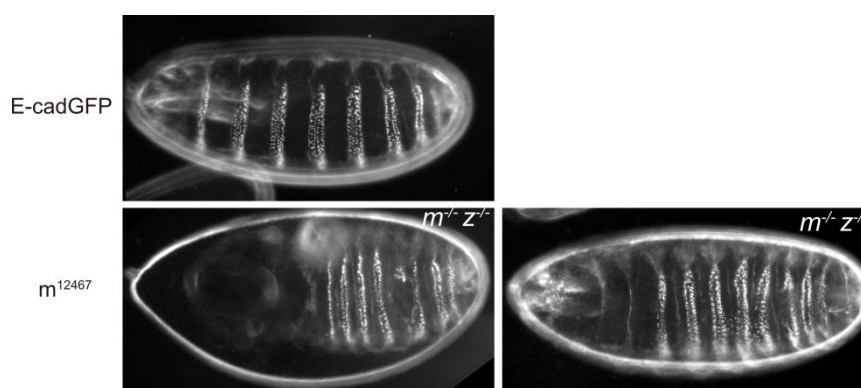
Figure 3.7: Cuticle preparation in m5 and E-cad GFP knock-in larvae. Denticle patterns were changed in m5 $m^{-/-}z^{-/-}$. The larvae were fixed and mounted by Hoyer's.

3.2.2 Impaired germband extension in E-cad hypoglycosylation mutants

Our lab found that *xit* specifically affected the germband extension in *Drosophila* (Zhang et al., 2014). Additionally, the germband extension was incomplete in injected E-cadherin RNAi embryos (Zhang et al., 2014). To further identify the role of E-cadherin *N*-glycosylation in germband extension, I recorded DIC time-lapse movies to check how much the germband has extended in E-cadherin *N*-glycosylation mutants. I found the *N*-glycosylation mutants also exhibited an incomplete germband extension like *xit* (**Figure 3.8**). I first measured how far the germband could extend and normalized it to the whole embryo's length (**Figure 3.8**). In OrR and E-cad GFP knock-in embryos, the germband could extend to around 53% of the embryo length. In contrast, the germband only expanded by 30% in *xit* (Zhang et al., 2014) (**Figure 3.8**). Nevertheless, in E-cadherin *N*-glycosylation mutants with 3, 4, and 5-point mutations,

the germband stretched between 40% and 50% of the egg length. Among them, m3 with sites 2, 4, and 6 mutations had the strongest effect on germband extension, which only moved to 40%. M4 with sites 1, 4, and 7 mutations showed the weakest impact, while m5 and m4 varied between two m3 mutants (**Figure 3.8**). Furthermore, it is also worth noticing that the germband extension was stopped in *xit* and m5, but only slowed down in other mutants (**Figure 3.8**).
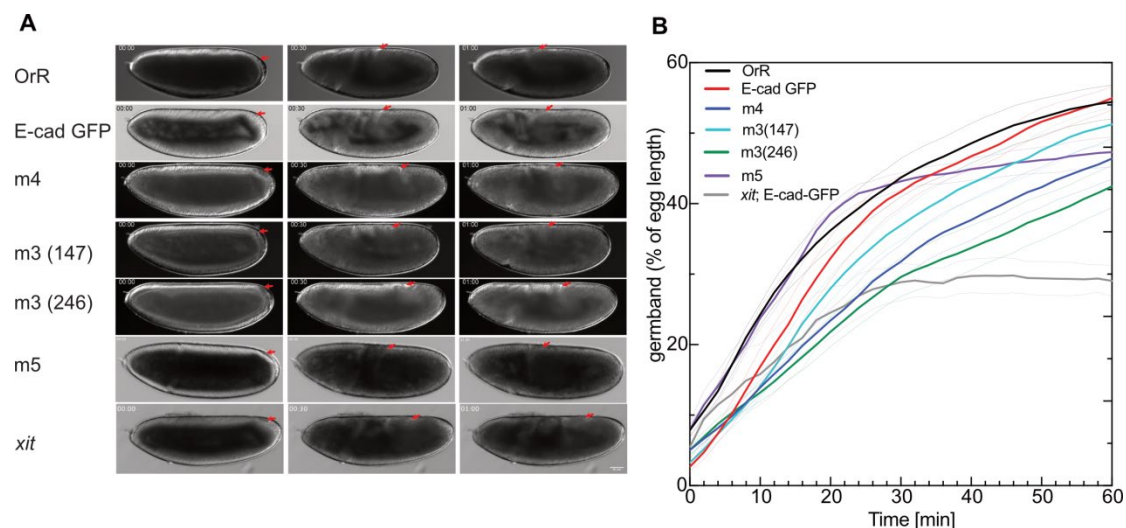
Figure 3.8: Impaired germband extension in *xit* and E-cadherin *N*-glycosylation mutants. (A) DIC images at the onset of germband extension, half-hour, and 1 hour after germband extension of the indicated genotypes. The red arrow marks how much the germband has extended. (B) The normalized distance between the posterior midgut invagination and the posterior pole cells. The standard error of the mean is represented by dashed lines with a 95% confidence interval. m5 (n = 13), xit (n = 11), and other genotypes (n = 20). Sandra recorded DIC movies of OrR, E-cadherin GFP, m3, and m4. M5 and *xit* were recorded by me.

3.2.3 E-cadherin localization and clustering

Despite the hypo-*N*-glycosylation in *xit*, the DE-cadherin total protein level remained unchanged (Zhang et al., 2014). In addition, the adherens junctions were curved and bent in *xit* as opposed to straight as in the wild type (Zhang et al., 2014) (**Figure 3.9**). However, the structure of junctions remained constant in *xit* and other *N*-glycosylated mutants (**Figures 3.9 and 3.10**). The junctions were stained with discs-large (DLG) and E-cadherin (GFP-booster) in wild type and *xit*. When the *N*-glycosylated mutants were stained with GFP-booster, they all showed a normal

junction, indicating the hypo-*N*-glycosylation did not change the junctional structure (**Figures 3.9 and 3.10**). However, in m4, some junctions were curved like in *xit* (**Figure 3.10**).
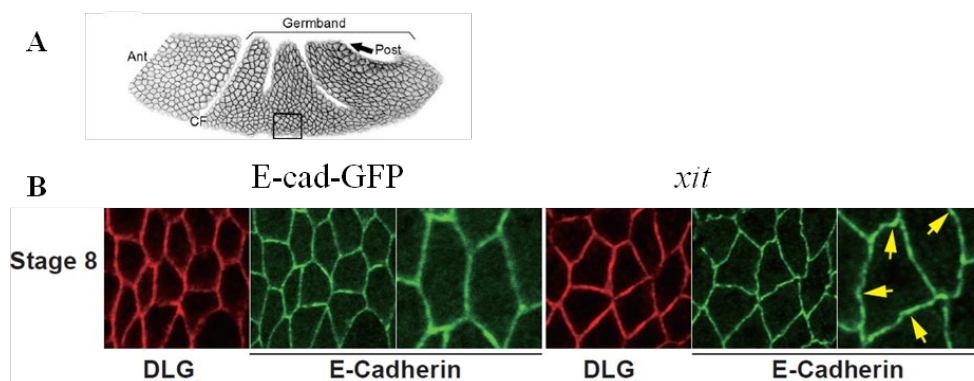
Figure 3.9: Hypo-*N*-glycosylation does not affect the epithelial cell-cell contacts. (A) The scheme shows the position of stained images on panel B. (B) Confocal images of DLG and E-cadherin (GFP booster) staining in E-cadherin GFP knock-in and *xit* stage8 embryos. DLG (Discs-large) is the marker of cell junction. The figure was kindly provided by Dr. Kong.

Even though the junctions in E-cadherin hypo-*N*-glycosylation mutants remained unchanged, the localization of E-cadherin was altered in m3 (**Figure 3.11**). The E-cadherin distribution was polarized (**Figure 3.11**) in E-cadherin GFP knock-in embryos, which is consistent with the previous report (Guillot and Lecuit, 2013a) that
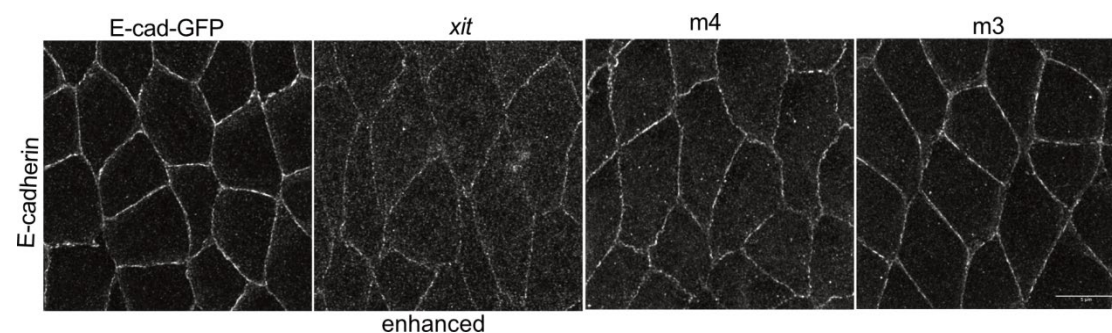
Figure 3.10: Adherens junctions remain unchanged in E-cadherin hypo-*N*-glycosylation mutants. DE-cadherin stained with indicated genotypes (wild type, *xit*, m4, and m3) by GFP booster. Airycan joint deconvolution images of fixed embryos at stage 7 in the indicated genotypes. A maximum intensity projection (MIP) was used. Scale bar 5μm.

the majority of E-cadherin is enriched at the apical domain at stage 8, while E-cadherin is abundant at the subapical domain at stage 6. However, in the m3 mutant, E-cadherin

co-localized with F-actin on the lateral side (**Figure 3.11**), indicating the maturation of E-cadherin is disturbed.
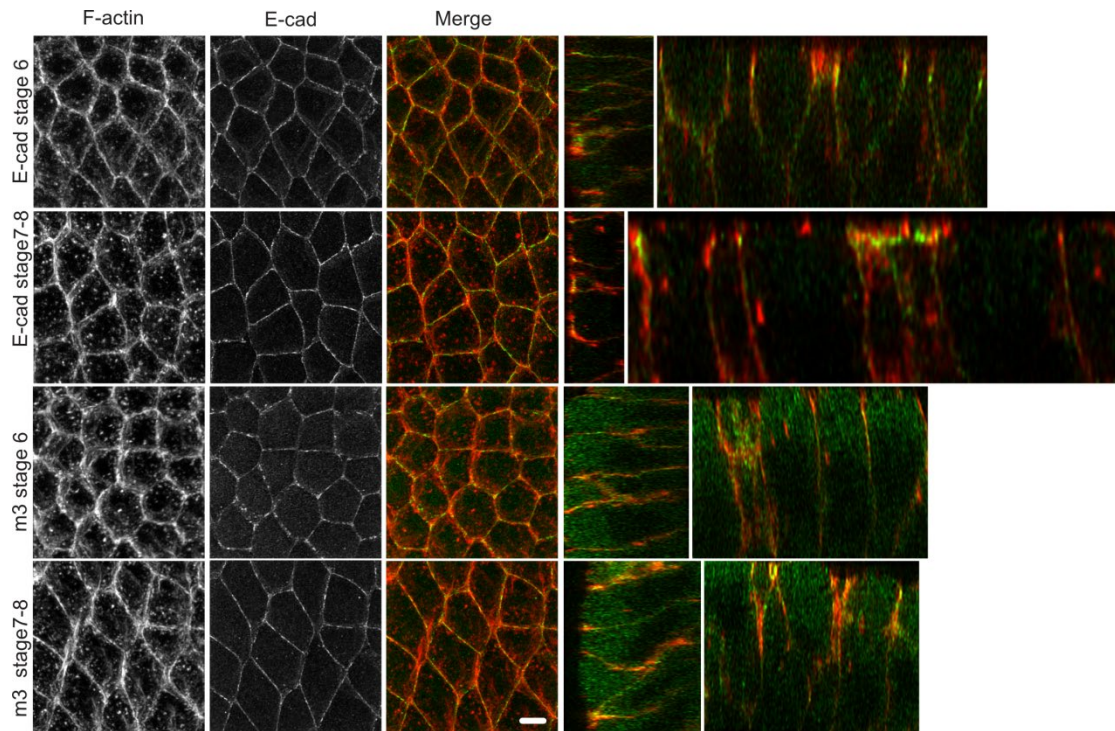
Figure 3.11: The location of E-cadherin is changed in the E-cadherin *N*-glycosylation mutant. Airycan joint deconvolution images of fixed embryos at indicated stages in endogenous E-cad GFP knock-in and m3 stained with F-actin (Phalloidin, red) and E-cadherin (GFP booster, green). Scale bar 5μm.

So far, we know that E-cadherin localization is changed in the E-cadherin *N*-glycosylation mutant (**Figure 3.11**). Additionally, the actomyosin network regulates the quantity, size, and intensity of E-cadherin clusters (Engl et al., 2014; Quang et al., 2013). Meanwhile, cortical actomyosin promotes the E-cadherin clustering process and strengthens the adhesion caused by force (Shewan et al., 2005; Smutny et al., 2010). Based on this, I proposed the hypothesis that *xit* affects the size of E-cadherin clusters, which in turn impacts E-cadherin mobility and tension. To confirm, I checked the size of E-cadherin clusters by using a super-resolution microscope-Airycan joint deconvolution system. The resolution of this method is down to 90 nm, depending on the sample. Afterward, I fixed and stained stage 7 embryos with GFP-booster, phalloidin, and p-myosin II in E-cadherin GFP, m3, and m4. I started by measuring

the average and total E-cadherin intensities at each junction. Additionally, I found the intensity of E-cadherin was sharply decreased in *xit* and m3, m4 (**Figures 3.12A, B, C, D**), which is consistent with figure 3.11. Afterward, I measured the variance of E-cadherin intensity among junctions, and I found the variation of E-cadherin intensity was significantly reduced in *N*-glycosylation mutants (**Figure 3.12B, E**). Figures 3.12A and B show the intensity of E-cadherin at a single junction. Figure 3.12B shows that the fluctuation between the maximum and minimum E-cadherin intensity levels was considerably more in the wild-type than in mutants, which is consistent with quantification (**Figure 3.12E**).
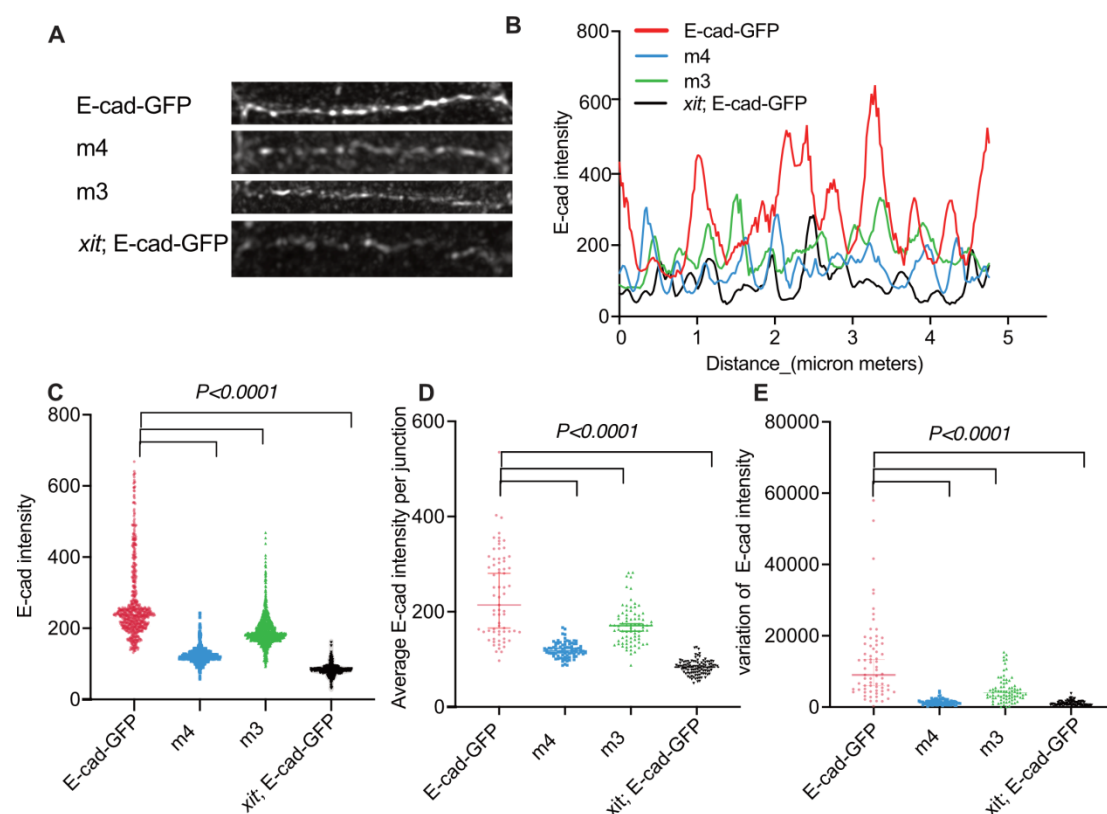
Figure 3.12: E-cadherin *N*-glycosylation regulates the size and intensity of E-cadherin clusters. (A) Airycan Joint Deconvolution images of E-cadherin clusters at a single junction in WT, m3, m4, and *xit*. (B) E-cadherin intensity in panel A. (C) E-cadherin total intensity at adherens junctions. (D) The average intensity of E-cadherin at each junction, excluding the vertices. (E) The variation of E-cadherin intensity across junctions. Statistical significance was estimated by an unpaired t-test, n > 60. A maximum intensity projection (MIP) was used.

3.2.4 Mobility of hypoglycosylated E-cadherin

By forming clusters, E-cadherin plays a critical role in tissue morphogenesis, thereby supporting intercellular adhesion and transmitting tension (Cavey et al., 2008; Quang et al., 2013; Takeichi, 1991; Zhu et al., 2003). In addition, the spot-like junctions become denser during *Drosophila* embryogenesis (Cavey et al., 2008). Moreover, clustered E-cadherin is more stable than unclustered E-cadherin (Cavey et al., 2008). In other words, E-cadherin clustering plays a fundamental role in tissue morphogenesis (Biswas, 2020). According to reports, the actomyosin network regulates E-cadherin size, number, and mobility (Engl et al., 2014; Quang et al., 2013). Interestingly, we found the mobile fraction was considerably increased in *xit* and other hypo-*N*-glycosylated mutants during germband extension (**Figures 3.13, 3.14, and 3.15**). To investigate the function of E-cadherin *N*-glycosylation in E-cadherin mobility, I performed the fluorescence recovery after photobleaching (FRAP) experiments in *xit* and *N*-glycosylated mutants during germband extension, and I focused on the clustered E-cadherin, so the entire bleached region was E-cadherin clusters. I quantified the fluorescence recovery and did a fitting by nonlinear regression and one-phase decay in GraphPad Prism. We found that there were more unclustered E-cadherin as the bleached E-cadherin-GFP molecular exchange was faster than an unbleached molecule in *xit* and m3, m4, and m5 mutants (**Figures 3.13, 3.14, and 3.15**). The incomplete recovery was due to the immobilized E-cadherin molecule (**Figures 3.13, 3.14, and 3.15**). The E-cadherin mobile fraction was 18% in E-cadherin GFP, whereas in *xit*, it increased to 43% (**Figure 3.13**).
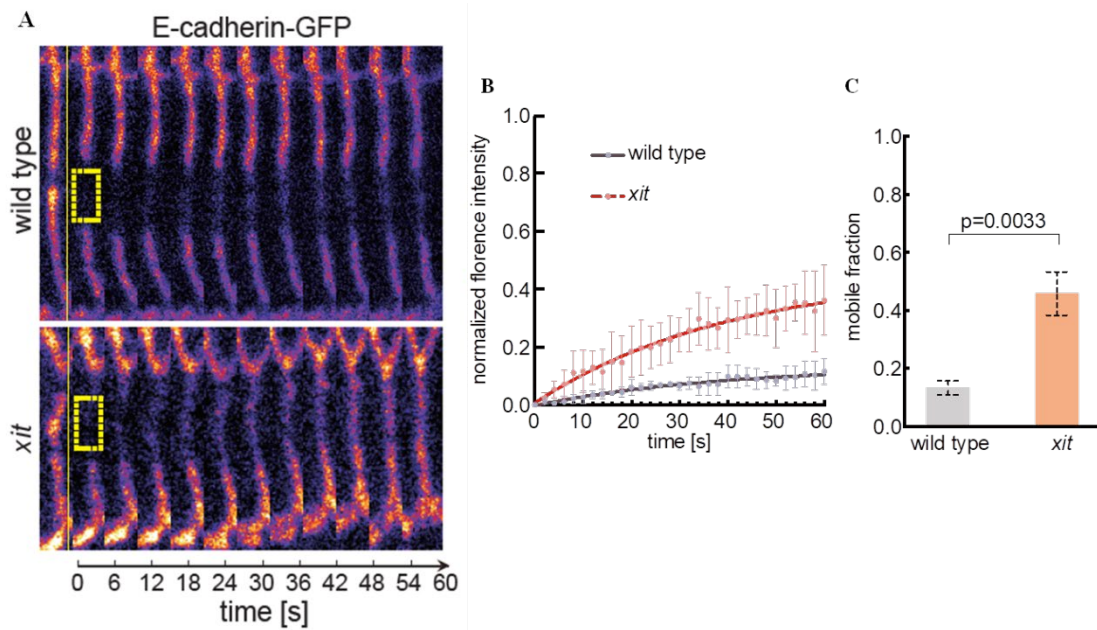
Figure 3.13: The E-cadherin mobile fraction is increased in *xit*. (A) Kymograph of E-cadherin after the FRAP experiment spanning one minute during stage 7. The yellow rectangle is the region of interest, which shows the bleached E-cadherin clusters. (B) E-cadherin fluorescence recovery curves in E-cad GFP knock-in and *xit*. A fitting curve was performed by nonlinear regression and one-phase decay using GraphPad Prism. (C) Mobile fraction of E-cadherin in panel A. Error bars represent the standard error of the mean (SEM) of the mobile fraction. Statistical significance was estimated by an unpaired t-test. Wild type means E-cadherin GFP knock-in in the figure. This figure was kindly provided by Dr. Kong.
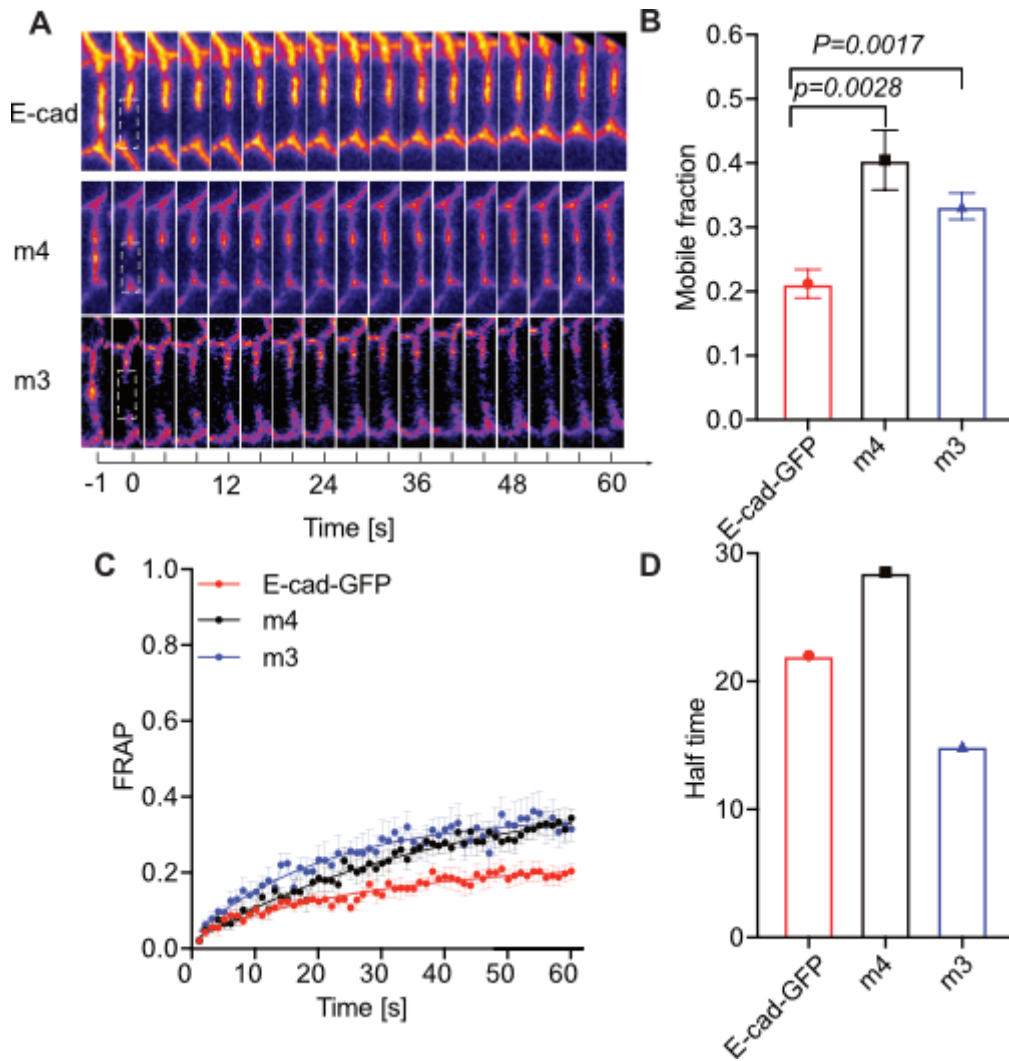
Figure 3.14: The mobile fraction is increased in E-cadherin *N*-glycosylation mutants. (A) Kymograph of E-cadherin after the FRAP experiment spanning one minute during stage 7. The white rectangle is the region of interest, which shows the bleached E-cadherin clusters. (B) Mobile fraction of E-cadherin in panel A. Error bars represent the standard error of the mean (SEM) of the mobile fraction. (C) E-cadherin GFP fluorescence recovery curves in E-cad GFP knockin (n = 10) and E-cadherin with three *N*-glycosylated point mutations (m3) (n = 7) and E-cadherin with four *N*-glycosylated point mutations (m4) (n = 9). A fitting curve was performed by nonlinear regression and one-phase decay in GraphPad Prism. Error bars represent the standard error of the mean (SEM) for the normalized E-cadherin intensity. (D) Half-time is the time when the intensity reaches half of its maximum intensity. Statistical significance was estimated by an unpaired t-test.

And the E-cadherin mobile fraction was 21% in E-cadherin GFP, 40% in m4, 33% in m3, 39% in m5$^{-/-}$z$^{-/-}$, and 30% in m5$^{-/-}$z$^{-/+}$ (**Figures 3.13, 3.14, and 3.15**). The recovery time is the time when the intensity can reach half of its maximum intensity. It

is worth pointing out that m5 is homozygous lethal and germline clones need to be generated. The mobility of m5$^{-/-}$z$^{-/-}$ and m5$^{-/-}$z$^{-/+}$ showed some differences. Compared to E-cadherin GFP knock-in and m5 maternal mutants (m5$^{-/-}$z$^{-/+}$), maternal and zygotic double mutants (m5$^{-/-}$z$^{-/+}$) had a larger effect on E-cadherin dynamics (**Figure 3.15**).
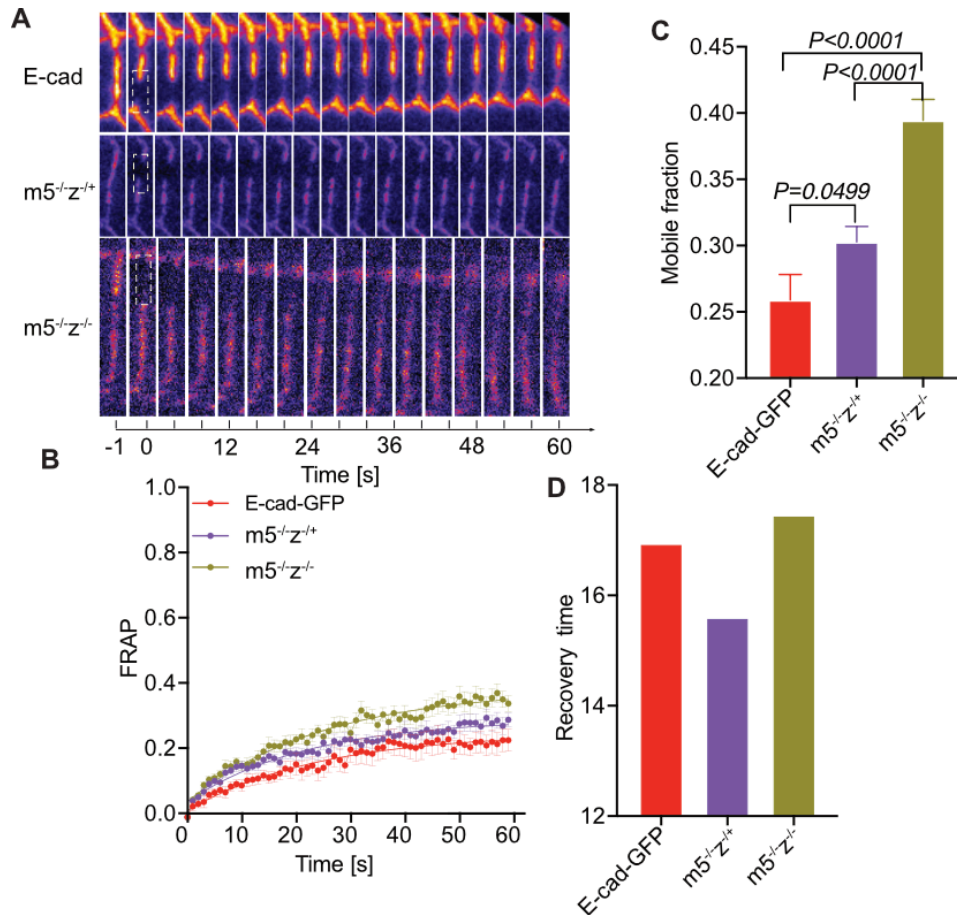
Figure 3.15: The mobile fraction is increased in E-cadherin *N*-glycosylation mutants. M5 germline clones were generated and crossed with m5/Cyo twist GFP. (A) Kymograph of E-cadherin after the FRAP experiment spanning one minute during stage 7. The white rectangle is the region of interest, which shows the bleached E-cadherin clusters. (B) E-cadherin GFP fluorescence recovery curves in E-cad GFP knockin and E-cadherin with five *N*-glycosylated point mutations (m5). A fitting curve was performed by nonlinear regression and one-phase decay using GraphPad Prism. Error bars represent the standard error of the mean (SEM) for the normalized E-cadherin intensity. (C) The mobile fraction of E-cadherin in panel A. Error bars represent the standard error of the mean (SEM) of the mobile fraction. (D) Recovery time is the time when the intensity reaches half of its maximum intensity. Statistical significance was estimated by an unpaired t-test. m5$^{-/-}$z$^{-/+}$, n = 13, m5$^{-/-}$z$^{-/-}$, n = 15.

In conclusion, the immobilization of E-cadherin clusters depends on

N-glycosylation.

3.2.5 Junction recoil after laser ablation

Cell shape change and cell rearrangement are driven by actomyosin-dependent cortical tension during development (Lecuit and Yap, 2015, Rauzi and Lenne, 2011). E-cadherin mediates cell-cell contact and plays an important role in contractile force (Lecuit and Yap, 2015). However, it is difficult to measure the junctional tension because of the mechanical properties of cell-cell contact (Sugimura et al., 2016). Researchers have lately been able to quantify the dynamics of cell-cell interaction with the development of laser-cutting technology (Krzic et al., 2012; Marinari et al., 2012), optical tweezers (Mazuel et al., 2015), FRET (Förster resonance energy transfer) tension sensor (Gayrard and Borghi, 2016) and other microscopy techniques. Subcellular laser ablation is the easiest way to measure mechanical tension compared with other techniques (Liang et al., 2016). The junctional tension can be measured by initial recoil (Liang et al., 2016). However, the viscous drag (friction) is also another regulator of junctional tension, so it is difficult to tell whether the increased vertexes' displacement and initial recoil velocities are because of increased junctional tension or reduced friction (Sugimura et al., 2016). On the other hand, wound healing occurs within seconds of laser cutting, and mechanical tension changes in turn (Wood, 2012), and the cell behavior after initial recoil may depend on secondary processes of the active materials like wound response. Therefore, I only measured the recoil velocities within 10 seconds.

Cadherins have three main functions in the formation and maintenance of cell-cell contacts, which are involved in adhesion tension, adhesion signaling, and the adhesion coupling process (Maître and Heisenberg, 2013). By interacting with the actomyosin network, cadherins can reduce interfacial and adhesion stress (Maître and Heisenberg, 2013).
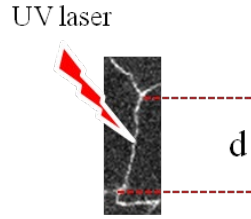
Figure 3.16: Schematic representation of the laser ablation experiment in the amnioserosa. In a single junction, a UV cut was performed, and displacements between two vertices were measured, as well as initial recoil velocities computed over time.
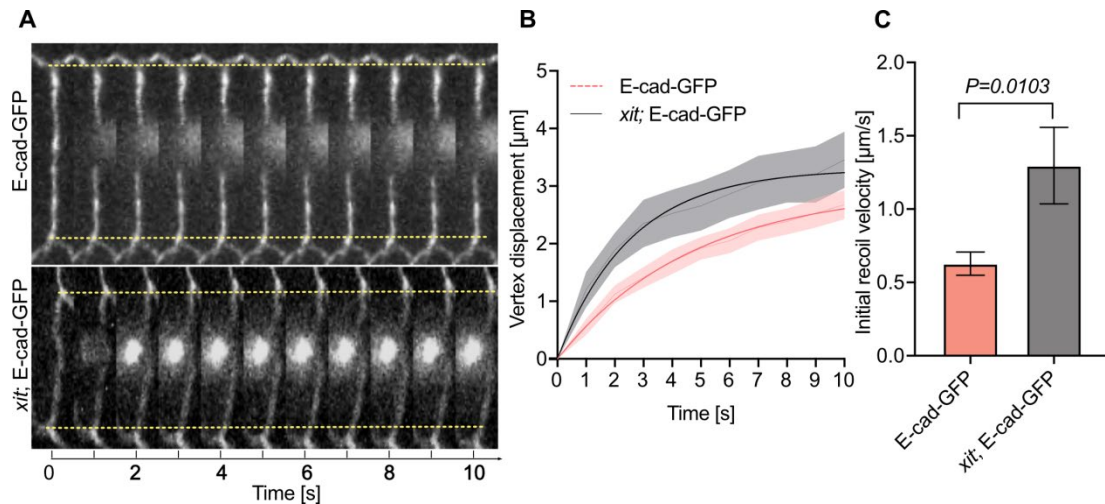
Figure 3.17: Junctional recoil is increased in *xit*. (A) Slices of movie stills from laser ablation experiments measuring cell-cell junction tension before and 10 seconds after ablation in E-cadherin GFP knock-in (WT) and *xit* in amnioserosa. Vertices' initial positions before laser ablation are indicated by yellow lines. (B) Vertex displacements in WT and *xit* were measured and normalized. (C) Initial recoil velocities were calculated based on vertex displacement and time in WT and *xit*. The error bars represent the mean with SEM. Statistical significance was estimated by an unpaired t-test. n = 15 (E-cadherin GFP), n = 11 (*xit*).

To check the role of hypo-*N*-glycosylation of E-cadherin for cell-cell adhesion, laser ablation experiments were performed in amnioserosa among mutants. By performing junction cut at cell-cell adhesion, which is labeled with E-cadherin GFP, tension is visualized by measurement of displacements between two vertices and recoil velocities (Liang et al., 2016). A schematic representation of displacement is shown in Figure 3.16. I found that *xit* and hypo-*N*-glycosylated mutants had considerably higher vertex displacements and initial recoil velocities (**Figures 3.17, 3.18, and 3.19**). Vertex

displacements were found to be three times greater in m3, m4, and m5$^{-/-}$z$^{-/+}$ embryos than in the wild type. However, in the m5$^{-/-}$z$^{-/-}$, the displacement increased by almost 4 times (**Figures 3.17, 3.18, and 3.19**). In the m5 mutant, maternal and zygotic double mutants, as well as maternal mutants, have the same effect on recoil (**Figure 3.19**).

Figure 3.18: Junctional recoil is increased in m3 and m4. (A) Movie stills from laser ablation experiments measuring cell-cell junction tension before and 10 seconds after ablation in E-cadherin GFP knock-in (WT) (n = 10) and E-cadherin *N*-glycosylation mutants (m3 and m4) (m3, n = 11, m4, n = 10) amnioserosa. Vertex positions before laser ablation are shown by yellow lines. (B, C) Vertex displacements in WT and mutants were measured and normalized. (D) Initial recoil velocities were calculated based on vertex displacement and time in WT and mutants. (E) WT and mutant viscoelasticity. The error bars represent the mean with standard deviation. An unpaired t-test was used to calculate statistical significance.

The E-cadherin GFP knock-in embryos had an initial recoil velocity of 0.36 μm/s, 0.85 μm/s in the m5$^{-/-}$z$^{-/+}$, and 0.74 μm/s in the m5$^{-/-}$z$^{-/-}$ (**Figure 3.19**). The GraphPad prism was also used to calculate viscoelasticity (K) (**Figures 3.18E and 3.19D**). In conclusion, E-cadherin hypo-*N*-glycosylation regulates junctional recoil.
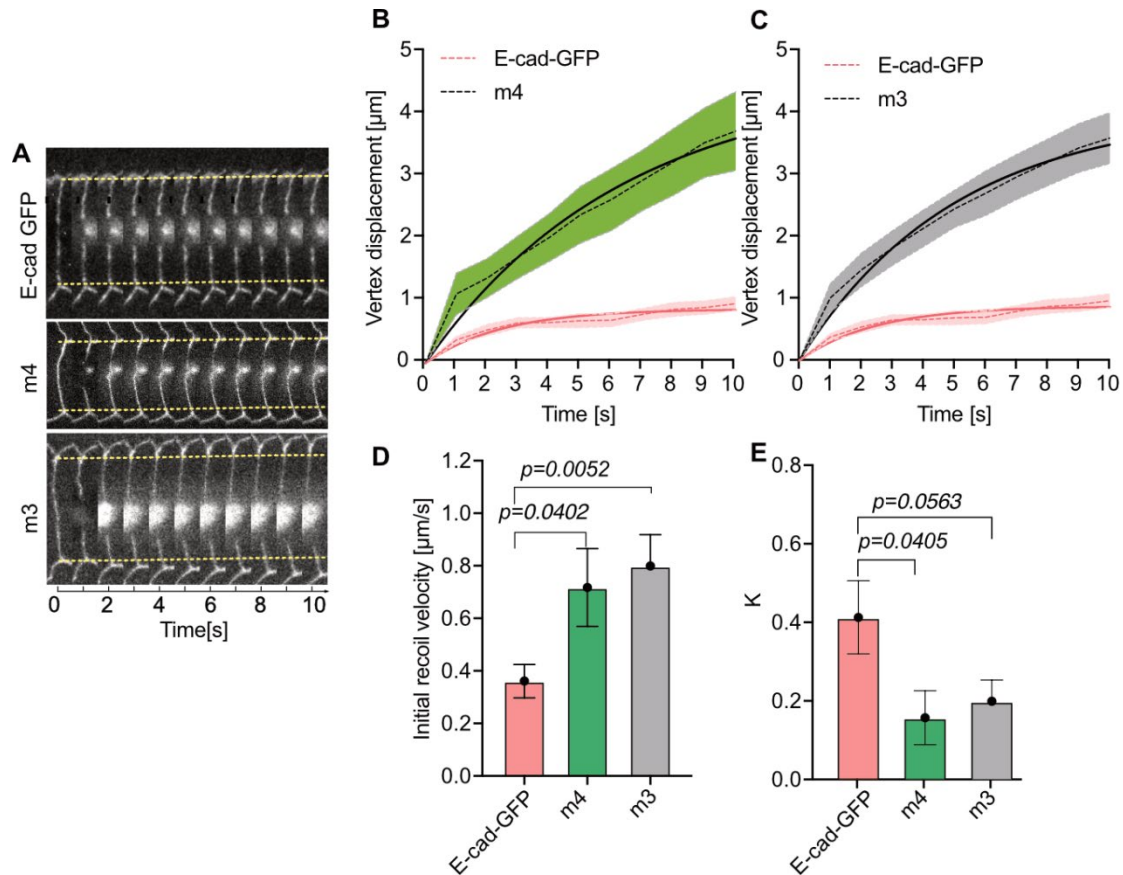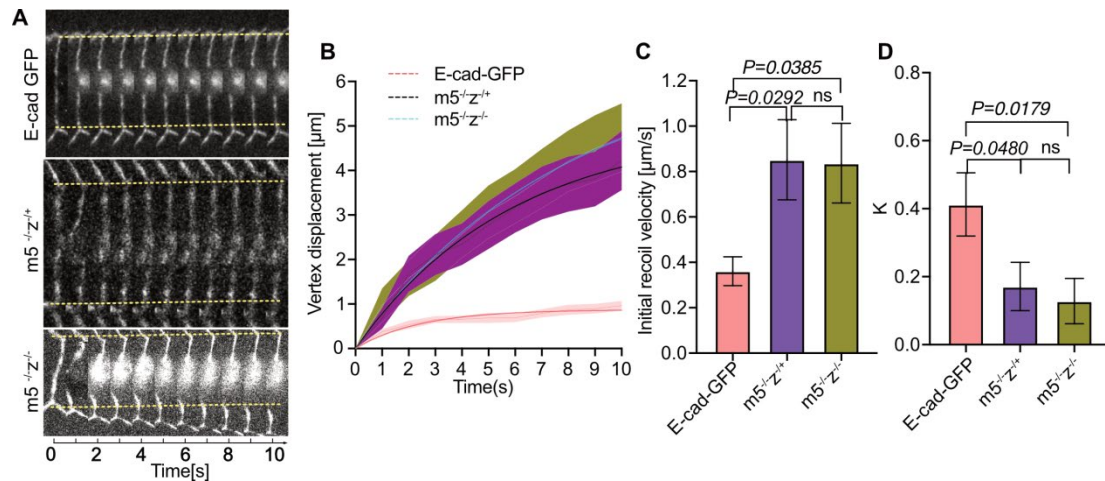
Figure 3.19: Junctional recoil is increased in m5. (A) Slices of movie stills from a laser ablation experiment measuring cell-cell junction tension before and 10 seconds after ablation in E-cadherin GFP knock-in (WT) and m5 amnioserosa. M5 germline clones were generated and crossed with m5/Cyo twist GFP. Vertex positions before laser ablation are shown by yellow lines. (B) Vertex displacements in WT and m5 were measured and normalized. (C) Initial recoil velocities were calculated based on vertex displacement and time in WT and mutants. (D) WT and mutant viscoelasticity. The error bars represent the mean with an SEM. Statistical significance was estimated by an unpaired t-test. m5$^{-/-}$z$^{-/+}$, n = 13, m5$^{-/-}$z$^{-/-}$, n = 15.

3.3 Impaired link of hypoglycosylated E-cadherin to cortical actomyosin

E-cadherin *trans* and *cis* interactions regulate E-cadherin clustering and immobilization. On the other hand, E-cadherin is physically linked to F-actin, and the cadherin-catenin complex also regulates the E-cadherin clustering process (Guillot and Lecuit, 2013b). In addition, *N*-glycosylation also has an impact on the stability of the E-cadherin junction (Liwosz et al., 2006; Zhao et al., 2008). Moreover, I found that hypo-*N*-glycosylation regulates E-cadherin dynamics and cell-cell tension. However, it is unclear why *N*-glycosylation was so important for E-cadherin dynamics. Because E-cadherin interacts with the cadherin-catenin complex and is physically linked to F-actin via α-catenin, I used a Co-IP experiment to look at the cadherin-catenin complex in E-cadherin *N*-glycosylation mutants. The standard protocol from (Oda et al., 1994) was used.

3.3.1 Increase mobility of hypoglycosylated E-cad depends on actomyosin contractility

The E-cadherin cytoplasmic domain binds to p120-catenin directly, p120-catenin interacts with β-actin, and β-actin binds to α-catenin, which then recruits vinculin, binds to F-actin, and finally links the cadherin-catenin complex to the actin cytoskeleton (Abe and Takeichi, 2008). Myosin II promotes actin organization and junctional tension (Harrison et al., 2011; Wu et al., 2015). Therefore, I wanted to know the reason for the phenotypes observed. Myosin II is a nice candidate. Deqing then injected Y-compound into *xit* embryos at stage 7. Y-compound activates myosin II. Water was injected into *xit* embryos as an additional control. We discovered that the E-cadherin mobility was reduced in the *xit* with 2 mM of Y-compound compared to the *xit* with water (**Figure 3.20**). The injection procedure had no significant effects on E-cadherin dynamics since there was no detectable difference in *xit* and *xit* injected with water (**Figure 3.20**). The mobility fraction was considerably lower in *xit* embryos when 2 mM of Y-compound was injected than in *xit* embryos. In conclusion, *xit* affects the actomyosin network within adhesion complexes.
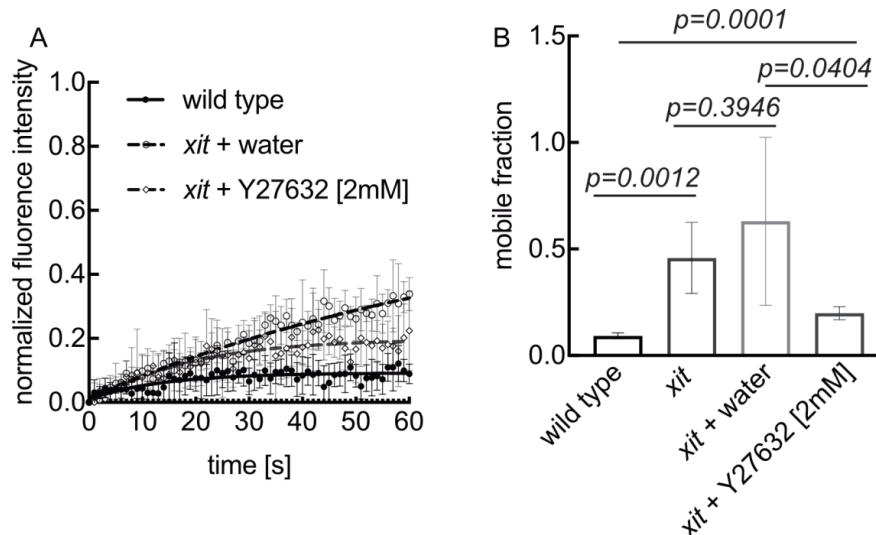
Figure 3.20: *xit* affects the interactions of actin-myosin within adhesion complexes.
(A) Normalized fluorescence intensity of FRAP experiments in wild type, *xit* injected with water and 2 mM of Y-compound. (B) E-cadherin mobile fraction in wild type, *xit*, and *xit* injected with water and 2 mM of Y-compound. This figure is kindly provided by Dr. Kong.

3.3.2 Increased association of hypoglycosylated E-cad with a-catenin

Firstly, to test the system, I performed a Co-IP experiment with E-cadherin GFP knock-in overnight embryos and GFP-trap agarose. Then, I did a western blot with an E-cad antibody and a GFP antibody designed to detect the *N* and *C*-terminal of E-cadherin, respectively. The GFP antibody can recognize the *C*-terminal of the E-cadherin protein because of the proteolytic cleavage between the amino acids 1010 and 1011 (**Figure 3.21**).
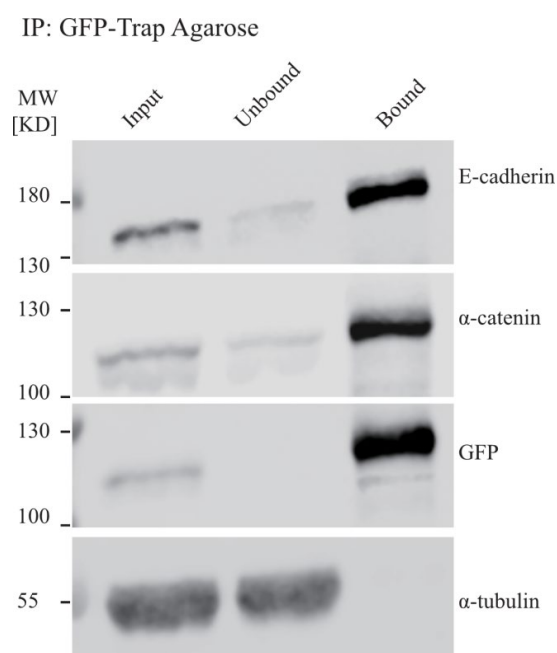
Figure 3.21: Co-IP experiments with overnight E-cadherin GFP knock-in embryos. E-cadherin, α-catenin, GFP, and α-tubulin antibodies were used for blotting.

Afterward, I generated *xit* germline clones, and three to six-hour of embryos were collected as well as E-cadherin GFP knock-in embryos. Most of the embryos are in the period of germband extension during a three to six-hour period. Later, I did the Co-IP experiment and quantified how E-cadherin and α-catenin interact (**Figure 3.21A, B, C**). Each band's integrated density and background density were measured, and the gray value was calculated by subtracting the sample's integrated density from the background density, and normalization was performed using the smallest value.

Surprisingly, E-cadherin and α-catenin interactions were enhanced at both the *N*-terminus and the *C*-terminus of E-cadherin (**Figure 3.16D, E**).
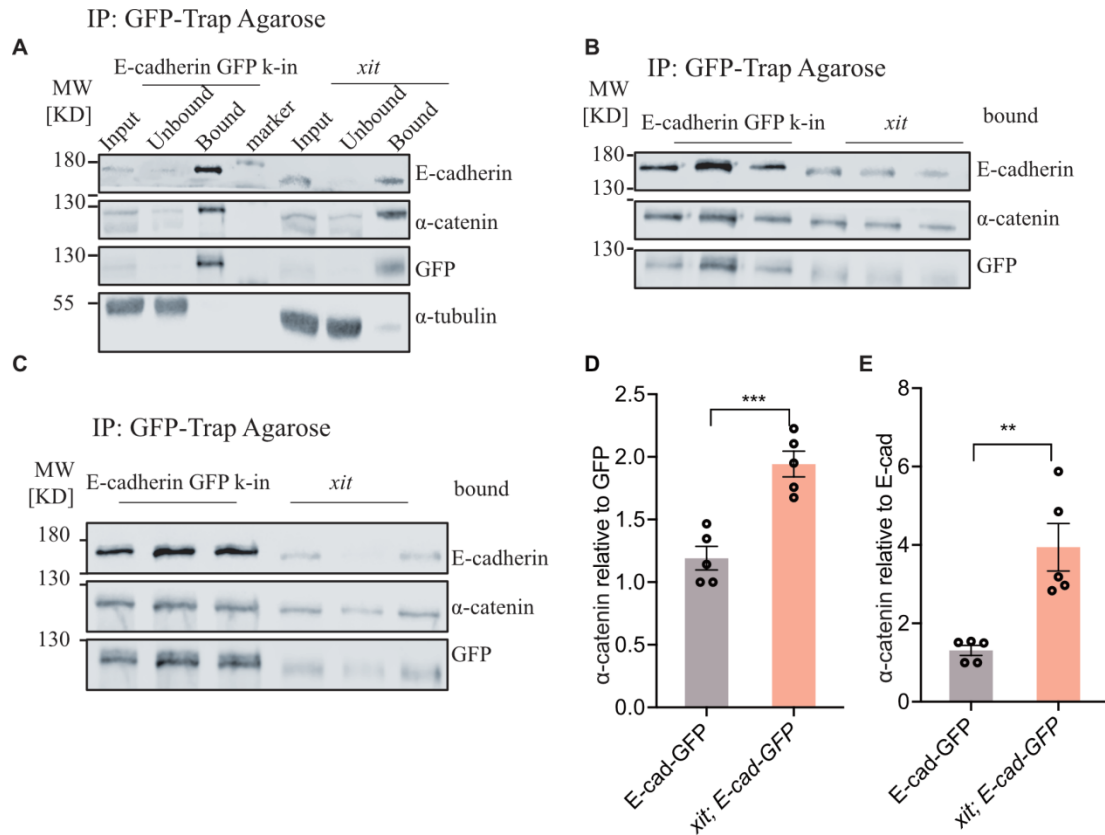
Figure 3.22: Increased E-cad-catenin complexes formation in *xit* mutants. (A) Co-IP experiment in three to six-hour embryos with GFP-trap agarose in E-cad GFP knock-in and *xit*. A western blot was performed using E-cadherin, α-catenin, and GFP antibodies. (B, C) Co-IP experiments in E-cad GFP knock-in and *xit* with 6 repeats of the bound part. (D) The relative expression level of α-catenin to GFP was quantified from panels B and C. (E) Quantification of the relative expression level of α-catenin to E-cadherin in panels B and C. Statistical significance was estimated by an unpaired t-test. ** $p \leq 0.01$, *** $p \leq 0.001$. The error bars represent the mean with SEM.
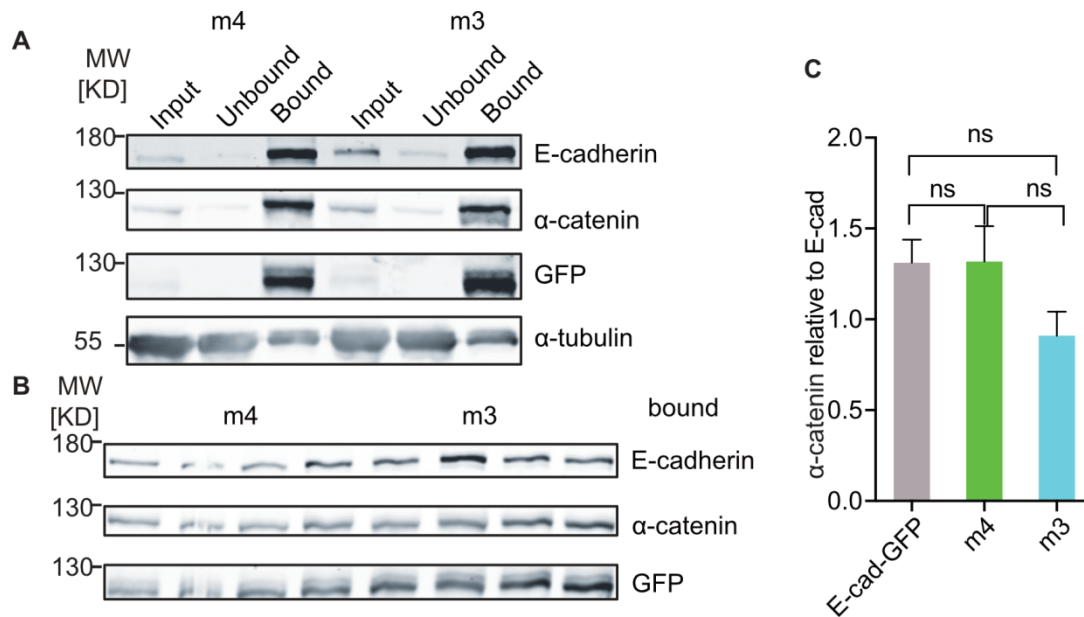
Figure 3.23: M3 and m4 do not affect E-cad-catenin complexes' formation. (A) Co-IP experiments in three to six-hour embryos with GFP-trap agarose for E-cadherin *N*-glycosylation mutants m3 and m4. A western blot was performed using E-cadherin, α-catenin, GFP, and α-tubulin antibodies. (B) Co-IP experiments with 4 repeats of the bound part in m3 and m4 lines. (C) Quantification of the relative expression level of α-catenin to E-cadherin in panel B. Statistic significance was estimated by an unpaired t-test. The error bars represent the mean with SEM. ns, p > 0.05.

Meanwhile, to check the cadherin-catenin complex formation in hypo-*N*-glycosylation mutants, I performed Co-IP experiments in m3 and m4 with three to six-hour of embryos as described before (**Figure 3.17**). However, the ratio of α-catenin to E-cadherin remains constant in m3 and m4 (**Figure 3.18**).

3.3.3 E-cad-catenin complexes in chimeric E-cad-α-catenin flies

We already know that E-cad-catenin complexes formation is significantly increased in *xit* (**Figure 3.22**). Furthermore, β-catenin linked cortical F-actin to E-cadherin by α-catenin (Liang and Gomez, 2015; Yonemura, 2011), and one β-catenin molecule could bind to one α-catenin molecule and form a 1:1 heterodimeric complex (Aberle et al., 1994). However, it is largely unknown how many α-catenin molecules could bind to the cadherin-catenin complex.
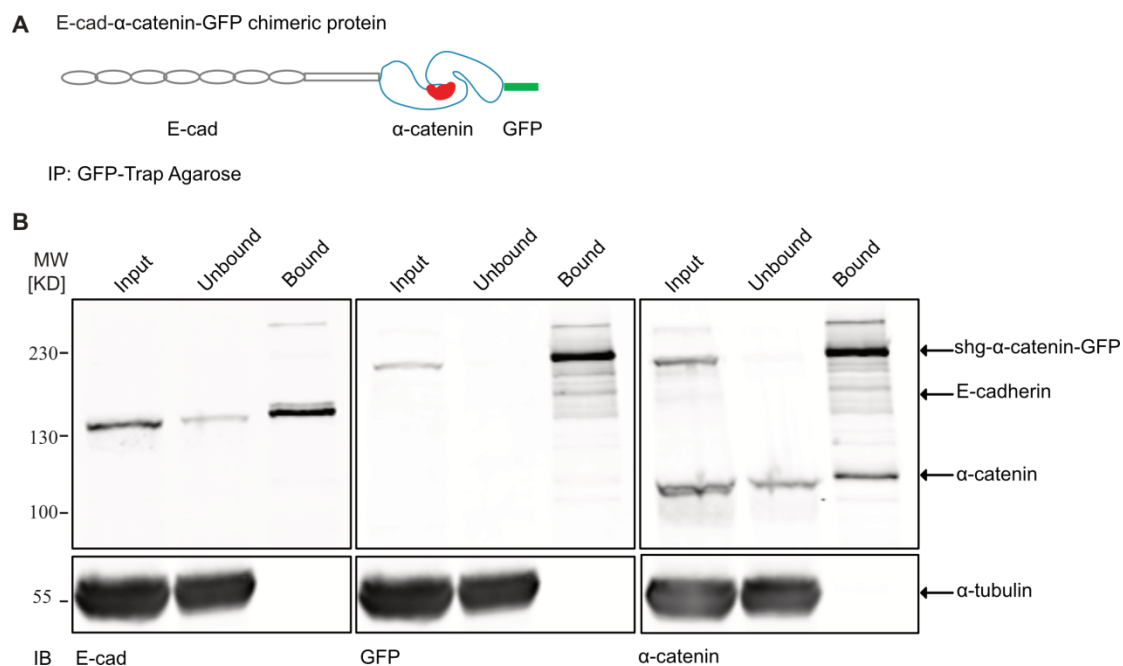
Figure 3.24: More α-catenin is recruited to the E-cad-catenin complexes in chimeric E-cad-α-catenin-GFP flies. (A) Schematic representation of E-cad-α-catenin-GFP chimeric flies. (B) A Co-IP experiment with GFP-trap agarose in three to six-hour embryos of E-cad-catenin chimeric flies. A western blot was carried out using E-cadherin, α-catenin, GFP, and α-tubulin antibodies.

I performed a Co-IP experiment with E-cad-α-catenin-GFP chimeric embryos to further investigate the molecular interactions between catenins and the E-cadherin (**Figure 3.24A**). This fly contains both GFP labeled E-cad-α-catenin and endogenous α-catenin, so I could check how many α-catenin could be recruited to the cadherin-catenin complex. I used GFP trap agarose to do the Co-IP experiment and did blotting with GFP, α-catenin, and E-cadherin antibodies. The GFP antibody could recognize the chimeric C-terminal-E-cad-α-catenin-GFP, and the α-catenin antibody could detect the endogenous α-catenin. If only GFP-tagged α-catenin is detected, it means that only one α-catenin molecule goes to the cadherin-catenin complex, and if endogenous α-catenin can also be detected, it indicates that there are more α-catenin molecules in this complex. I detected the *N*-terminal of E-cadherin when incubated with E-cadherin protein. The *C*-terminal of E-cadherin and the α-catenin fusion protein were found by GFP and α-catenin antibodies (**Figure 3.24B**). It should be noted that I

also detected endogenous α-catenin by α-catenin antibody (**Figure 3.24B**).

Taken together, more α-catenin could be recruited to the E-cad-catenin complexes, and the affinity is increased when the spatial locus is sufficient. Previous results showed that the *xit* mutant has a higher ratio of α-catenin to E-cadherin than the wild-type (**Figure 3.22**).
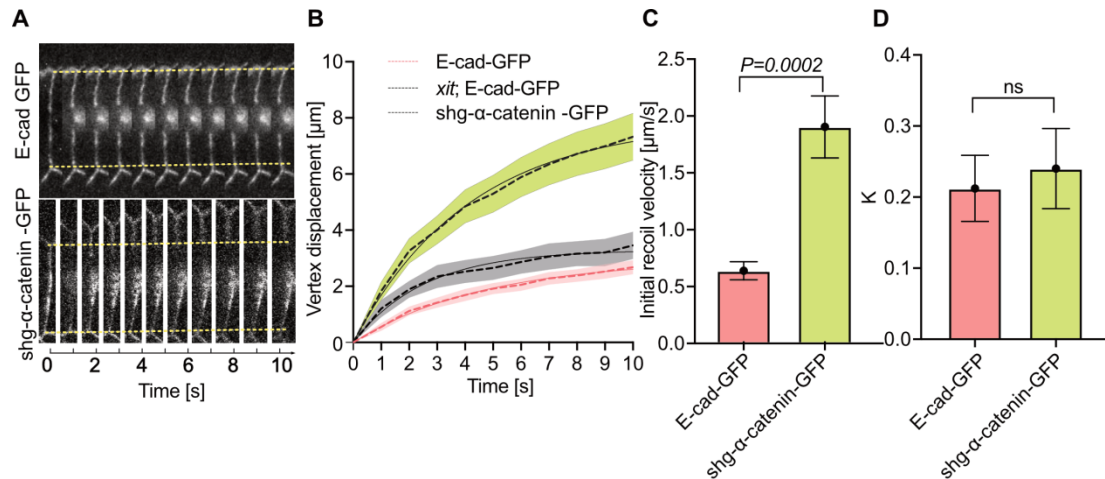
Figure 3.25: Larger initial recoil in E-cad-α-catenin GFP chimeric embryos. (A) Slices of movie stills of laser ablation experiments in WT and E-cad-α-catenin GFP chimeric amnioserosa to measure cell-cell junction tension. Vertex positions before laser ablation are shown by yellow lines. (B) Vertex displacements were measured and normalized in WT, *xit*, and E-cad-α-catenin GFP chimeric embryos. (C) Initial recoil velocities in WT and E-cad-α-catenin GFP chimeric embryos. (D) Viscoelasticity in two lines. All error bars represent SEM. E-cadherin GFP knockin, n = 15, E-cad-α-catenin-GFP, n = 17.

Furthermore, force is driven by actomyosin contractility and cell-cell adhesion (Heisenberg and Bellaïche, 2013). Actomyosin networks also play an important role in force transmission (Kong et al., 2017; Mogilner and Oster, 2003). In addition, we already know that the interaction between α-catenin and E-cadherin is increased in *xit* embryos (**Figure 3.25**). Moreover, α-catenin could bind to F-actin and link the cadherin-catenin complex to the actomyosin network. By applying the laser cutting experiment in E-cad-α-catenin-GFP chimeric amnioserosa, where the interactions between E-cadherin and α-catenin were artificially enhanced, I found a clue that when more α-catenin binds to E-cadherin, how will tension react? I found that vertex displacements and initial recoil velocities were increased in shg-α-catenin-GFP

chimeric embryos compared with wild-type and *xit* with an unchanged viscoelasticity (**Figure 3.25**), suggesting the junctional tension was increased in shg-α-catenin-GFP chimeric embryos (**Figure 3.25**), which also proves the larger recoil I observed in E-cadherin *N*-glycosylation mutants in turn.
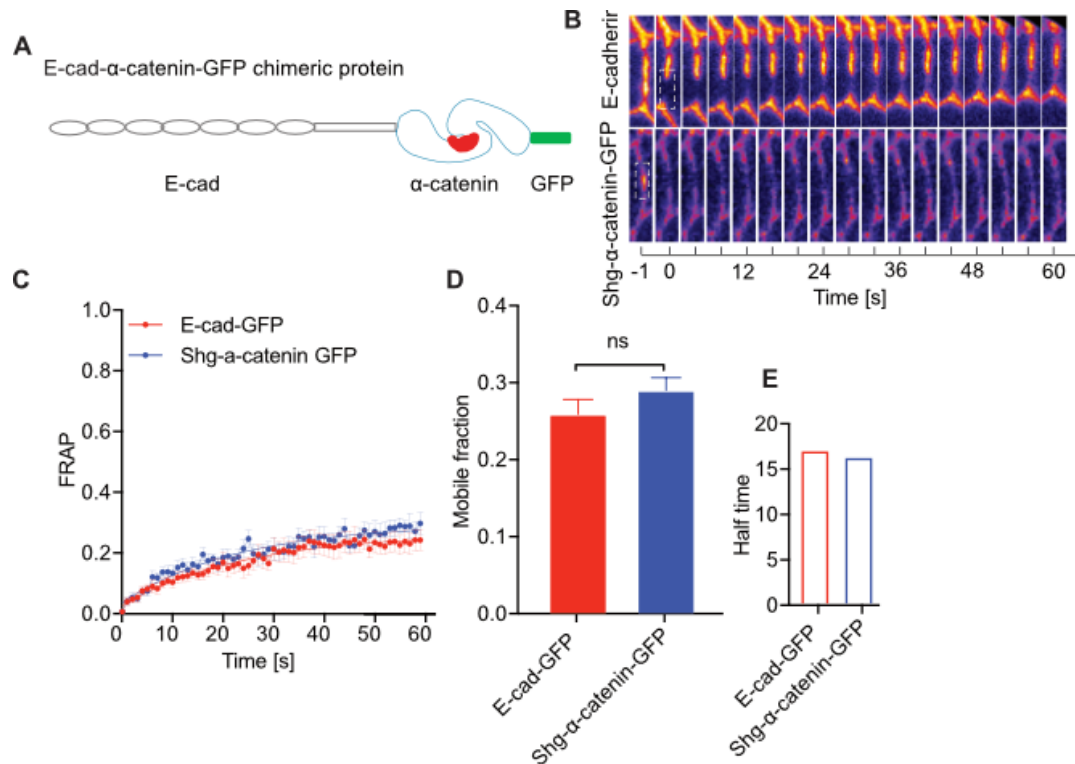
Figure 3.26: The fusion protein of E-cadherin and α-catenin alone does not change the mobility of E-cadherin. (A) Schematic representation of E-cad-α-catenin-GFP chimeric flies. (B) Kymograph of the E-cadherin FRAP experiment. The white rectangle is the region of interest, which shows the bleached E-cadherin clusters. (C) Fluorescence recovery curves for the E-cad GFP knock-in embryos at stage 8. Error bars represent the standard error of the mean (SEM) for the normalized E-cadherin intensity. A fitting curve was performed by nonlinear regression and one-phase decay in GraphPad Prism. (D) The E-cadherin mobile fraction in panel B. The error bars are the standard error of the mean (SEM) of the mobile fraction. (E) Half-time is the time when the intensity reaches half of its maximum intensity. E-cadherin GFP knockin, n = 10, E-cad-α-catenin-GFP , n = 11.

The actomyosin network regulates E-cadherin mobility (Engl et al., 2014; Quang et al., 2013). During germband extension, DE-cadherin migrates to the apical and forms stable clusters at adherens junctions (Harris and Peifer, 2004). However, I found that E-cadherin mobility increased in E-cadherin hypo-*N*-glycosylation mutants, including

xit and E-cadherin sites *N*-glycosylation mutations (**Figures 3.12, 3.13, 3.14**). And the cadherin-catenin complex formation is remarkably increased in *xit* (**Figure 3.22**). Moreover, the tension is also increased in E-cad-α-catenin GFP chimeric embryos.

So I wanted to check if this stronger cadherin-catenin interaction could have a role in the dynamics of E-cadherin afterward. Therefore, I did a FRAP experiment with E-cad-α-catenin GFP chimeric embryos at stage 7. However, I found no difference in E-cadherin dynamics during germband extension between wild-type and E-cad-α-catenin GFP chimeric embryos (**Figure 3.26B, C, D**).

The only difference between E-cadherin hypo-*N*-glycosylation mutants and E-cad-α-catenin GFP chimeric flies is the posttranslational modifications of E-cadherin. Hypo-*N*-glycosylation could cause increased E-cadherin mobilities, greater recoil, and increased cadherin-catenin complex formation. However, increased cadherin-catenin interactions alone would increase the junctional tension rather than alter the E-cadherin mobilities (**Figures 3.25 and 3.26**).

Taken together, one of the E-cadherin posttranslational modifications-*N*-glycosylation has an essential role in regulating the mobility of E-cadherin clusters.

3.4 Specificity of individual *N*-glycosylation sites

There are two principal mechanisms for the function of *N*-glycans. In the "bulk model," the number of *N*-glycans matters as long as they are distributed along the polypeptide chain. E-cad with 10 *N*-glycan will be more hydrophilic than a molecule with only three glycan moieties, irrespective of the actual Asn residues that are modified. Alternatively, in the "key model," the actual sites of *N*-glycosylation matter. Glycosylation at site A will have a different function than at site B. Beyond this, one has to consider the role of *N*-glycans in biogenesis and ER quality control. A polypeptide with nil *N*-glycans is likely to misfold and be subject to protein degradation. It may even have dominant effects by titrating the machinery.
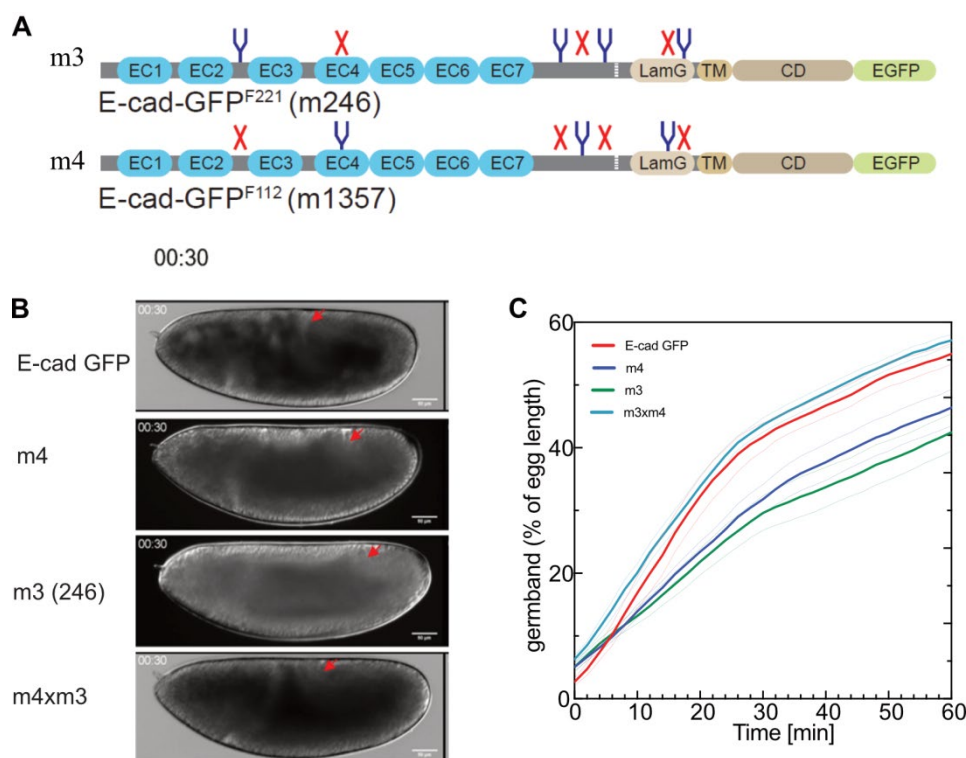
Figure 3.27: E-cadherin *N*-glycosylation mutations with site complementation show a normal germband extension. (A) Diagram of transheterozygous with specific *N*-glycosylation mutations in E-cadherin. (B) DIC images at the onset of germband extension, half an hour after germband extension of the indicated genotypes. The red arrow marks how much the germ band has extended. (C) The normalized distance between the posterior midgut invagination and the posterior pole cells. The standard error of the mean is represented by dashed lines with a 95% confidence interval. (n = 20). The DIC movies were recorded by Sandra.

We already know that E-cadherin dynamics, junctional tension, and cadherin-catenin complex formation are reliant on *N*-glycosylation (**Figures 3.11-3.13, 3.15-3.18**). However, there are 11 potential *N*-glycosylation sites in DE-cadherin (Zielinska et al., 2012). In the endoplasmic reticulum, *xit* encodes a glucosyltransferase (Zhang et al., 2014). Moreover, *xit* has multiple substrates. To confirm whether the number or the position of *N*-glycans is important for the DE-cadherin dynamics, I did a test by complementation of the different E-cadherin *N*-glucosylation mutants. The mutations of m3 and m4 carry mutations in m4, but not in m3 and vice versa, which means when crossed together, the embryos have seven normal E-cadherin *N*-glycosylation sites and seven mutated E-cadherin *N*-glycosylation sites. Then I
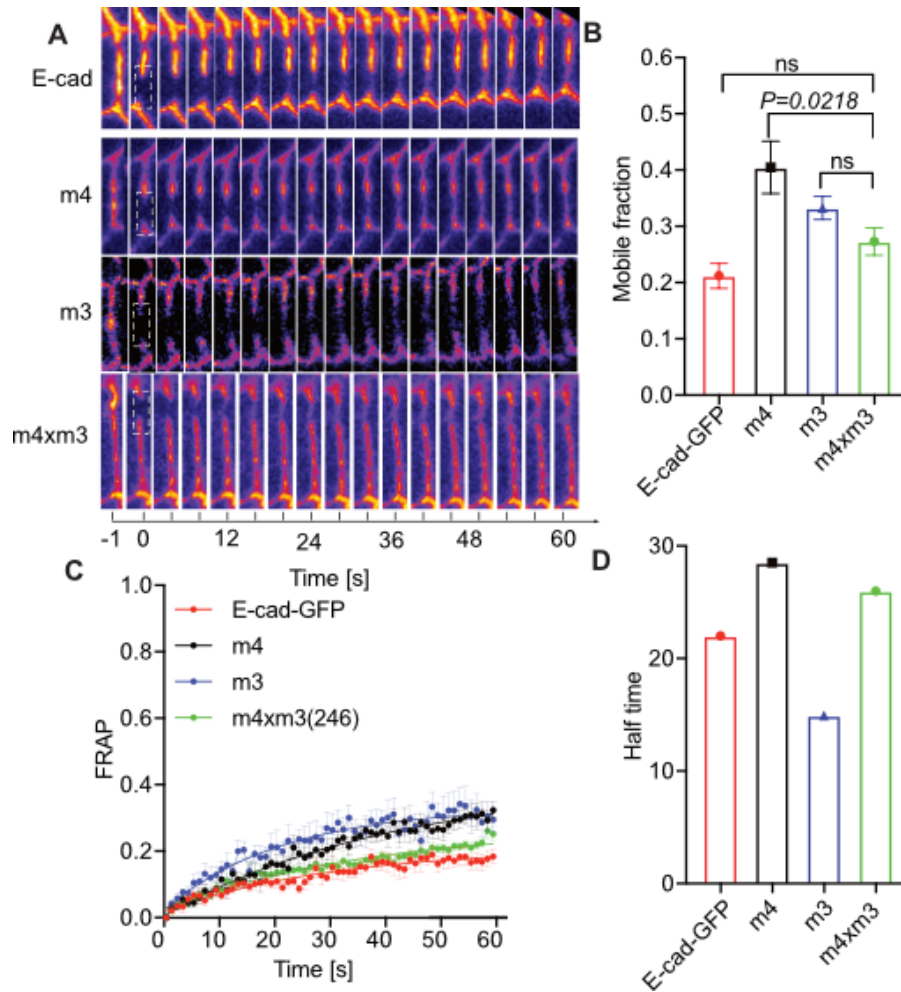
Figure 3.28: E-cad mobility is rescued in transheterozygous E-cadherin *N*-glycosylation mutants. M3 and m4 mutants were crossed together, and virgins of m3/m4 were crossed with males of m3 (m4/m3). (A) Kymograph of E-cadherin after the FRAP experiment spanning one minute during stage 7. The white rectangle is the region of interest, which shows the bleached E-cadherin clusters. (B) Mobile fraction of E-cadherin in panel A. Error bars represent the standard error of the mean (SEM) of the mobile fraction. (C) E-cadherin GFP fluorescence recovery curves in E-cad GFP knockin and m3, m4, and m3/m4. A fitting curve was performed by nonlinear regression and one-phase decay in GraphPad Prism. Error bars represent the standard error of the mean (SEM) for the normalized E-cadherin intensity. (D) Half-time is the time when the intensity reaches half of its maximum intensity. Statistical significance was estimated by an unpaired t-test. E-cadherin GFP knockin, n = 7, m3, n = 8, m4, n = 7, m4/m3, n = 8.

crossed the virgins of m3/m4 with males of m3 and recorded the DIC movies, FRAP, and laser ablation experiments with the offspring. So the maternal is m3/m4 in all the embryos. To my surprise, when crossing them together, the impaired germband extension in m3 and m4 was completely rescued instead of a pronounced slowing down

in germband extension (**Figure 3.27**). This suggests that *N*-glycans may have a position-dependent rather than a number-specific role in the E-cadherin complexes formation, as there would have been a significant delay in germband extension in m3/m4 transheterozygous.
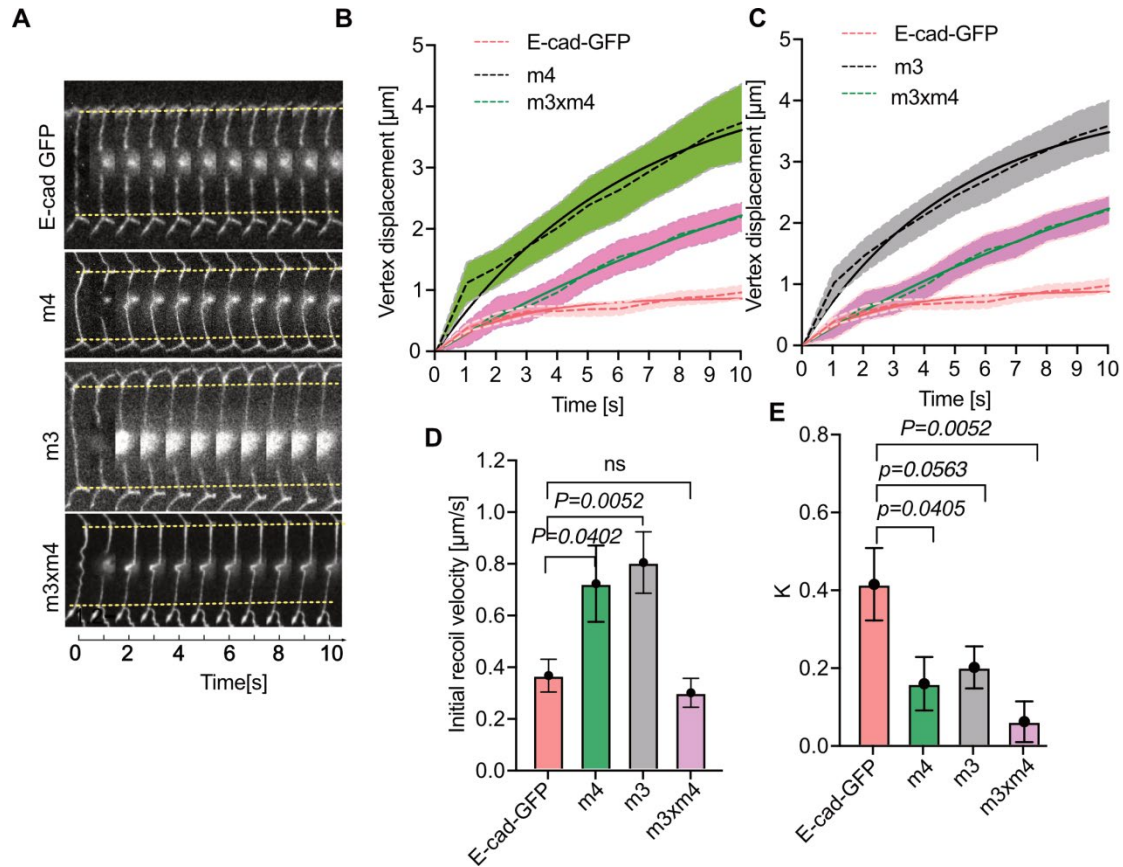
Figure 3.29: Junctional initial recoil is partially rescued in transheterozygous E-cadherin *N*-glycosylation mutants. (A) Slices of movie stills from a laser ablation experiment measuring cell-cell junction tension before and 10 seconds after ablation in E-cadherin GFP knock-in (WT), m4, and m4/m3(246) amnioserosa. Vertex positions before laser ablation are shown by yellow lines. (B) Vertex displacements in WT, m4, m3, and m4/m3(246) were measured and normalized. (C) Initial recoil velocities were calculated based on vertex displacement and time in WT and mutants. (D) WT and mutant viscoelasticity. The error bars represent the mean with an SEM. Statistical significance was estimated by an unpaired t-test. E-cadherin GFP knockin, n = 10, m3, n = 11, m4, n = 10, m4/m3, n = 9.

To confirm the *N*-glycan position-dependent function in regulating E-cadherin dynamics, I did a FRAP experiment with m3/m4 transheterozygous at stage 7. And I found the mobile fraction of m3/m4 transheterozygous was decreased compared to

m4 and m3 mutants (**Figure 3.28A, B, C**). However, the mobile fraction did not show a considerable difference in m3 and m3/m4 transheterozygous embryos (**Figure 3.28B**). This suggests that *N*-glycans may have a number-dependent role in E-cadherin dynamics. In addition, there was no difference between E-cadherin GFP knock-in and m3/m4 transheterozygous embryos (**Figure 3.28B**). This further suggests that *N*-glycans have a position-specific role in E-cadherin dynamics.

To further investigate the position-dependent role of E-cadherin *N*-glycosylation in junctional recoil, I did a laser-cutting experiment with m3/m4 transheterozygous in amnioserosa. I found that m3/m4 transheterozygotes have significantly less vertex displacement than m3 and m4 (**Figures 3.29A, B, C**). The initial recoil velocity was dramatically reduced in m3/m4 transheterozygous compared with m3 and m4 (**Figures 3.29A, D**). The initial recoil velocity is 0.36 μm/s in the E-cadherin GFP knock-in, 0.72 μm/s in m4, 0.80 μm/s in m3, and 0.29 μm/s in m3/m4 (**Figure 3.29**). This suggests that *N*-glycans may have a position-specific role in E-cadherin-mediated tension. In addition, I did not find any remarkable difference in initial recoil velocity among wild type and m3/m4 transheterozygous (**Figure 3.29D**). Taken together, *N*-glycans may have a position-specific role and may also have a number-specific effect in cadherin-catenin complex formation (**Figures 3.27, 3.28, and 3.29**).

To further explore the site-specific role of *N*-glycans in the cadherin-catenin complex formation, I repeated the same experiments that were done in m3 (246)/m4. Firstly, I checked the germband extension in m3 (147)/m4 mutants. I crossed m3 (147) and m4 together and collected virgins of m3 (147)/m4, then I crossed them with males of m4. Therefore, the maternal genotype in all offspring is m3 (147)/m4. This fly contains 7 E-cadherin *N*-glycosylation site mutations like m3 (246)/m4, but the difference is that some of the sites in site mutations are identical in m3 (147) and m4 (1357).

Afterward, I recorded DIC movies and quantified how much the germband had extended in m3 (147)/m4 mutants (**Figure 3.30**). In contrast to what we observed in

m3 (246) /m4 (**Figure 3.27**), the germband extension did not rescue in m3 (147)/m4 mutants, and it was more like m4 in one hour after germband extension, which reached only 42% of full embryo length (**Figure 3.30**). But it is faster than the m4 by half an hour after the germband extension (**Figure 3.30**).

At the same time, to check the mobility of E-cadherin, I performed the FRAP experiment in m3 (147)/m4 embryos. To my surprise, there was no significant difference in the E-cadherin mobile fraction in m3 (147)/m4 mutants and m4 (**Figure 3.31**). However, they both increased compared to E-cadherin GFP knock-in embryos (**Figure 3.31**). During germband extension, the E-cadherin mobile fraction is 25% in E-cadherin GFP knock-in, 40% in m4, and 27% in m3 (147)/m4 mutants (**Figure 3.31**).
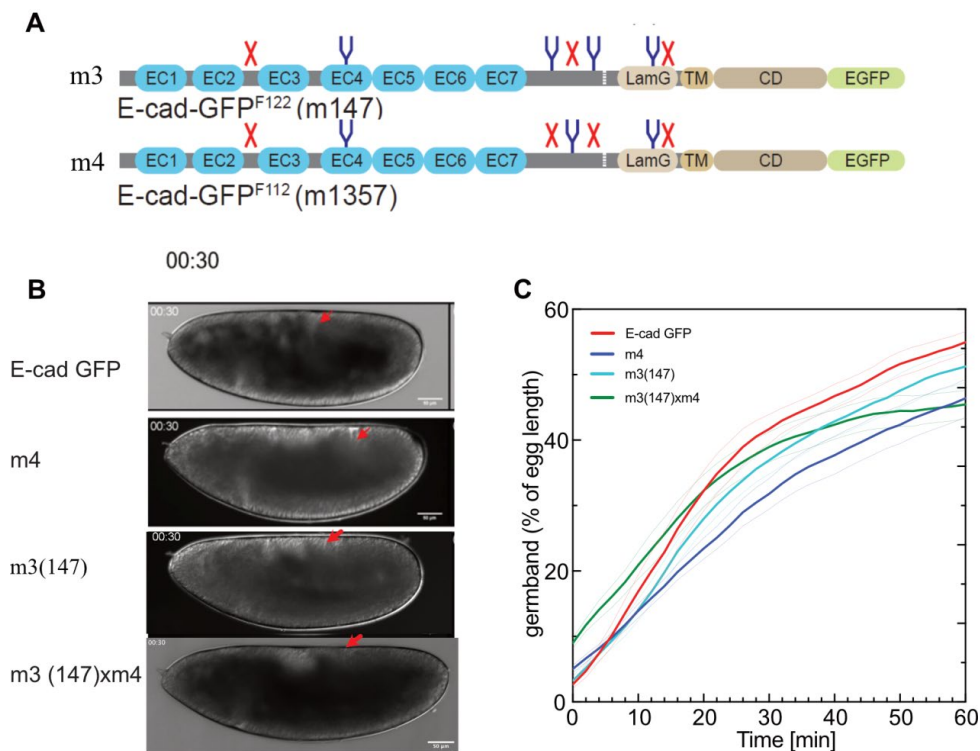
Figure 3.30: Impaired germband extension in m3 (147)/m4 mutants. (A) Scheme of m3 (147)/m4 flies with specific *N*-glycosylation site mutations. (B) DIC images at the onset of germband extension, half an hour after germband extension of the indicated genotypes. The red arrow marks how much the germ band has extended. (C) The normalized distance between the posterior midgut invagination and the posterior pole cells. The standard error of the mean is represented by dashed lines with a 95% confidence interval. n = 18 (m3 (147) x m4), n = 20 (others). The DIC movies (E-cadherin GFP, m4, and m3) were recorded by Sandra.
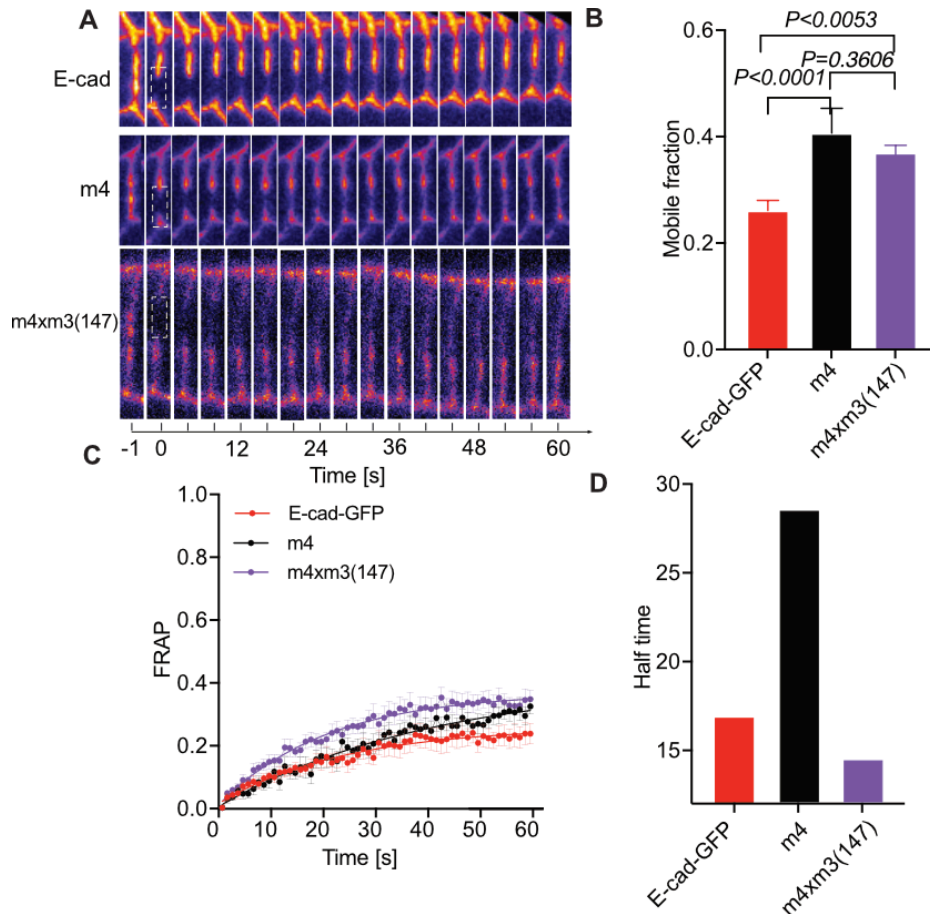
Figure 3.31: Increased E-cadherin mobile fraction in m3 (147)/m4 mutants compared with E-cadherin GFP knock-in embryos. M3(147) and m4 mutants were crossed together, and virgins of m3/m4 were crossed with males of m3 (m4/m3(147)). (A) Kymograph of E-cadherin after the FRAP experiment spanning one minute during stage 7. The white rectangle is the region of interest, which shows the bleached E-cadherin clusters. (B) Mobile fraction of E-cadherin in panel A. Error bars represent the standard error of the mean (SEM) of the mobile fraction. (C) E-cadherin GFP fluorescence recovery curves in E-cad GFP knockin and m4 and m4/m3(147). A fitting curve was performed by nonlinear regression and one-phase decay in GraphPad Prism. Error bars represent the standard error of the mean (SEM) for the normalized E-cadherin intensity. (D) Half-time is the time when the intensity reaches half of its maximum intensity. Statistical significance was estimated by an unpaired t-test. E-cadherin GFP knockin, n = 10, m4, n = 7, m4/m3, n = 12.

We already know that *N*-glycans may have a position-specific role in cadherin-catenin complex formation (**Figures 3.27, 3.28, and 3.29**).To look further into the position-specific role of *N*-glycan in the E-cadherin-mediated junctional tension during germband extension, I did a laser-cutting experiment with m3 (147)/m4 mutants and m4 embryos during germband extension. Consistent with FRAP results,

the vertex displacement has no noticeable difference among m3 (147)/m4 mutants and m4 (**Figure 3.32**) but rather increases compared to m4 and E-cadherin GFP knock-in embryos (**Figure 3.32**). The initial recoil velocity is 0.36 μm/s in the E-cadherin GFP knock-in, 0.72 μm/s in m4, but 0.84 μm/s in m3 (147)/m4 (**Figure 3.32**). However, there is no significant difference between E-cadherin GFP knock-in embryos and m3 (147)/m4 mutants (**Figure 3.32**).
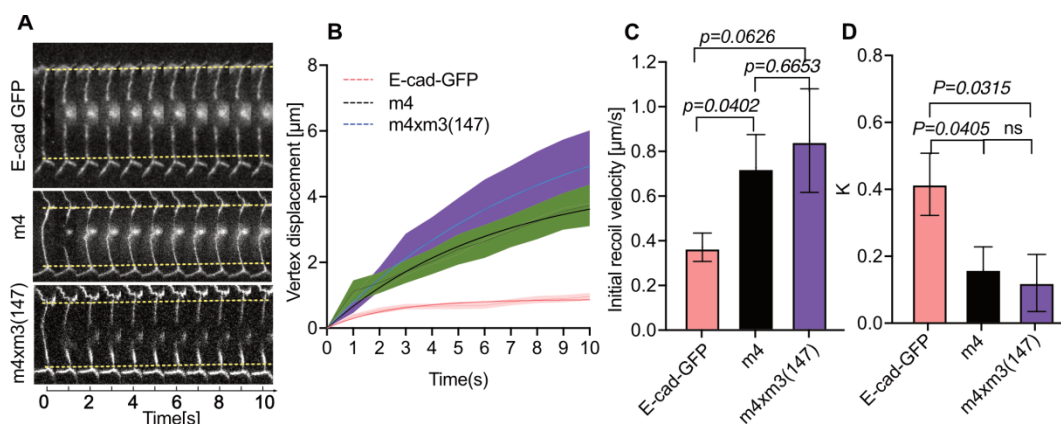
Figure 3.32: Larger E-cadherin junctional initial recoil in m3 (147)/m4 mutants compared with E-cadherin GFP knock-in embryos. (A) Slices of movie stills from a laser ablation experiment measuring cell-cell junction tension before and 10 seconds after ablation in E-cadherin GFP knock-in (WT), m4 and m4/m3(147) amnioserosa. Vertex positions before laser ablation are shown by yellow lines. (B) Vertex displacements in WT, m4, and m4/m3(147) were measured and normalized. (C) Initial recoil velocities were calculated based on vertex displacement and time in WT and mutants. (D) WT and mutant viscoelasticity. The error bars represent the mean with an SEM. Statistical significance was estimated by an unpaired t-test. E-cadherin GFP knockin, n = 10, m4, n = 10, m4/m3, n = 10.

Taken together, *N*-glycans have a position-specific role in cadherin-catenin complex formation (**Figures 3.27-3.32**).

4. Results-2

4.1 Developmental control of E-cadherin during germband extension

4.1.1 E-cad expression in *Drosophila* embryos

Germband extension is a vital morphological process in development. During this process, DE-cadherin plays an essential role (Halbleib and Nelson, 2006) by interacting with an actin filament and myosin II (Bertet et al., 2004). DE-cadherin is also crucial for apicobasal polarity, for which it moves to the apical domain and forms adherens junctions during germband extension (Harris and Peifer, 2004). Furthermore, during tissue morphogenesis, E-cadherin produces clusters that transfer tension and support adhesions (Harris and Peifer, 2004; Quang et al., 2013; Zhu et al., 2003). However, germband extension is a very fast process, which lasts about 1.5 hours in *Drosophila*. The number of E-cadherin increases by about 50% during gastrulation in *Drosophila* embryos by the quantitative imaging system (Quang et al., 2013) (from stage 7b to stage 9). Why does E-cadherin, despite its numbers sharply increasing over a short period, play such a significant role in tissue morphogenesis? To investigate the developmental control role of E-cadherin during germband extension, I first checked the E-cadherin protein level during the onset of gastrulation (stage 6) and germband extension (stage 8) by live image and western blot in E-cadherin GFP knock-in embryos. Via live imaging, I found the intensity of E-cadherin sharply increased from the onset of gastrulation to germband extension (**Figures 4.1B, C, D**). In parallel, I did a western blot using staged 5, 6, and 8 OrR embryos and I found the E-cadherin total protein level increased from cellularization to gastrulation (**Figures 4.1E, F**). Taken together, there is a significant increase in E-cadherin protein levels during germband extension (**Figure 4.1**).

59
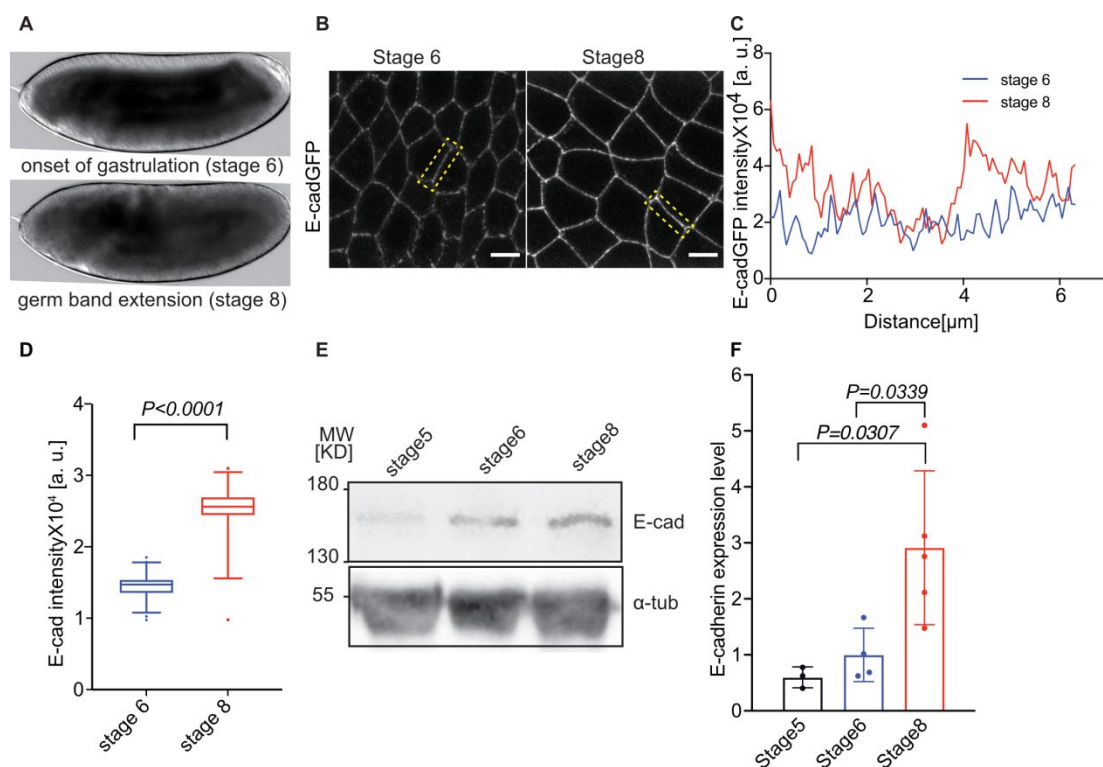
Figure 4.1: The E-cadherin intensity increases during germband extension. (A) DIC images of *Drosophila* embryos at stage 6 and stage 8. (B) Live confocal images of E-cad GFP knock-in embryos at the onset of gastrulation and germband extension. (C) Plot profile of a single junction in panel B showing the E-cadherin gray value in staged *Drosophila* embryos. (D) Mean E-cadherin intensity across all junctions (n = 5). (E) Western blot of OrR embryos during cellularization, the onset of gastrulation, and germband extension. (F) Quantification of panel E. (stage5, n = 3, stage 6, n = 4, stage 8, n = 5.) The error bars represent the mean with a 95% confidence interval.

Following that, I wanted to know if E-cadherin protein expression is caused by an increase in mRNA levels, so I carried out an RT-PCR to examine the mRNA expression of staged embryos. However, I found no significant elevation of E-cadherin mRNA (**Figure 4.2**). Therefore, I would like to find the reason for the upregulation of the E-cadherin protein.
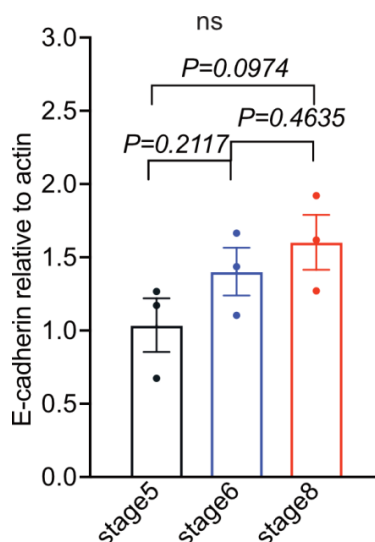
Figure 4 2: The E-cad mRNA level does not significantly change during cellularization and gastrulation in OrR *Drosophila* embryos. Q-PCR analysis of E-cadherin mRNA levels in staged *Drosophila* embryos (n = 3). Statistical significance was estimated by an unpaired t-test.

4.1.2 Decreased mobile fraction of E-cad during junction maturation

Stabilization of adhesions requires the immobilization of E-cadherin clusters (Cavey and Lecuit, 2009). Also, clustered E-cadherin is more stable than unclustered E-cadherin (Cavey et al., 2008). So to test the dynamics of E-cadherin, I carried out a FRAP experiment in E-cadherin clusters at the onset of gastrulation (stage 6) and germband extension (stage 8) (**Figure 4.3**). And I found the E-cadherin mobile fraction is significantly reduced by 40% from early to late germband extension (**Figures 4.3B and C**). In stage 8 embryos, the recovery of the normalized E-cadherin fluorescence is much faster compared with stage 6 (**Figure 4.3A**). This suggests that E-cadherin may have a developmental control role in E-cadherin maturation. And then I want to investigate the potential regulators of E-cadherin maturation during germband extension.
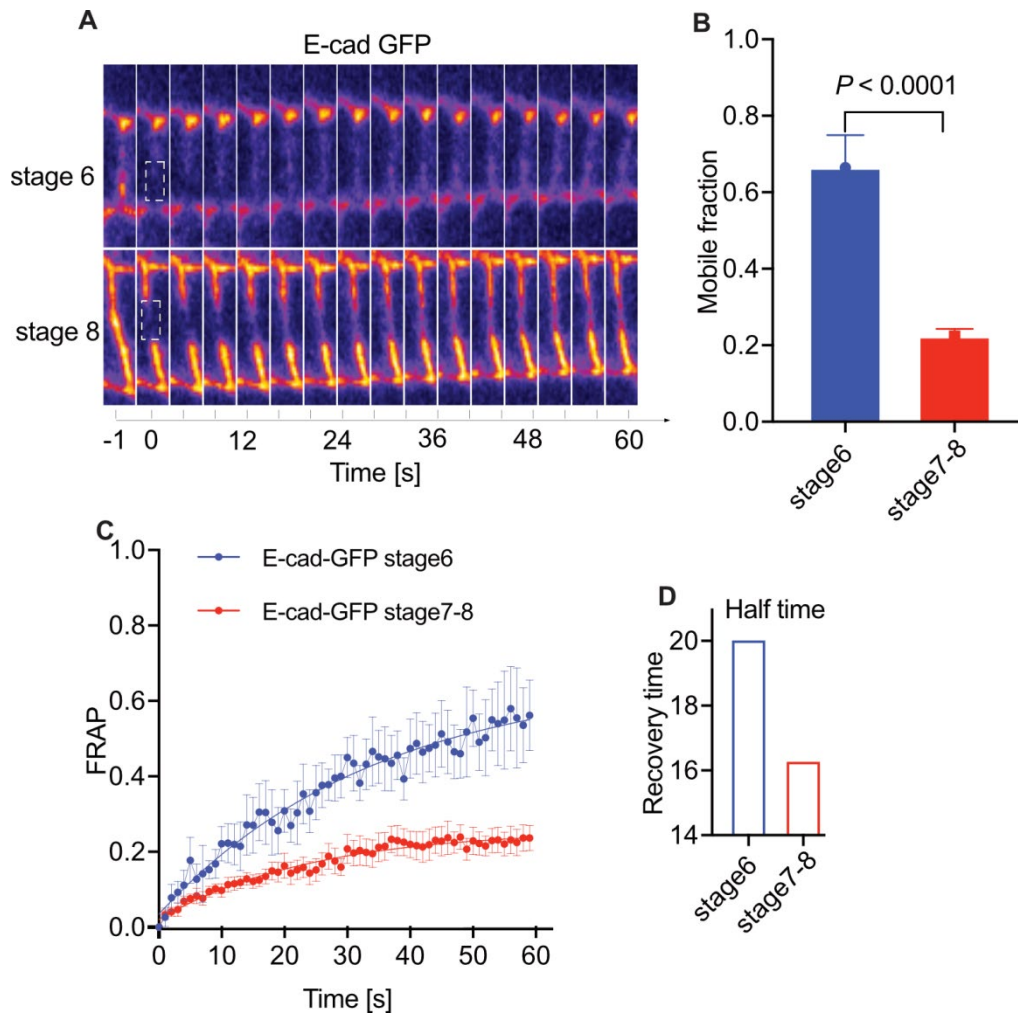
Figure 4.3: The E-cadherin mobile fraction is significantly decreased during gastrulation in E-cad GFP knock-in embryos. (A) E-cadherin kymograph before and after the FRAP experiment spanning one minute. The white rectangle is the region of interest, which shows the bleached E-cadherin clusters. (B) The E-cadherin mobile fraction is shown in figure A. Error bars represent the standard error of the mean (SEM) of the mobile fraction. (C) Fluorescence recovery curves for the E-cad GFP knock-in embryos at stage 6 (n = 6) and stage 8 (n = 10). A fitting curve was performed by nonlinear regression and one-phase decay in GraphPad Prism. Error bars represent the standard error of the mean (SEM) for the normalized E-cadherin intensity. (D) Recovery time is the time when the intensity reaches half the maximum intensity. Statistical significance was estimated by an unpaired t-test.

4.2 Role of RhoGEF2 in E-cad dynamics and junction maturation

Gerband extension is driven by cell intercalation and cell rearrangements (Bertet et al., 2004; Irvine and Wieschaus, 1994; Rice and Garen, 1975). Cell shape changes

require a reconstruction of the actin cytoskeleton and cell cortex, which is dependent on the Rho family of GTPases (Etienne-Manneville and Hall, 2002; Großhans et al., 2005; Hanna and El-Sibai, 2013; Kardash et al., 2010; Schmidt and Grosshans, 2018). In addition, Rho activates formin, promotes the polymerization of unbranched actin, and mediates myosin contractility (Collinet and Lecuit, 2013). Moreover, RhoGEF2 (guanyl-nucleotide exchange factor) and Rho1 play an important role in *Drosophila* gastrulation. Therefore, I proposed that Rho GEF2 may have a pivotal role in controlling E-cadherin dynamics to a large degree. Therefore, I did a western blot to check the E-cadherin protein level in various Rho mutants. I crossed the virgins of mat-gal 67-15 with males of constitutively activated Rho1 balanced with Cyo (Rho1-v14 (CA)/Cyo) or dominant-negative Rho1 balanced with TM6B (Rho1-N19 (DN)/TM6B). I found the E-cadherin total protein level does not change in both cases. Following that, Rho GFF2 germline clones were generated, and the total E-cadherin protein level remained unchanged (**Figure 4.4**).
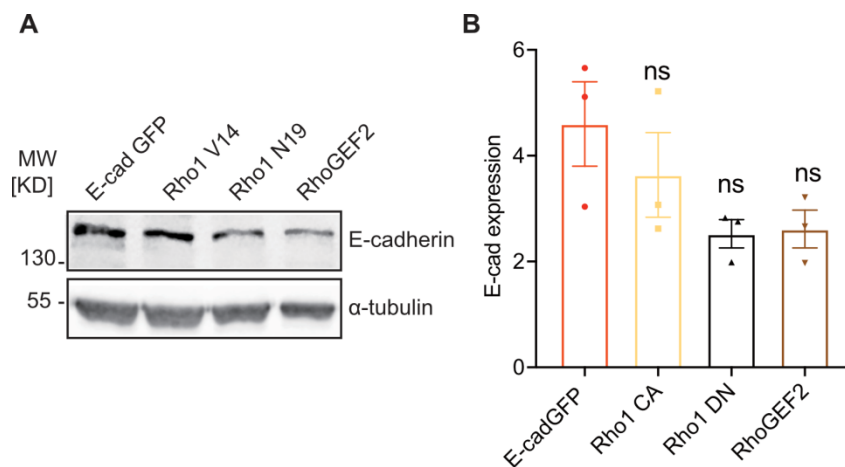
Figure 4.4: Rho1 does not regulate the E-cadherin expression level. (A) WB. The mat-gal 67-15 females were crossed with the males of Rho1-v14 (CA)/Cyo and Rho1-N19 (DN)/TM6B. RhoGEF2 germline clones were generated. Embryos aged 3 to 6 hours were collected. (B) Quantification of A (n = 3). ns, $p > 0.05$. Statistical significance was estimated by an unpaired t-test.

4.2.1 RhoGEF2 regulates myosin II activation

Myosin II contractility controls cell shape change and cell intercalation during germband extension (Bertet et al., 2004; Rozbicki et al., 2015). Also, Rho1 activates

myosin II during tissue morphogenesis (Kerridge et al., 2016). However, there is no report to check the total myosin II protein level *in vivo*. To check this, I did a western blot with Rho1 CA, Rho1 DN, and Rho GEF2 for 3 to 6-hour embryos as described before. I found that total myosin II levels are significantly decreased in Rho1 DN and Rho GEF2 in 3 to 6-hour embryos (**Figure 4.5**). Surprisingly, myosin II also decreased in Rho1-constitutively-active embryos (**Figure 4.5**).
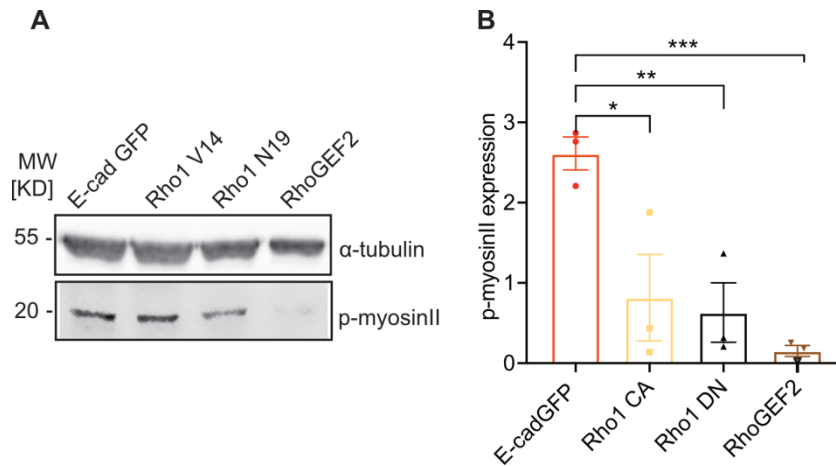
Figure 4.5: Rho1 regulates p-myosin II expression levels. (A) WB. The mat-gal 67-15 females were crossed with the males of Rho1-v14 (CA)/Cyo and Rho1-N19 (DN)/TM6B. RhoGEF2 germline clones were generated. Embryos aged 3 to 6 hours were collected. (B) Panel A quantification (n = 3). Statistical significance was estimated by an unpaired t-test. *, $p < 0.05$, **, $p < 0.01$, ***, $p < 0.001$.

4.2.2 Junctional E-cadherin intensity is decreased in RhoGEF2 mutants

Later, I stained RhoGEF2 germline clones for E-cadherin and discovered that activated E-cadherin was significantly lower in RhoGEF2 germline clones compared to controls (**Figure 4.6**), which is consistent with the previous report (Kerridge et al., 2016). Taken together, I found that RhoGEF2 regulates the myosin II total protein level and junctional E-cadherin.
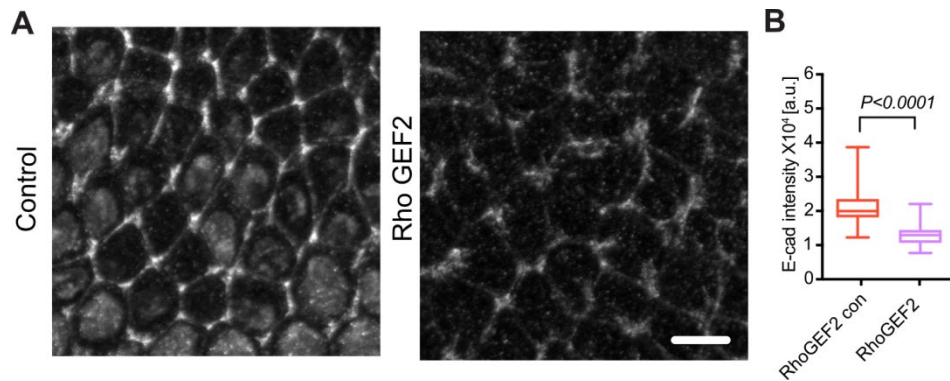
Figure 4.6: Junctional E-cadherin intensity is decreased in *RhoGEF2* mutants during germband extension. (A) E-cad GFP was stained with a GFP booster. Histone-GFP and Rho GEF2 were stained in one tube. RhoGEF2 con (n = 3), RhoGEF2 (n = 3). scale bar 5 μm. A maximum intensity projection (MIP) was used. Statistical significance was estimated by an unpaired t-test.

4.2.3 E-cadherin cluster dynamics are RhoGEF2 dependent

To investigate RhoGEF2's function in E-cadherin-mediated adhesion maturation further, I performed a FRAP experiment in staged RhoGEF2 Ubi-E-cad GFP embryos (control) and RhoGEF2 germline clones. Because E-cadherin is overexpressed in RhoGEF2 Ubi-E-cad GFP embryos, first I checked the E-cadherin dynamics pattern in RhoGEF2 Ubi-E-cad GFP control embryos. I found the E-cadherin mobile fraction was decreased from the onset of gastrulation to germband extension (Figure 4.7), like that in the E-cadherin GFP knock-in embryos (Figure 4.3). However, the relative mobile fraction is higher in this control compared to the wild-type (**Figures 4.3, 4.7**). At stage 6, the E-cadherin mobile fraction is around 50% in E-cadherin GFP knock-in embryos but 60% in RhoGEF2 Ubi-E-cad GFP control embryos (**Figures 4.3 and 4.7**). At stage 8, the mobile fraction is 20% and 50%, respectively. (**Figures 4.3 and 4.7**). From the kymograph of E-cadherin after the FRAP experiment, we see that the E-cadherin recovered slower in RhoGEF2 Ubi-E-cad GFP control embryos compared to E-cadherin GFP knock-in embryos (**Figures 4.3, 4.7**). However, the pattern is indeed the same; the E-cadherin clusters become more stable at stage 8. Therefore, we can use this fly to investigate the role of RhoGEF2 in E-cadherin dynamics.
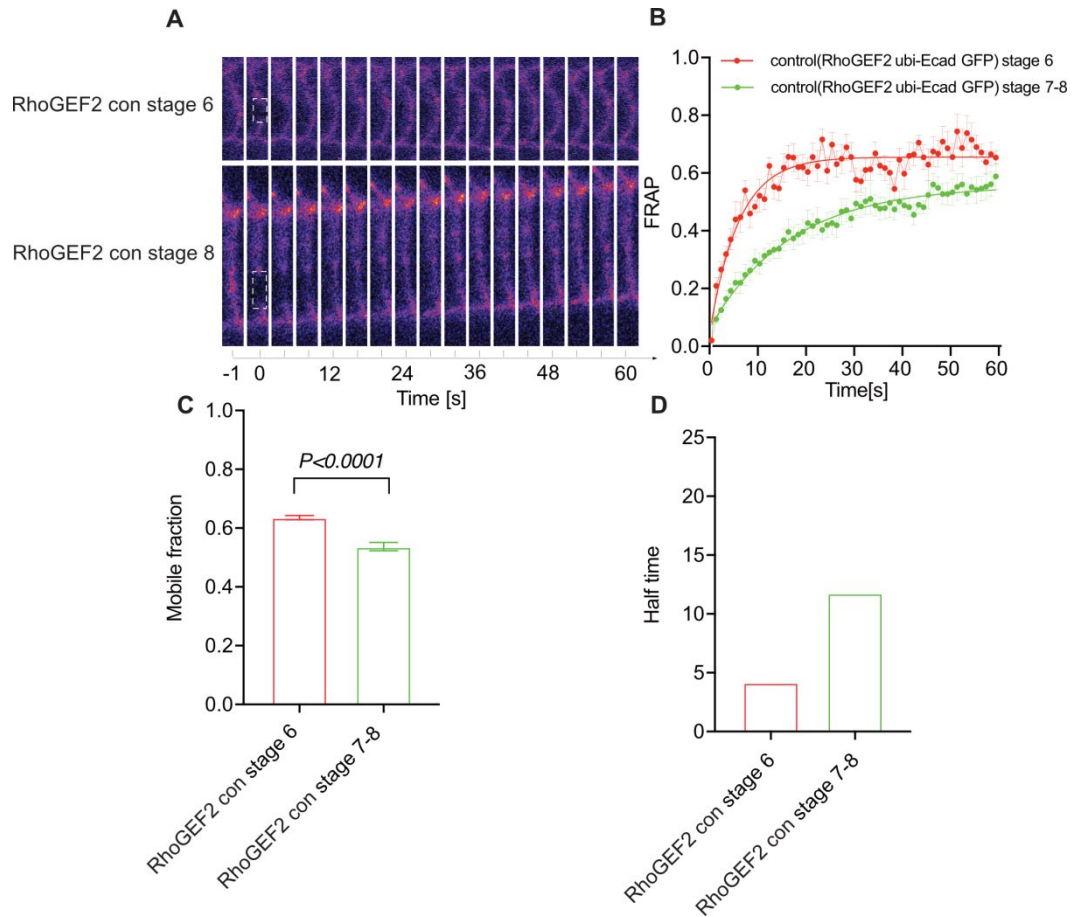
Figure 4.7: The E-cadherin mobile fraction is decreased during gastrulation in *RhoGEF2* control embryos. (A) E-cadherin kymograph before and after the FRAP experiment spanning one minute. The white rectangle is the region of interest, which shows the bleached E-cadherin clusters. (B) Fluorescence recovery curves for Rho GEF2 control embryos at stage 6 (n = 9) and stage 8 (n = 11). A fitting curve was performed by nonlinear regression and one-phase decay in GraphPad Prism. Error bars represent the standard error of the mean (SEM) of the normalized E-cadherin intensity. (C) The E-cadherin mobile fraction is shown in panel A. (D) Half-time is the time when the intensity can reach half of its maximum intensity. Control is Rho GEF2 Ubi-E-cad GFP.

To further illuminate the role of RhoGEF in E-cadherin dynamics, RhoGEF2 germline clones were generated in the background of Ubi-E-cad GFP. The E-cadherin cluster mobility in RhoGEF2 germline clones is increased as shown by the FRAP experiment when compared to the control (**Figure 4.8**), suggesting that RhoGEF2 regulates E-cadherin cluster dynamics.
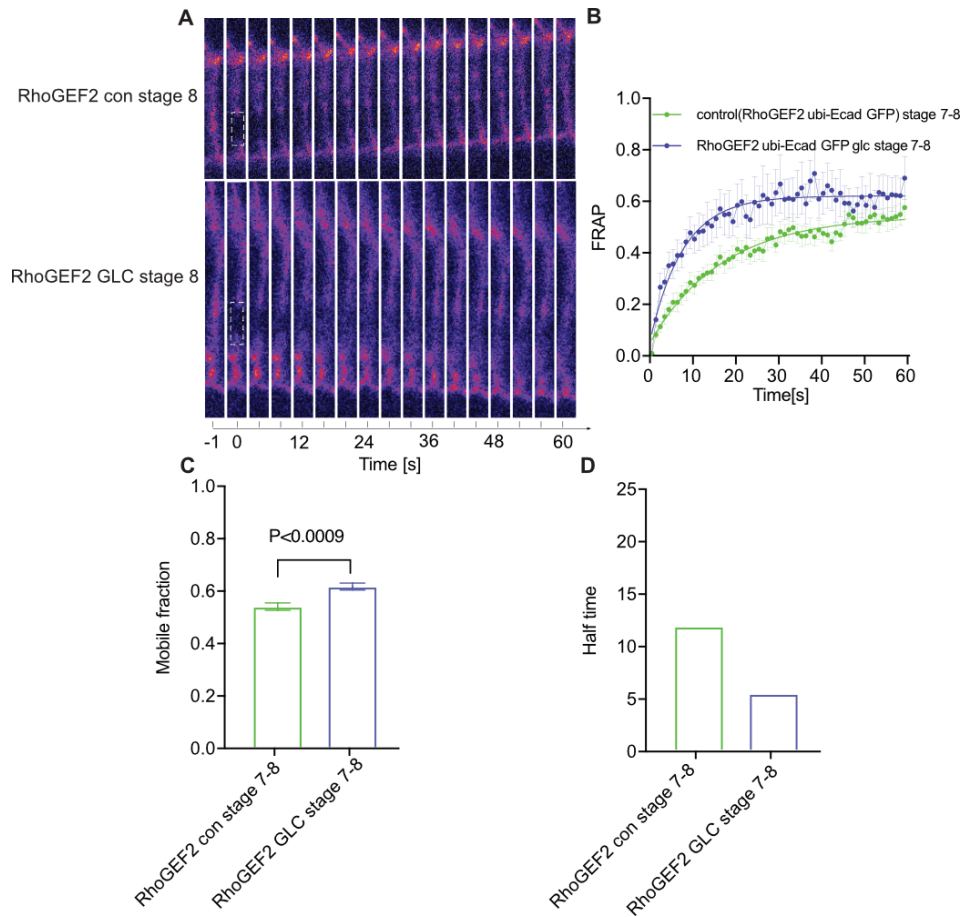
Figure 4.8: The E-cadherin mobile fraction is increased during germband extension in *RhoGEF2* GLC. (A) E-cadherin kymograph before and after the FRAP experiment spanning one minute. The white rectangle is the region of interest, which shows the bleached E-cadherin clusters. (B) Fluorescence recovery curves for stage 8 RhoGEF2 control and germline clone embryos. The error bars are the standard error of the mean (SEM) of the mobile fraction. A fitting curve was performed by nonlinear regression and one-phase decay in GraphPad Prism. (C) The E-cadherin mobile fraction is shown in panel A. (D) Half-time is the time when the intensity reaches half of its maximum intensity. Control is Rho GEF2 Ubi-E-cad GFP, n = 11, *RhoGEF2* GLC, n = 10.

4.3 E-cadherin dynamics and junction maturation depend on Src42A

Tyrosine kinase src (c-Src) modulates cell adhesion in mammalian cells by regulating E-cadherin expression, distribution, and function (Liu et al., 2015). In *Drosophila*, there are two c-Src homologs, Src-family kinases Src42 and Src64, which are both expressed and active during convergent extension and myosin contractility (Tamada et al., 2021). Src42A, a conserved tyrosine kinase, is important for polarized

cell shape changes and cell reorganization (Förster and Luschnig, 2012). Based on this, I would like to check the role of Src in *Drosophila* E-cadherin dynamics. So I first crossed homozygous males of Src42A CA (constitutively active) and Src42A DN (dominant-negative) with females of mat gal 67-15. The embryos were then collected after 3-6 hours and stained with the Zipper antibody. In parallel, His-GFP was used as a control and stained in the same tube with Src42A CA or Src42A DN embryos. For the analysis, a maximum intensity projection (MIP) was used. I found the intensity of Zipper is increased in Src42A CA embryos and sharply decreased in Src42A DN embryos (**Figure 4.9**), which means Src42A regulates the intensity of Myosin II (**Figure 4.9**).
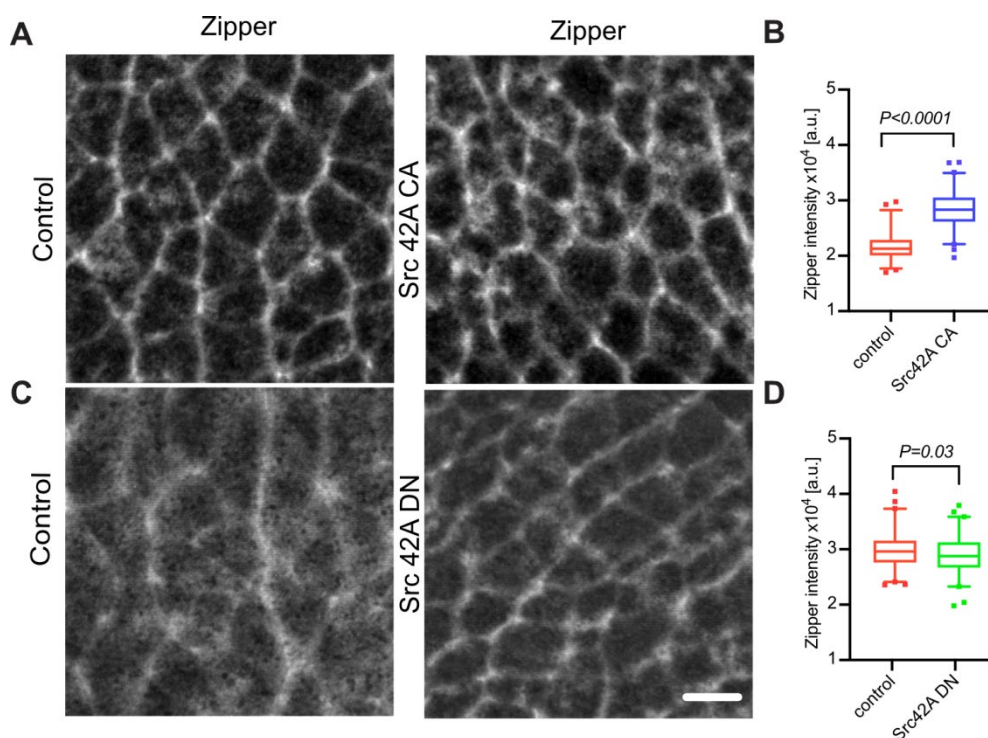
Figure 4.9: Src 42A activates myosin II. Myosin II was stained with a zipper antibody. Histone-GFP, Src CA, and Src DN 3-6h embryos were stained in one tube, respectively. (A, C) Zipper staining of the indicated genotypes. Images were gained with z-stacks and maximum intensity was used by Fiji. (B, D) Zipper intensity quantifications in panels A and C. Tissue analyzer projection was used to quantify the junctional Zipper intensity. Src CA control (n = 3), Src CA (n = 4), Src DN control (n = 3), Src DN (n = 4), scale bar 5 μm. The error bar is the mean with a 95% confidence interval. A maximum intensity projection (MIP) was used. An unpaired t-test was used to determine statistical significance.

However, when checking the p-myosin expression level in indicated genotypes, there was no significant difference in Src42A CA, Src42A DN, and Src42A RNAi lines (**Figure 4.10**). However, it is important to know that this p-myosin antibody is a phospho-Myosin light chain (smooth muscle) rather than non-muscle myosin II.
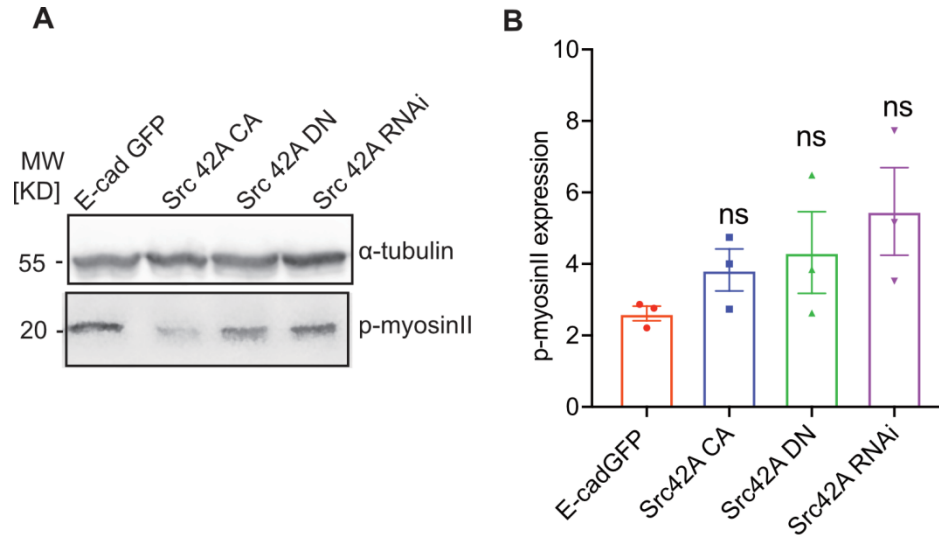
Figure 4.10: Src42A does not regulate the total p-myosin expression level. (A) WB. Homozygous males of Src42A CA and Src42A DN were crossed with females of mat gal 67-15. Embryos aged 3 to 6 hours were collected. (B) Quantification of panel A (n = 3). An unpaired t-test was used to determine statistical significance ([ns,] $p > 0.05$).

4.3.1 Src42A regulates junctional E-cadherin intensity during germband extension

Src is required for localized myosin contractility and planar polarity (Tamada et al., 2021). Moreover, DE-cadherin plays an essential role in *Drosophila* germband extension through interactions with F-actin and myosin II (Bertet et al., 2004). Src regulates E-cadherin expression and EMT (Nagathihalli and Merchant, 2012). However, some experiments revealed that Src could downregulate E-cadherin (Avizienyte et al., 2004; Kale et al., 2018). To further check the role of Src in E-cadherin maturation during germband extension and also check the role of Src in E-cadherin expression *in vivo*, I stained E-cadherin with control (Histone-GFP) and Src42A CA or Src42A DN in one tube, respectively. Surprisingly, I found the

junctional E-cadherin intensity was increased in Src42A CA 3-6h embryos, and the junctional E-cadherin intensity was decreased in Src42A DN 3-6h embryos compared to control (**Figure 4.11**), which is consistent with previous reports.
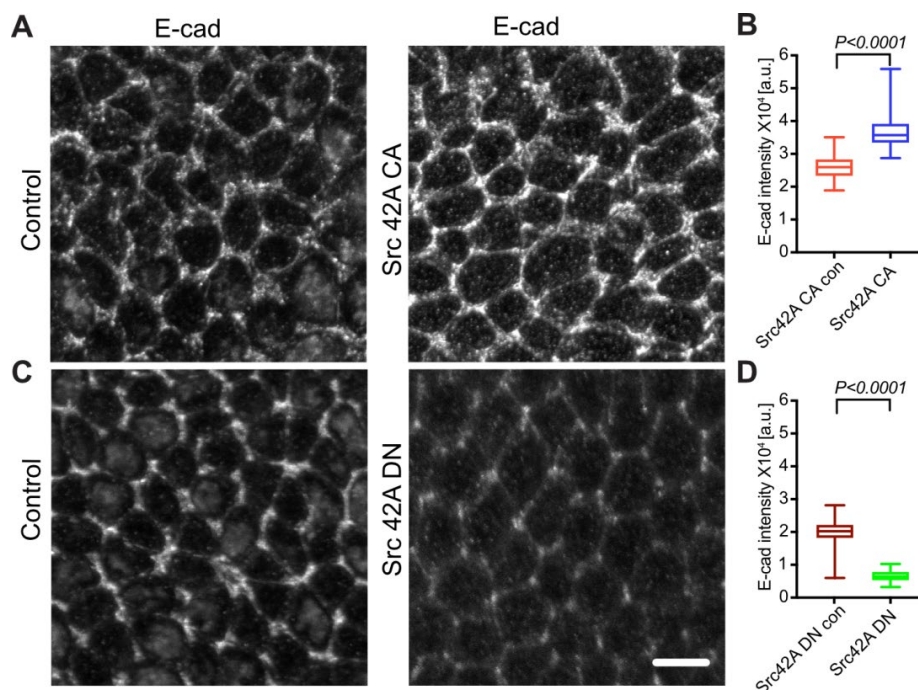
Figure 4.11: Src42A regulates membrane E-cadherin intensity during germband extension. E-cad GFP was stained with the DCAD2 antibody. Histone-GFP and Src CA, Src DN 3-6h embryos were stained in one tube, respectively. (A, C) The E-cadherin staining of the indicated genotypes. Images were gained with z-stacks and the maximum intensity was used by Fiji. (B, D) Panel A and C quantifications. Tissue analyzer projection was used to quantify the junctional E-cadherin intensity. Src CA control (n = 6), Src CA (n = 8), Src DN control (n = 8), Src DN (n = 5), scale bar 5 μm. A maximum intensity projection (MIP) was used. Statistical significance was estimated by an unpaired t-test.

To further identify the role of Src on E-cadherin protein level, I did a WB with Src42A CA, Src42A DN, and Src42A RNAi 3-6h embryos. However, I found the E-cadherin total protein level was significantly decreased in Src42A CA and Src42A DN (**Figure 4.12**). However, the E-cadherin expression level does not change in Src42A RNAi (**Figure 4.12**). One possible reason is that there are two c-Src homologs in *Drosophil*a, Src-family kinases Src42 and Src64. In addition, Src regulates E-cadherin expression bidirectionally. On the one hand, at the adherens junctions, high

levels of Src suppressed E-cadherin expression (Matsuyoshi et al., 1992). Src, on the other hand, may promote adhesions, and E-cadherin can activate Src in turn (McLachlan et al., 2007).
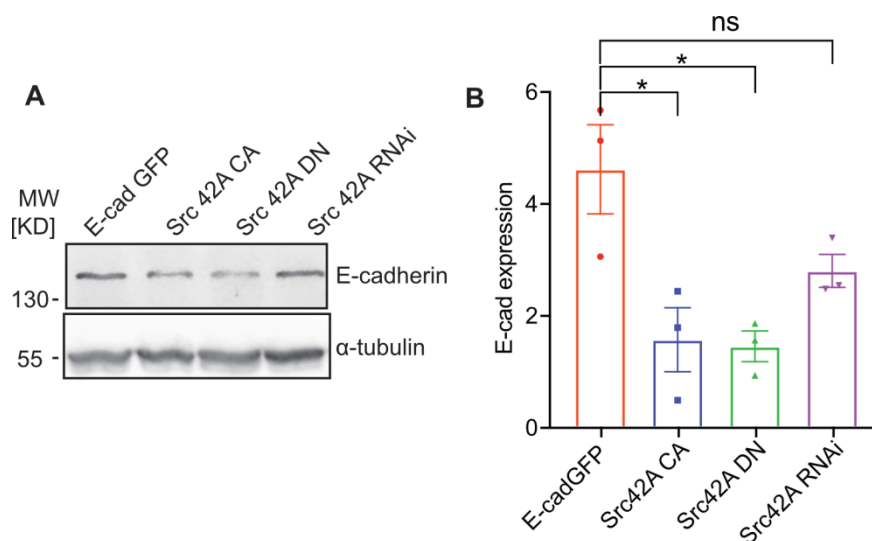
Figure 4.12: Src42A CA and Src DN downregulate the E-cadherin total protein level. However, the downregulation of Src 42A by RNAi does not change the E-cadherin expression level. (A) WB. Homozygous males of Src42A CA and Src42A DN were crossed with females of mat gal 67-15. Embryos aged three to six-hour were collected. (B) Quantification of panel A (n = 3). An unpaired t-test was used to determine statistical significance. *$p <$ 0.05, [ns] $p > 0.05$.

4.3.2 E-cadherin cluster dynamics are independent of Src42A

We already know that Src42A regulates E-cadherin expression (**Figures 4.10, 4.11, and 4.12**). Later, we would like to check the role of Src42A in E-cadherin dynamics during germband extension. Thus, I performed a FRAP experiment using Src42A RNAi with E-cadherin GFP embryos. I found the intensity of E-cadherin fluorescence recovery was not changed in Src42A RNAi compared to E-cadherin GFP knock-in embryos during germband extension (**Figure 4.13**). The mobile E-cadherin in Src42A RNAi is identical to the wild type (**Figure 4.13**). In summary, E-cadherin cluster dynamics are independent of Src42A.
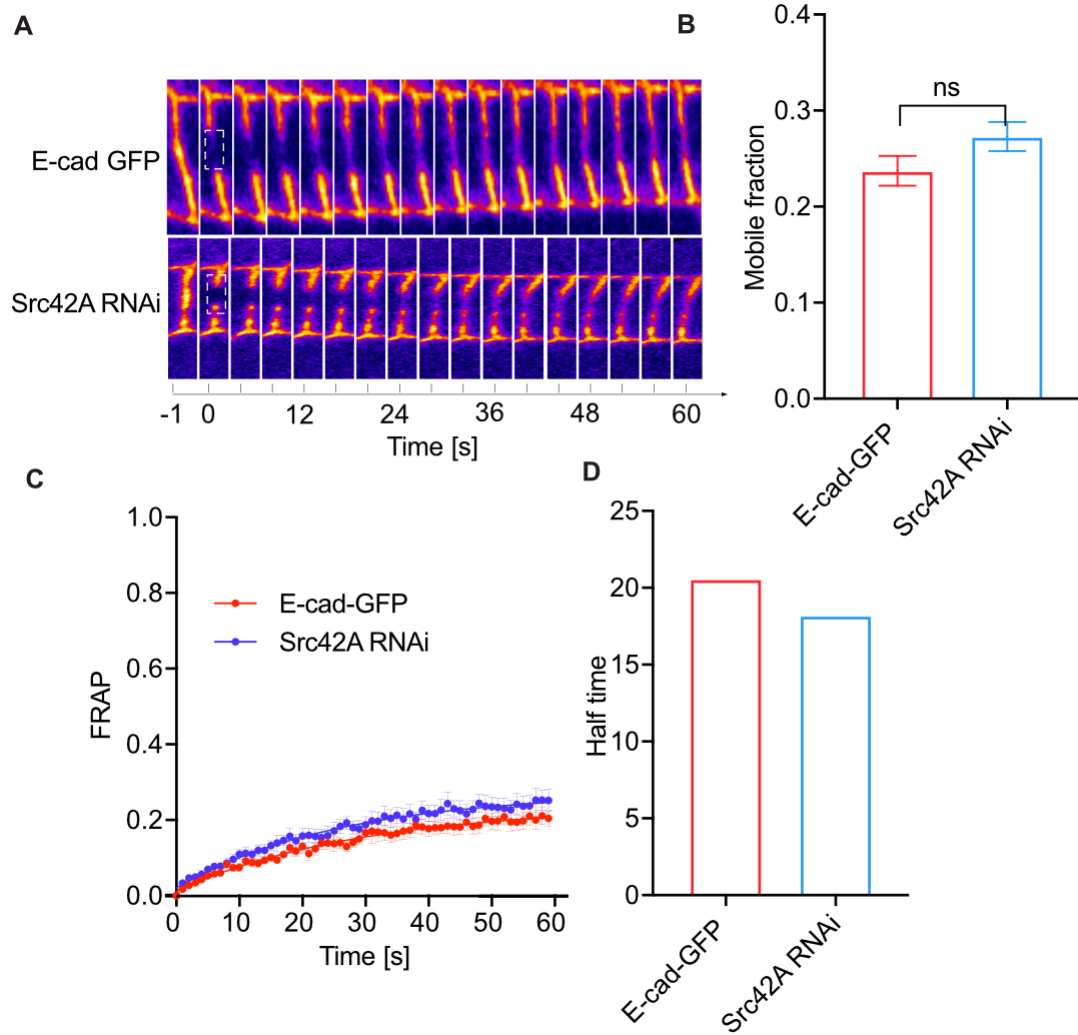
Figure 4.13: The mobile fraction of E-cadherin does not change during germband extension in Src42A RNAi embryos. (A) E-cadherin Kymograph of a FRAP experiment in wild type and Src42A RNAi embryos over a one-minute course. The white rectangle is the region of interest, which shows the bleached E-cadherin clusters. (B) The E-cadherin mobile fraction is shown in panel A. The error bars are the standard error of the mean (SEM) of a mobile fraction. (C) Fluorescence recovery curves for the Src42A RNAi embryos at stage 8. A fitting curve was performed by nonlinear regression and one-phase decay in GraphPad Prism. (D) Recovery time is the time when the intensity reaches half of its maximum intensity in wild-type and Src 42A RNAi embryos. An unpaired t-test was used to determine statistical significance. n = 7.

4.4 The maturation of E-cadherin is *N*-glycosylation-dependent

4.4.1 Mobile E-cadherin does not change in E-cadherin *N*-glycosylation mutations during germband extension
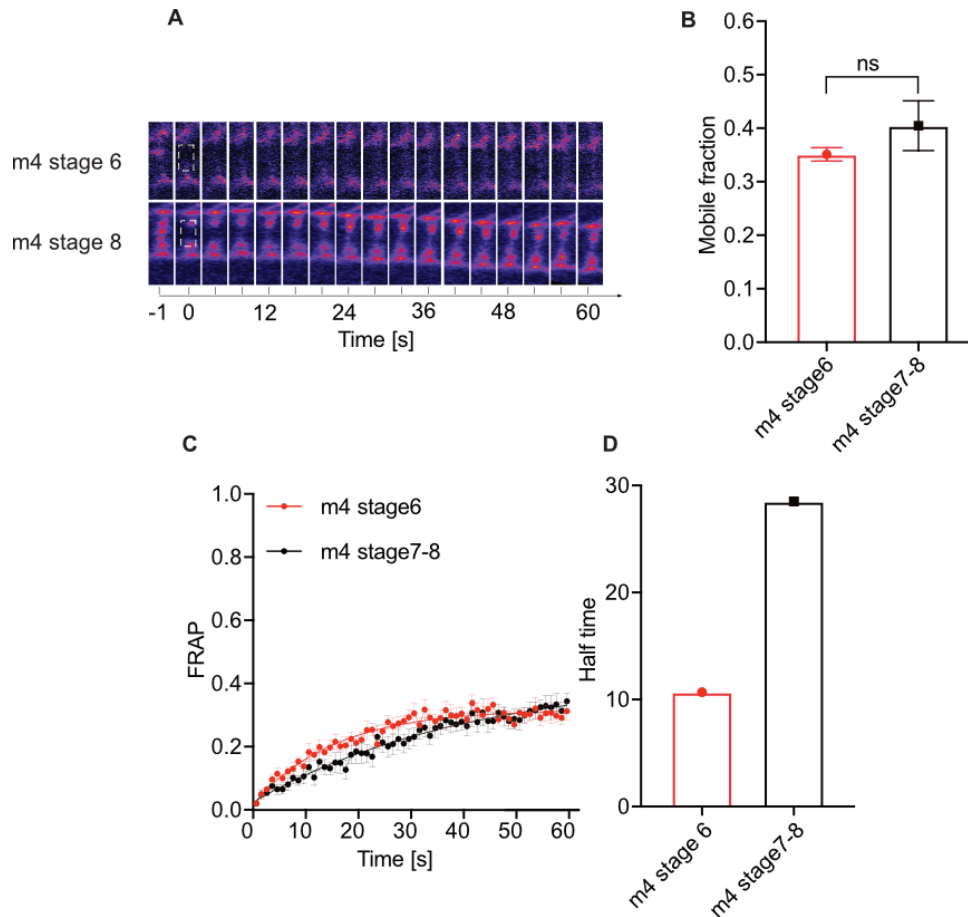
Figure 4.14: Immobile E-cadherin does not change during gastrulation in E-cadherin with four *N*-glycosylation site mutations. (A) E-cadherin kymograph of a FRAP experiment in E-cadherin *N*-glycosylation mutant. The white rectangle is the region of interest, which shows the bleached E-cadherin clusters. (B) The E-cadherin mobile fraction is shown in panel A. (C) Fluorescence recovery curves for the endogenous E-cadherin-GFP with four *N*-glycosylation mutations at stage 6 (n = 8) and stage 8. (n = 7) A fitting curve was performed by nonlinear regression and one-phase decay in GraphPad Prism. (D) Recovery time is the time when the intensity can reach half of its maximum intensity.

N-glycosylation of E-cadherin is one of the most significant posttranslational modifications. We have already looked into the role of *N*-glycosylation in E-cadherin-medicated tissue morphogenesis (**results 3**). Here we wanted to check the

role of *N*-glycosylation during E-cadherin maturation. Therefore, I did a FRAP experiment with E-cadherin *N*-glycosylation mutants m3 and m4. However, I did not see the E-cadherin mobile fraction change in m3 and m4 (**Figures 4.15 and 4.16**), suggesting that *N*-glycosylation regulates E-cadherin maturation during germband extension.
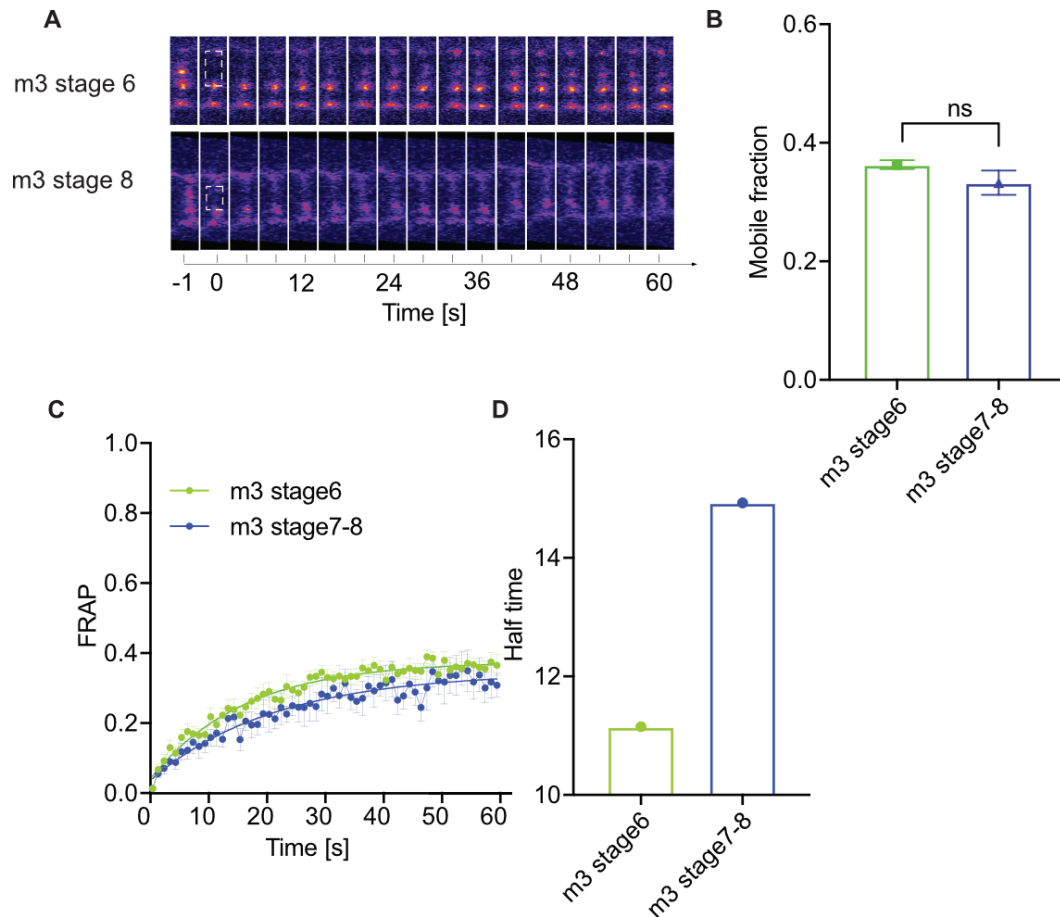
Figure 4.15: Immobile E-cadherin does not change during gastrulation in E-cadherin with three *N*-glycosylation site mutations. (A) Kymograph of E-cadherin in a FRAP experiment in m3. (B) The E-cadherin mobile fraction is shown in panel A. (C) Fluorescence recovery curves for m3 at stage 6 (n = 11) and stage 8 (n = 7). A fitting curve was performed by nonlinear regression and one-phase decay in GraphPad Prism. (D) Recovery time is the time when the intensity can reach half of its maximum intensity.

4.4.2 The localization of E-cadherin is changed in the E-cadherin *N*-glycosylation mutant during germband extension

This part is already presented in Figure 3.10.

5. Discussion

5.1 E-cadherin hypo-*N*-glycosylation and tissue morphogenesis

N-glycosylation is one of the most important post-translational modifications. In addition, *N*-glycosylation, the most evolutionary conserved biological process, is crucial for protein stabilization, immunological response regulation, ER quality regulation, and other significant biological functions (Helenius and Aebi, 2004). Glycosylation deficiencies impair protein folding and maturation. Furthermore, it was reported that a large amount of protein hypo-*N*-glycosylation was demonstrated to show disorders across different systems in patients. Even though proteins' hypo-*N*-glycosylation is strongly associated with cell dysfunction, it is still unclear how hypo-*N*-glycosylation affects cell dynamics, particularly in mechanotransduction.

During epithelial morphogenesis, E-cadherin forms clusters and facilitates junction remodeling and force transmission (Kale et al., 2018). Moreover, the homophilic binding of E-cadherin is the basis of E-cadherin's function in adhesion. E-cadherin interacts with F-actin through β-actin, α-catenin, and vinculin, and links the cadherin-catenin complex to the actin cytoskeleton (Abe and Takeichi, 2008), which is crucial for cell-cell adhesion (Drees et al., 2005; Jamora and Fuchs, 2002). The initial discovery of the *xiantuan* (*xit*) mutant came from the oogenesis X chromosome screen. The homology of *xit*, ALG8, catalyzes the second glucose in *yeast* (Helenius and Aebi, 2004). Moreover, *Drosophila* mutants in *wollknäuel* (*wol*) and *garnystan* (*gny*) are the homologs of ALG5 and ALG6. These mutations produce specific morphogenetic abnormalities and are lethal (Burda and Aebi, 1998; Reiss et al., 1996; Stagljar et al., 1994; Zhang et al., 2014). Additionally, our group has demonstrated that E-cadherin is hypo-*N*-glycosylated and germband extension is incomplete in *xit* (Zhang et al., 2014). In the endoplasmic reticulum, *xit* also encodes a glucosyltransferase (Zhang et al., 2014).

To further identify the role of E-cadherin hypo-*N*-glycosylation in germband extension, site-specific Asn–>Gln mutations in E-cadherin protein at *N*-glycosylation sites introduced at the endogenous genetic locus in *Drosophila* with different combinations were generated. From the DIC movies, we knew that m3 (246) inhibited germband extension the most among these mutants, except for *xit* (**Figure 3.8**), even though m5 is homozygous lethal. Surprisingly, in terms of germband extension, the m5 most closely resembled the *xit* phenotype; they both delayed the germband extension and terminated it afterward (**Figure 3.8**). M4 (1357) showed a weaker phenotype in comparison to m3 (246), but a stronger phenotype than m3 (147) concerning the effect on germband extension (**Figure 3.8**). It appears that some *N*-glycosylation sites are more important than others because a greater number of mutations in E-cadherin *N*-glycosylation sites did not result in more disorders in germband extension. This is also consistent with the following results (**Figures 3.27 and 3.30**).

To find which sites are crucial for the *xit* genotypes, I performed the MS experiment with Co-IP samples. And we know from the MS results (**Figure 3.2**) that site 317 is not important for impaired germband extension. Sites 617 and 1274 are rather important. However, this did not explain that m3 (147) slowed down the germband extension more than m5 (12467) did. Additional evidence for this was provided by transheterozygous mutants, which demonstrated that *N*-glycans may play a position-dependent role in the germband extension (**Figure 3.27**). Together, I made the argument that E-cadherin *N*-glycosylation has both number-dependent and position-dependent functions in E-cadherin dynamics. To test this, transgenes of single-site mutations as well as site mutations in various combinations can be introduced to E-cadherin at the locus. As a result, each site can be examined individually to determine which sites would contribute to the impaired germband extension. However, I postulated that the germband extension would not be weakened by just one site. Simultaneously, the site mutations identified in the MS experiment were then generated, and the same experiments will be carried out to check how far the germband would extend and what function it would play in E-cadherin dynamics.

Using this method, it might be possible to identify the crucial E-cadherin *N*-glycosylation sites involved in germband extension and E-cadherin dynamics.

Furthermore, hypo-*N*-glycosylated E-cadherin affects cell-cell contact in the mammalian cell. For instance, hypo-glycosylated E-cadherin (mutant V13) promotes intercellular adhesion in carcinoma A253 cells (Jamal et al., 2009). In addition, hypo-glycosylated E-cadherin promotes the recruitment of γ-catenin and vinculin to adherens junctions and as well as junction stabilization in CHO cells (Liwosz et al., 2006; Palovuori and Eskelinen, 2000). The question is, how does E-cadherin *N*-glycosylation affect tissue morphogenesis? *xit* and hypo-*N*-glycosylated E-cadherin mutants were employed to discover the solution. And hypo-*N*-glycosylated E-cadherin mutants did not exhibit any abnormalities in cell-cell contact (**Figures 3.9 and 3.10**). However, the localization of E-cadherin has changed in E-cadherin hypo-*N*-glycosylation mutants and m3, E-cadherin with three *N*-glycosylated point mutations, delayed E-cadherin migration to the apical domain as well as E-cadherin maturation (**Figure 3.11**). Only the efficient expression of E-cadherin changes in *xit*, with the overall protein amount remaining constant (Zhang et al., 2014), suggesting that E-cadherin is not subjected to ERAD despite hypo-*N*-glycosylation. Consequently, hypo-*N*-glycosylation does not contribute to the expression of E-cadherin. What, then, is the reason for the observed phenotypes and the underlying mechanism? This will be covered in the paragraphs that follow.

5.2 Roles of *N*-glycosylation in the E-cadherin immobilization and clustering

E-cadherin is not evenly distributed but forms *cis* and *trans* clusters at adherens junctions, which stabilizes adhesion (Quang et al., 2013; Takeichi, 1991; Zhu et al., 2003) and acts as a force transmitter (Hong et al., 2010; Patel et al., 2006). Although E-cadherin endocytosis has been demonstrated, the acton-myosin network, *cis,* and *trans*-interactions have also been shown to mediate E-cadherin sizes and intensities (de Beco et al., 2009; Engl et al., 2014; Indra et al., 2018; Quang et al., 2013; Song et al.,

2013). It will be of considerable interest to investigate the other E-cadherin clustering mediators.

It has been reported that E-cadherin *N*-glycosylation affects its functionality (Pinho et al., 2011). *xit* and E-cadherin hypo-*N*-glycosylation mutants were employed to determine the function of hypo-*N*-glycosylation in E-cadherin dynamics. According to the laser ablation experiments, we knew that E-cadherin mobile fraction and vertex displacement were both noticeably elevated in E-cadherin hypo-*N*-glycosylation mutants, both the *xit* and site hypo-*N*-glycosylation mutants (**Figures 3.13-3.15, 3.17-3.19**). And the laser-cutting experiment's primary goal, nevertheless, is to examine the junctional tension. However, it is challenging to tell if the increased recoil velocity is due to the higher junctional tension or lower friction. We can assume that the higher vertex displacements and initial recoil velocities are caused by the increased tension if the viscoelasticity (K) stays constant (Sugimura et al., 2016). However, if the K value is changed, it could be preferable to use atomic force microscopy to verify the force. It may be possible to measure the junctional tension by doing a fitting with a few parameters, but it is still challenging to do so. On the other hand, wound healing starts to take place shortly after laser cutting, resulting in mechanical tension changes in turn (Wood, 2012). These may have an impact on how cells behave after initial recoil and depend on secondary processes of the active materials like wound response. The recoil velocities were therefore only measured for the first 10 seconds.

It has been reported that E-cadherin *trans* and *cis* interactions are important for the clustering process (Wu et al., 2010; Wu et al., 2011; Zhang et al., 2009). We proposed that E-cadherin hypo-*N*-glycosylation regulates E-cadherin dynamics by affecting the size and intensity of E-cadherin clusters (**Figure 5.1**). To test this hypothesis, E-cadherin was stained with GFP-booster and the intensities and variance of junctions were measured (**Figure 3.12**). I noticed that, during germband extension, the intensities (both the overall intensities and junctional intensities) and sizes of E-cadherin (variance of clusters) were significantly reduced in *xit* and E-cadherin

hypo-*N*-glycosylation mutants, including *xit* compared to E-cadherin GFP knock-in embryos (**Figure 3.12**), and smaller E-cadherin clusters in *xit* and hypo-*N*-glycosylated mutants, which may indicate that *N*-glycosylation regulates the size and intensity of the clusters (**Figure 3.12**).

Regarding the role of *N*-glycosylation in E-cadherin cluster sizes and intensities, Super-Resolution Microscopy, such as Stimulated Emission Depletion (STED), or Stochastic Optical Reconstruction Microscopy (STORM), could also be used to check the structure of E-cadherin clusters in E-cadherin *N*-glycosylation mutants and wild-type embryos during germband extension.

The other regulator that controls E-cadherin clustering is actin (Engl et al., 2014; Quang et al., 2013). Therefore, further investigation is still required to determine how *N*-glycosylation influences actin organization. Although the F-actin staining has already been done in *xit*, m3, m4, and m5 embryos, a proper method to quantify the interaction between E-cadherin and F-actin is still required. In addition, the cadherin-catenin complex serves as a linker between E-cadherin and F-actin (Abe and Takeichi, 2008; Hazan et al., 1997; Imamura et al., 1999; Song et al., 2013). I will therefore investigate how E-cadherin hypo-*N*-glycosylation affects the cadherin-catenin complex formation (**Figures 3.22 and 3.23**). Additionally, when compared to E-cadherin GFP knock-in embryos (WT), *xit* significantly increased the cadherin-catenin complex formation by Co-IP assays during germband extension (**Figure 3.22**). But, why did I not observe a difference between the cadherin-catenin complex formation in m3 and m4 mutants? One explanation is that m3 and m4 have a less significant impact on E-cadherin *N*-glycosylation than *xit*. The MS results showed that E-cadherin *N*-glycosylation sites 617 and 1274 are *xit*-dependent (**Figure 3.2**). Among m3 and m4, only m3 contains the mutation site 1274, hence m3 had a stronger influence on germband extension than that of m4 but weaker than *xit* (**Figure 3.8**). Neither of them contains the mutation site 617, as it's the new *N*-glycosylation site in E-cadherin that I identified from the MS experiment (**Figure 3.2**). Therefore, this could be a reason why I failed to identify the enhanced cadherin-catenin complex

formation in m3 and m4.

To further confirm the role of E-cadherin hypo-*N*-glycosylation in cadherin-catenin complex formation, α-catenin and E-cadherin staining need to be carried out in wild-type and E-cadherin hypo-*N*-glycosylation mutants. Afterward, I will quantify the ratio of α-catenin and E-cadherin. While staining can precisely detect the E-cadherin on the junctions, the Co-IP experiment measured the overall E-cadherin. Another argument is that there might be a difference in the number of hypo-*N*-glycosylation sites, which is different between m3 and m4. However, due to the limitations of Co-IP experiments, no difference was detected between them and E-cadherin-GFP knock-in embryos (**Figure 3.23**). More sensitive experiments to investigate E-cadherin and α-catenin interactions may be required later.

At the same time, the new transgene was being created with mutations at positions 617 and 1274, which I identified from the MS experiments. The dynamics of E-cadherin's function, as well as the cadherin-catenin complex formation and the effects on germband extension in this transgene, will be further examined. Additionally, a comparison between this new transgene and *xit's* phenotypic and functional impacts on E-cadherin dynamics is required.

Furthermore, myosin II promotes junctional tension and actin organization (Harrison et al., 2011; Wu et al., 2015). Consequently, Y-compound was injected into *xit* embryos to activate myosin II during germband extension to determine whether myosin II affects the E-cadherin dynamics in E-cadherin hypo-*N*-glycosylation mutants. We found the mobile fraction of E-cadherin was significantly lower in *xit* with 2 mM Y-compound compared with *xit* embryos, suggesting myosin II was required for the enhanced E-cadherin dynamics in *xit* embryos and the E-cadherin dynamics in *xit* is dependent on myosin II (**Figure 3.20**).
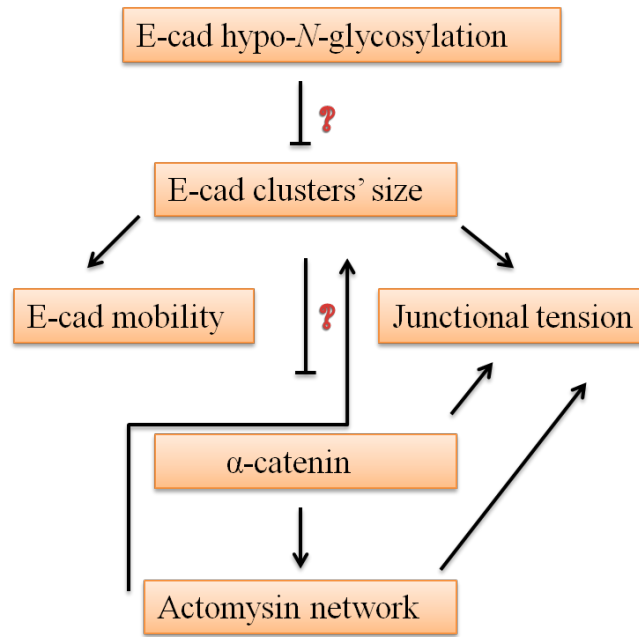
Figure 5.1: A hypothesis regarding how hypo-*N*-glycosylation regulates E-cadherin dynamics. E-cadherin *N*-glycosylation regulates the dynamics and E-cadherin-dependent tension by controlling the sizes and intensities of E-cadherin clusters. As a result, additional α-catenin could be recruited to the E-cadherin-catenin complex, which would then regulate junctional tension in turn.

In conclusion, E-cadherin hypo-*N*-glycosylation modulates E-cadherin dynamics, and *xit* affects the interactions of actin-myosin with adhesion complexes (**Figures 3.13-15, 3.17-3.20, 3.22**).

To further clarify the role of E-cadherin hypo-*N*-glycosylation in cadherin-catenin complex formation, I used E-cad-α-catenin-GFP chimeric embryos, which have both endogenous and GFP-labeled α-catenin. Additionally, different antibodies can be used to detect different types of α-catenins. Based on this, I can conclude that how many molecules of α-catenin interact with E-cadherin? Through a Co-IP experiment, I found both endogenous and GFP-labeled α-catenin, which means E-cadherin can be combined with multiple α-catenins and additional α-catenin can be recruited to the E-cad-catenin complexes (**Figure 3.24B**). This is made feasible by the fact that, as there are more open places, a larger E-cadherin cluster fragments into numerous little clusters (**Figure 5.2**). And this may be an explanation for why the E-cadherin

hypo-*N*-glycosylation mutants have smaller E-cadherin clusters (**Figure 3.12**).

It was reported that monomeric α-catenin interacts more strongly with E-cadherin-β-catenin, while dimeric α-catenin binds to F-actin more (Drees et al., 2005). Unfortunately, I was unable to figure out which subtype of α-catenin was elevated in the complexes. Taken together, E-cadherin *N*-glycosylation regulates E-cadherin dynamics by modifying the E-cadherin's size, intensity, and E-cadherin-catenin complex formation *in vivo* (**Figures 3.12, 3.22, and 3.24**).

Furthermore, I found that in m3 and m4 mutants, the interaction of α-catenin with the *C*-terminal of E-cadherin was decreased (which was not shown in the figures). At the *C*-terminal of DE-cadherin, m3 only affects *N*-glycosylation at site 1274, and m4 has hypo-*N*-glycosylation at site 1290, which suggests that these two sites are important for the interactions of E-cadherin and α-catenin. However, this is different from what we observed in *xit* (**Figure 3.22D**). As a result, a closer examination of this section is still required.
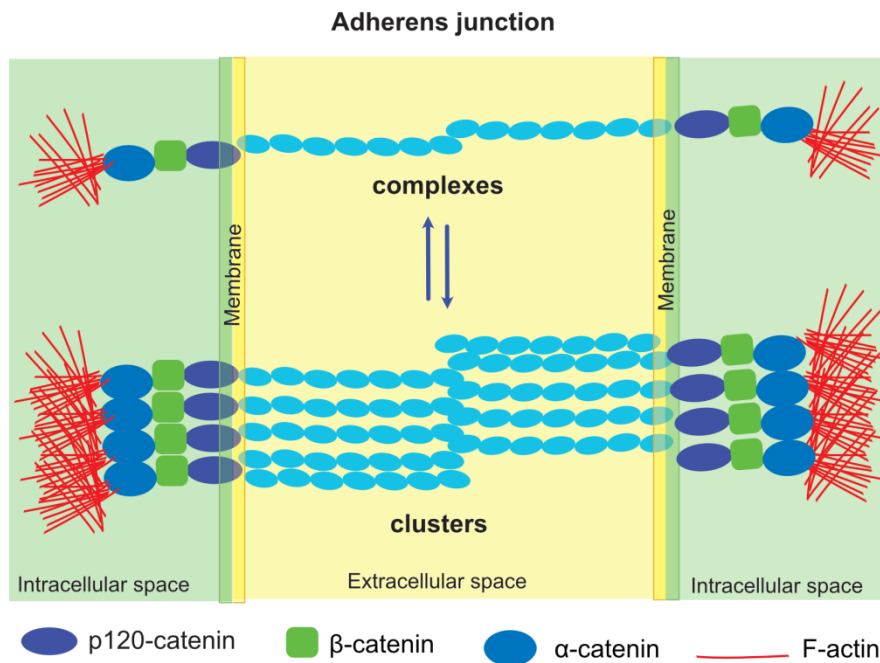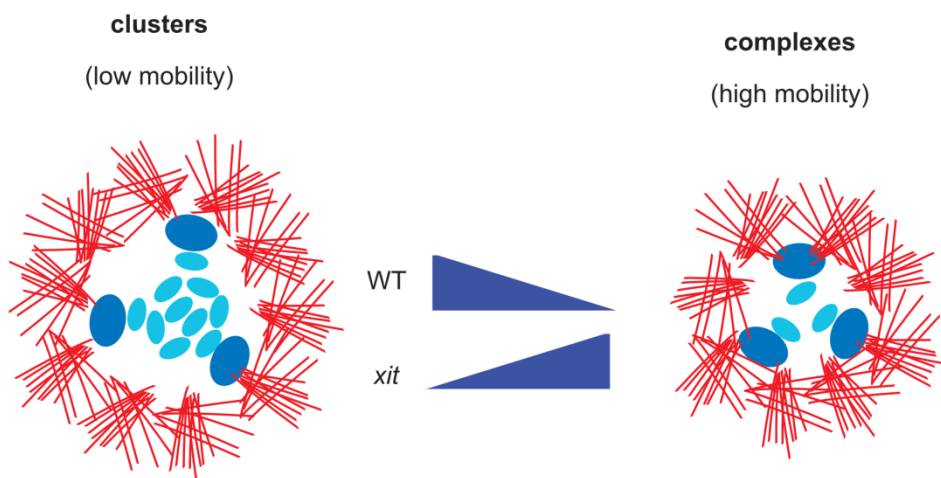
Figure 5.2: A model of increased cadherin-catenin complex formation in *xit* versus wild-type. Side views of E-cadherin-catenin complexes. E-cadherin directly binds with p120-catenin, p120-catenin interacts with β-catenin, β-catenin binds to α-catenin, and α-catenin interacts with F-actin. Top views of E-cadherin-catenin complexes in E-cadherin GFP knockin and *xit*. E-cadherin is more mobile in *xit* than in wild-type, indicating that there are more clusters in wild-type other than complexes. More α-catenin can be recruited to the cadherin-catenin complex in *xit*. And the E-cadherin clusters' size is smaller with a reduced area of the cadherin-catenin complex in the figure. This figure is modified from (Guillot and Lecuit, 2013b; Wu et al., 2015).

5.3 Position-dependent role of *N*-glycans in E-cadherin dynamics

N-glycosylation is essential for protein function. However, deglycosylation results in a less significant or even increased role of enzyme activity compared to the individual *N*-glycosylation site mutations (Skropeta, 2009), which means some *N*-glycan sites are more important than others with their unique functions, and this may be because the different structures of each *N*-glycan (Skropeta, 2009). One of the examples is that the *N*-glycosylation site (N384) mutation leads to a two-time increase in LCAT (Lecithin–cholesterol acyltransferase) activity in COS cells (Skropeta, 2009). On the other hand, a protein with more *N*-glycans will be more hydrophilic, and the number of *N*-glycans is essential for protein secretion and folding. To summarize, there are two principal mechanisms for the function of *N*-glycans: the numbers of *N*-glycans or the positions of *N*-glycans are important for the proteins' functions.

Based on this, to further check whether the number or position of E-cadherin *N*-glycosylation is more important for the dynamics of E-cadherin, I crossed m4 (1357) with different m3, m3 (246), and m3 (147), and then virgins of m3 (246)/m4 (1357) or m3 (147)/m4 (1357) were crossed with males of m3 or m4 with stronger effects on germband extension, separately (**Figure 5.3**). The progeny of m3 (246)/m4 (1357) and m3 (147)/m4 (1357) both contain seven mutated *N*-glycosylation sites in E-cadherin. However, in m3 (246)/m4 (1357), every *N*-glycosylation mutation site is distinct, while some E-cadherin *N*-glycosylation sites are the same in m3 (147)/m4 (1357) (**Figure 5.3**).

Regarding the *N*-glycan position-dependent role in E-cadherin dynamics, only the m3 (246)/m4 (1357) mutant shows the site complementation effect (**Figures 3.27-3.29**), but not the m3 (147)/m4 (1357) (**Figures 3.30-3.32**). To further check the site complementation function of E-cadherin hypo-*N*-glycosylation, more new transgenes would be produced. For instance, E-cadherin with five-site *N*-glycosylation and two-site mutations with different combinations will be generated, and the position-dependent role of *N*-glycan in E-cadherin dynamics will be further investigated.
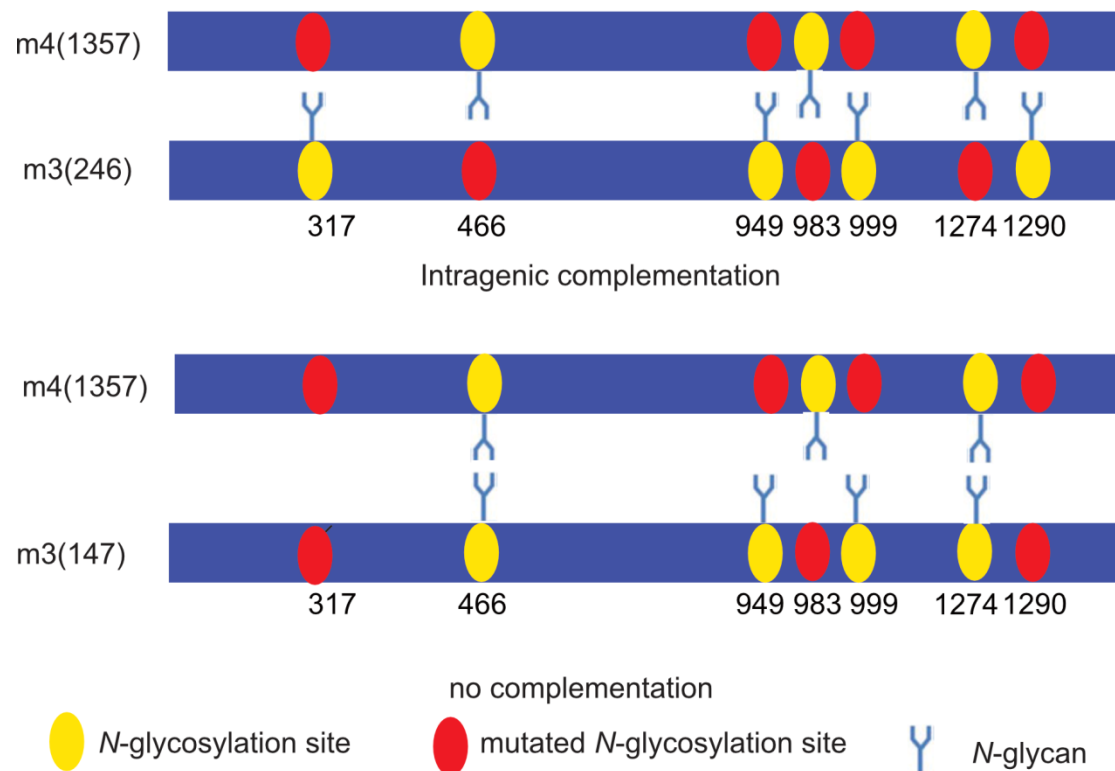
Figure 5.3: *N*-glycans have a position-dependent role in E-cadherin dynamics. The m3 (246) and m4 (1357), two E-cadherin hypo-*N*-glycosylation mutants, have mutations in one line but not in another. However, when crossed together, the offspring contains seven normal *N*-glycosylation sites and seven mutated *N*-glycosylation sites within E-cadherin. While crossing the mutant m3 (147) and m4 (1357) together, the progeny also contains 7 mutated *N*-glycosylation sites within E-cadherin. However, some of the mutation sites are the same (sites 1 and 7), and certain *N*-glycosylation sites are missing (sites 2 and 6), suggesting every *N*-glycosylation site has to be present. However, the line it presents does not matter at all. The mutated *N*-glycosylation sites represent an N (asparagine) to Q (glutamine) mutation. The scheme is modified from (Pinho et al., 2011; Zielinska et al., 2012).

In the m3 (246)/m4 (1357) mutant, the germband extension was normal like wild-type, as well as the E-cadherin dynamics (**Figures 3.27-3.29**). The E-cadherin position-dependent function has been further examined with other E-cadherin hypo-*N*-glycosylation mutants, m3 (147)/m4 (1357) (**Figures 3.30-3.32**). To my astonishment, the m3 (147)/m4 mutant showed impaired germband extension (**Figure 3.30**). Additionally, during germband extension, the m3 (147)/m4 mutant exhibited considerably lower E-cadherin mobile fraction, vertex displacement, and initial recoil velocity compared to m4 and E-cadherin GFP knock-in embryos (**Figures 3.31 and**

3.32), which means there is no site complementation function in m3 (147)/m4. Unfortunately, one more control (m3) is missing for the FRAP and ablation experiments. On the other hand, m4 had a weaker effect on germband extension than m3 (147), but not m3 (246) (**Figure 3.8**), which strongly illustrated the position-dependent role of E-cadherin in germband extension as well as E-cadherin dynamics in turn (**Figure 5.3**).

In other words, each of the seven *N*-glycosylation sites in E-cadherin must be present to maintain its function in cell-cell dynamics as well as in the germband extension process. However, the line where they are present is completely irrelevant.

In addition, hypo-*N*-glycosylation of E-cadherin does not affect the overall protein levels of E-cadherin (Zhang et al., 2014). This means the hypo-*N*-glycosylation does not alter the enzyme activity, which also supports the E-cadherin position-dependent role.

Concerning the position-dependent role of *N*-glycan in E-cadherin dynamics, I could also investigate the role of *N*-glycosylation in adhesion in S2 cells. After transfecting S2 cells with plasmids carrying different *N*-glycosylation mutations and wild-type E-cadherin plasmids, cellular clumping and chelation will be assessed. The contacts between neighbor junctions in E-cadherin hypo-*N*-glycosylation mutants and wild-type could also be measured using an atomic force microscope (AFM). Alternatively, it can be determined whether hypo-*N*-glycosylation of E-cadherin controls its rigidity and cell adhesion. However, the better way to compare the force in wild-type and mutants is to measure the force directly with embryos by AFM. It is also possible to measure how much force will be needed to pull two cells together after cell disassociation. After that, cell aggregation may also be measured by AFM using wild-type and mutant cells with a fixed pulling force.

It will be of great interest to study the position-dependent role of *N*-glycans in E-cadherin dynamics in detail; specifically, only a few numbers of sites have this function, or seven potential *N*-glycosylation sites must be presented at the same transgene, or perhaps some other sites (for example, the sites which I identified from

the MS experiment-sites 617 and 692) also contribute to the position-dependent function in E-cadherin dynamics. These can be tested by more hypo-*N*-glycosylated mutations in E-cadherin.

Taken together, our research on E-cadherin hypo-*N*-glycosylation mediated cell dynamics *in vivo* provides hints for the understanding of posttranslational modifications in E-cadherin-medicated mechanotransduction in living organisms, and E-cadherin hypo-*N*-glycosylation is important for the germband extension, as well as E-cadherin dynamics via regulating the size and intensity of E-cadherin's clusters and the cadherin-catenin complexes formation (**Figures 3.12, 3.13-3.15, 3.17-3.20,3.22, 3.24-3.26**). And *N*-glycans have a position-dependent role in the E-cadherin dynamics (**Figures 3.27-3.32**).

5.4 E-cadherin has a developmental control role during germband extension. (Regulators of E-cadherin maturation)

The formation and stabilization of cell-cell junctions are promoted by actin polymerization. Nascent adhesions have a shorter lifespan and are made up of tiny, dot-like adhesions (Choi et al., 2008; Vicente-Manzanares and Horwitz, 2011), while mature adhesions are larger and longer, which is due to actin polymerization and myosin II activation (Galbraith et al., 2007; Vicente-Manzanares and Horwitz, 2011). Focal adhesion kinase (FAK), Src, and force are additional factors that control the turnover of nascent adhesions (Choi et al., 2008; Galbraith et al., 2002; Katsumi et al., 2002; Riveline et al., 2001). Suppressing these signals may therefore promote adhesion maturation (Webb et al., 2004). Furthermore, nascent adhesion formation and turnover are myosin II-independent (Choi et al., 2008). However, actomyosin contractility regulates adhesion size (Galbraith et al., 2002). The goal of this work was to define the factors that influence adhesion maturation during germband extension.

Firstly, the E-cadherin intensity was significantly increased from the onset of gastrulation to germband extension (**Figure 4.1**). This was not, however, caused by a

rise in its mRNA level (**Figure 4.2**). Rho GEF2 and Src42A regulate E-cadherin intensity (**Figures 4.6 and 4.9**). However, Rho1 did not control the E-cadherin total protein level (**Figure 4.4**), suggesting that more E-cadherin could be recruited to the adhesions during E-cadherin maturation.

Furthermore, even though the E-cadherin along the junction was increased in Src42A CA embryos, the total E-cadherin was decreased (**Figures 4.9 and 4.12**), and both decreased in Src42A DN embryos (**Figures 4.9 and 4.12**). Since only half of the embryos had the correct genotype and it was challenging to distinguish between different genotypes, myosin II activity in Rho1 mutants could not be quantified. However, the myosin II intensity was quantified in Src42A CA and DN embryos as the males are homozygous and all the offspring are heterozygous. We found Src 42A activated myosin II by staining (**Figure 4.9**), which is consistent with the previous report (Tamada et al., 2021). Unfortunately, there was no difference in WB experiments. One potential explanation is Src64, another homology of c-Src in *Drosophila*. Src 42A CA alone could not change the *p*-myosin II total protein level. The second reason could be the *p*-myosin II antibody, which is a phospho-myosin light chain (smooth muscle) rather than non-muscle myosin II. The staining still allows us to conclude that Src42A controls the maturation of E-cadherin.

The modulators of E-cadherin dynamics would be another side I would like to check. To confirm this, a FRAP experiment was carried out using Rho GEF2 mutants with overexpressed E-cadherin GFP and Src42A RNAi coupled with E-cadherin GFP embryos (**Figures 4.7, 4.8, and 4.13**). The mobile E-cadherin fraction was increased during germband extension in RhoGEF2 GLC (**Figure 4.8**), indicating that E-cadherin mobility is dependent on RhoGEF2.

Src42A RNAi did not, however, cause a change in E-cadherin mobility, which does not imply that E-cadherin mobility is unrelated to Src (**Figure 4.13**). The efficiency of RNAi is different to measure, but I could also try the Src42A knockout line or the Src42A and Src64 double mutants. In addition, Src can bi-directionally regulate the expression of E-cadherin. On the one hand, high levels of Src suppress

junctional E-cadherin expression (Matsuyoshi et al., 1992). Src, on the other hand, may promote adhesions, and E-cadherin, in turn, may activate Src (McLachlan et al., 2007). As a result, the expression of Src and E-cadherin is complicated and dependent on both proteins at cell junctions. Therefore, further investigation should be performed to study the role of Src and E-cadherin at adherens junctions.

It's interesting to note that the E-cadherin *N*-glycosylation controlled the E-cadherin dynamics during germband extension (**Figures 4.14 and 4.15**). The E-cadherin mobile fraction was decreased from the onset of gastrulation to germband extension (**Figure 4.3**). In addition, there was no difference in E-cadherin *N*-glycosylation mutants (**Figures 4.14 and 4.15**), which was consistent with chapter 3 and indicated that E-cadherin *N*-glycosylation plays an essential role in the E-cadherin dynamics. Apart from that, the localization of E-cadherin was also changed during germband extension (**Figure 4.16**). In the wild type, E-cadherin is found in the subapical domain at stage 6 and is enriched in the apical domain at stage 8 (Guillot and Lecuit, 2013a). Co-localization with F-actin was not observed in either stage by the Airyscan Joint Deconvolution system (**Figure 4.16**). However, E-cadherin co-localized on the lateral side with F-actin at stage 6 and stage 8 in m3 embryos (**Figure 4.16**).

Furthermore, Rho kinase (ROCK) helps myosin II assembly. By injecting Y-compound in staged embryos, the role of myosin II would be confirmed during germband extension.

To sum up, Rho GEF2, Src42A, and E-cadherin *N*-glycosylation control E-cadherin dynamics and expression during germband extension.

6. Materials and Methods

6.1 Materials

6.1.1 Reagents

All standard chemicals and reagents were ordered from Carl Roth GmbH (Karlsruhe, Germany), AppliChem GmbH (Darmstadt, Germany), Invitrogen (Carlsbad, USA), Sigma-Aldrich (St. Louis, USA), Merck (Darmstadt, Germany) or Thermo Fisher Scientific (Waltham, USA) unless otherwise mentioned.

6.1.2 Media for flies

Fly food and apple juice plates

All the flies' food and apple juice plates are prepared by our technicians under the standard protocol.

http://wwwuser.gwdg.de/~jgrossh/protocols/Fliegenzucht/Fliegenfutter-HD.html.

6.1.3 General buffer

Name	Compositions
Blocking buffer	5% non-fat milk or 5% BSA
Embryos fixation buffer	4.5 mL PBS, 5 mL Heptane, 0.5 mL Formaldehyde (37%)
Embryos heat fixation buffer (salt buffer)	0.03% Triton X-100, 0.4% NaCl
PBS	7 mM Na_2HPO_4, 130 mM NaCl, 3 mM NaH_2PO_4 (pH 7.4)
PBT	PBS with 0.1% of Tween-20 or TritonX-100
TE buffer	10 mM Tris/HCl (pH 8), 1 mM EDTA
Buffer for WB and Co-IP	
Stacking gel buffer	0.5 M Tris/HCl (pH 6.8), 0.4% SDS
Separating gel buffer	1.5 M Tris/HCl (pH 8.8), 0.4% SDS

6x Laemmli's buffer	375 mM Tris/HCl, 10% SDS, 50% Glycerol, 0.6 M DTT, 0.06% Bromphenole blue
10x SDS-PAGE running buffer	0.25 M Tris, 2 M glycine,1% SDS
Wet transfer buffer	25 mM Tris, 175 mM Glycine, 20% Methanol
Extraction buffer	50 mM Tris/HCl (pH 7.6), 100 mM NaCl, 1% NP-40, 1%Triton X-100
Buffer for protein purification	
Lysis buffer	50 mM Tris/HCl (pH 8), 500 mM NaCl, 1 mM DTT
Wash buffer:	50 mM Tris/HCl (pH 8), 500 mM NaCl, 1 mM DTT
Elution buffer	50 mM Tris/HCl (pH 8), 50 mM NaCl, 30 mM Glutathione
Buffers for the DNA preparation	
Squishing Buffer	Tris-HCl 10 mM (pH 8.2), EDTA 1 mM, NaCl 25 mM, Proteinase K 200 μg/mL

6.1.4 Commercial kits

Name	Source
Plasmid Midi Kit Nucleobond AX	Macherey-Nagel, Düren, Germany
iQ SYBR Green Supermix	Bio-Rad, München, Germany
In-Fusion® HD Cloning	Takara Bio USA, Inc.

6.1.5 Other materials

Name	Source
Aquapolymount	Polysciences Inc., Warrington, USA
Complete Mini (EDTA-free) Protease Inhibitor Cocktail	Roche, Basel, Switzerland
Coverslips	Thermo Fischer, Braunschweig, Germany

Fly vials	Greiner, Kremsmünster, Austria
GFP-Trap-Agarose	Chromotek, Martinsried, Germany
Nitrocellulose membrane Protran 0.45 μm NC	GE Healthcare Life Sciences, Little Chalfont, UK
PCR tubes	Brand, Wertheim, Germany
Ribolock RNase inhibitor	Thermo Fischer, Braunschweig, Germany
Whatman 3 mm blotting paper	GE Healthcare Life Sciences, Little Chalfont, UK

6.1.6 Antibodies

Primary antibodies

name	reactivity	Working concentration staining	Western blot	source
E-cadherin	rat		1:100	T. Uemura (Oda et al., 1993)
DCAD2(E-cadherin)	rat	1:50		DHSB T. Uemura (Oda et al., 1993)
DCAT1(α-Catenin)	rat	1:2000	1:2000	DHSB (Oda et al., 1993)
α-tubulin	mouse		1:250	Hybridoma bank B512
p-myosin II	rabbit		1:2000	Cell signaling
Myosin II	gp+ rabbit	Serum 1:2000		Purified by myself
GFP	rabbit		1:1000	Sigma
GFP	chichen	1:2000		Abcam
Narf	gp	1:500	1:5000	Maria Kriebel
Nup153	rabbit	1:500		

Dm0	mouse	1:250	
Dlg	mouse	1:100	Hybridoma bank
			(Parnas et al., 2001)
Dia	rabbit	1:1000	

Second antibodies

	Name	Dilution	Source
Staining	Alexa Fluor 488 /568/647 Goat-anti mouse IgG (H+L)		
	Alexa Fluor 488/568/647 Goat-anti rabbit IgG (H+L)	1:500	Invitrogen
	Alexa Fluor 488/568/647 Goat-anti guinea pig IgG (H+L)		
	Alexa Fluor 488/568/647 Goat-anti rat IgG (H+L)		
WB	IRDye® 680RD/800CW Goat anti-mouse IgG (H + L)		
	IRDye® 680RD/800CW Goat anti-rabbit IgG (H + L)	1:15000	LI-COR Biosciences
	IRDye® 680RD/800CW Goat anti-guinea Pig IgG (H + L)		
	IRDye® 680RD/800CW Goat anti-rat IgG (H + L)		

Booster DAPI

name	Dilution	Source
GFP-booster	1:500(2 μg/mL)	Invitrogen
DAPI	1:250	Sigma

6.1.7 Plasmids generated during my Ph.D.

Name	Description Source

PattB GFP Narf knock-in	Amplification Narf promoter region by PCR (MK84/92), vector (PattB GMR) digested with NotI and BglII. Introduction GFP site by infusion (MK97/95), the vector (PattB Narf genomic (-ATG)) was digested with BglII.
Genomic FO GFP-Narf WT	The GFP site was introduced by digest from Frt GFP, and the vector (PattB Narf Flipout (+ATG)) was digested with BglII and AP.
Genomic FO GFP-Narf H/R	Introduction point mutation *via* PCR (MK32/33). The PCR product was digested with DpnI, and the vector was digested by NdeI and NheI.
UASt-GFP-Narf WT	Amplification of GFP by in-fusion (MK103/104). The template (GFP Narf knock-in) vector pUASt attbB was digested with NotI and AP. Amplification of 5'UTR by in-fusion (MK105/106), template (pUASt attbB Narf), the vector was opened with XhoI.
UASt-GFP-Narf H/R	Amplification of GFP by infusion (MK103/104). The template (GFP Narf knock-in) vector pUASt attbB was digested with NotI and AP. Amplification of 5'UTR by infusion (MK105/106). The template (pUASt attbB Narf H/R) and vector were opened with XhoI.
Genomic GFP-Narf (ectopic)	Amplification of genomic Narf by infusion (na3/4). The vector (GFP Narf knockin) was cut with NotI and AP.
UASt-mCherry-Narf	Amplification of 5'UTR by infusion (na3/4). The template (UASt-GFP-Narf) and the vector (UASt-GFP-Narf) were digested with BglII to remove the 5'UTR and GFP.

	Amplification of mCherry by infusion (na7/8). The template (PCS2-mCherry), the vector was cut with BglII.
UASt-mCherry-Narf H/R	Amplification of 5'UTR by infusion (na3/4). The template (UASt-GFP-Narf H/R) and the vector (UASt-GFP-Narf H/R) were digested with BglII to remove the 5'UTR and GFP.
	Amplification of mCherry by infusion (na7/8). The template (PCS2-mCherry) and the vector were cut with BglII.
Genomic FO GFP-Narf WT (HR) ectopic (51D, 86Fb)	Amplification of upstream sequence by infusion (na19/20). The vector (Genomic FO GFP-Narf WT (HR)) was cut with SphI.

6.1.8 Primers

All oligonucleotides were ordered from Eurofins Genomics (Ebersberg, Germany).

Oligo name	Sequence (5'-3')	Description
na-1	CTTCAGTTGAGGTGGAACAGTT	Sequence for Narf H/R flies (forward primer between Extron 3 and 4)
na-2	TTGTCACTAATCTCACCCCG	Sequence for Narf H/R flies
na-3	CTTGCATGCAATGCGGCCGCCTAG CATGAAAACGAAACACATTG	Infusion forward primer for genomic GFP-Narf (ectopic) with Not1
na-4	TGCAGTGAGCCAAGCTATCGTCA AAACATAGCGGTAATTG	Infusion reverse primer for genomic GFP-Narf (ectopic)

na-5	TGGGAATTCGTTAACGCTTGGCTCACTGCAC	Infusion forward primer for Narf 5'UTR
na-6	ACTTCCAGTAGATCTGGTTTTCGTAATAAATAATATTTAAC	Infusion for reverse primer for Narf 5'UTR
na-7	TTATTACGAAAACCAGATCTATGGTGAGCAAGGGCGAGG	Infusion forward primer for mCherry
na-8	GAACTTCCAGTAGATCTGTACAGCTCGTCCATGCC	Infusion reverse primer for mCherry
na-9	CCAAACCGCTTTCTGAACTT	Colony pcr primer for Narf 5'UTR
na-10	CTACGACGCTGAGGTCAAG	Forward primer for mCherry
na-11	CTTCGTATAGCATACATTATACGAAG	Reserve primer for loxp
na-12	GCCACTGACCCCAAACAAC	Forward primer 25C6
na-13	CTCGCAATTCTTCTCGCAG	Reserve primer 25C6
na-14	TGTGTATGATTGTCGCTCTCCT	Forward primer 55C4
na-15	CCAGTGTGTGCGATGTAAGC	Reserve primer 55C4
na-16	AACTGTTCCACCTCAACTGAAG	Sequence
na-17	CCCTTAGCATGTCCGTGG	A forward primer in 3p-element (PCR for attb and Frt sites)
na-18	CAGCGAGTGGAAATGCGAAC	Sequencing primer
na-19	CGAATTCTTGCATGCGGGAATTGGGAATTCGTTAAC	Infusion forward primer for FO genomic Narf (ectopic) with SphI
na-20	TGCAGTGAGCCAAGCTATCGTCAAAACATAGCGGT	Infusion reverse primer for FO genomic Narf (ectopic)
na-22	GTACTCCACGAATTCATGTCCAAGGGCGAGGA	Infusion forward primer for Pattb-GMR-GFP

na-23	CGAAGTTATGGTACCTTACTTGTACAGCTCGTCCATGC	Infusion reverse primer for Pattb-GMR-GFP
na-24	CCGAAGACGAGGATAACGCATCC	E-cadherin q-PCR forward primer
na-25	CCGTTGTGTAGTCGTCGTAGATTCC	E-cadherin q-PCR reverse primer
na-50	CACGGAGTACGAGCTGAAG	Sequening primer for N617Q
na-51	TGCGTTTGGTCAAGACGC	Sequening primer for N617Q
N617Q	GACTGCTCGAGGATGCCAATACGAATACCGAGGTCATTGAGGTAAAGGCCGAAGACGAGGATAACGCATCCCAGATCCTATACAGCATTGAGAGCGGTAACGTGGGTGATGCCTTTAAGATTGGTCTTAAGACCGGCAAAATCACGGTCAACCAGAAGTTGGACTACGAAACGATCACGGAGTACGAGCTGAAGGTGCGTGCGTTCGATGGAATCTACGACGACTACACAACGGTGGTTATCAAAATTGAAGACGTGCAGGACAACCCGCCGGTGTTTAGCAGGACTACAGCGTCACCATTCTGGAGGAGACCACATATGACGACTG	Site (617) mutation of E-cadherin
HS390	CACCGGTATCGTTCTGGACT	Actin 5c q-PCR forward primer
HS391	AGGGCAACATAGCACAGCTT	Actin 5c q-PCR reverse primer
MK32	GAAAAGGTATCAAATTACAGATTTGTTGAGGTAATGGCC	Introduction point mutation
MK33	GGCCATTACCTCAACAAATCTGTAATTTGATACCTTTTC	Introduction point mutation

MK34	CGAGAAGACGCTATCTGGC	Sequencing primer
MK35	CATGGTAACGGGTGTGCAG	Sequencing primer
MK37	CCACACCTATCTGATAGCG	Sequencing primer
MK38	CGCTATCAGATAGGTGTGG	Sequencing primer
MK39	GCCAGATAGCGTCTTCTCG	Sequencing primer
MK40	CTGCACACCCGTTACCATG	Sequencing primer
MK44	GCGAGGTTAATGGCGTTGTAGC	Sequencing primer
MK45	CCTGCGCCAATGGAATATTTAGG	Sequencing primer
MK56	GATAAGGCAAGGTCAAAGACTGG	Sequencing primer
MK84	ATATAGCGGCCGCGCTTGGCTCAC TGCAC	Amplification of Narf promoter
MK88	TCGAATTGCCGGCTGTACAC	Sequencing primer
MK90	AACCCTTAGCATGTCCGTGG	Sequencing primer
MK91	GTACCTACCTCGACTGCTAC	Sequencing primer
MK92	ATATAAGATCTGGTTTTCGTAATAA ATAATATTTAAC	Amplification of Narf promoter
MK93	ATATAAGATCTTCGAGGTTGAGCA GAGCG	PCR primer
MK94	TACGAAAACCAGATCTATGTCCAA GGGCGAGGAG	PCR primer
MK95	TCAACCTCGAAGATCTCTTGTACA GCTCGTCCATGC	Introduction GFP site by infusion
MK96	ATATAAGATCTATGTCGAGGTTGA GCAGAGC	PCR primer
MK97	TACGAAAACCAGATCATGTCCAA GGGCGAGGAG	Introduction GFP site by infusion
MK98	CTGTACAAGAGATCTACTGGAAGT TCTGTTCCAG	Amplification of Narf
MK99	TCAACCTCGAAGATCTACCTCGCC	Amplification of Narf (colony

	GGAGCC	pcr)
MK100	TACGAAAACCAGATCTTCGAGGTT GAGCAGAGCGC	Amplification of Narf promoter by infusion (did not work)
MK101	GCGCCTCGAGACTAGTTGTTGAG CCATGTTACCACGC	Amplification of Narf promoter by infusion
MK102	TACGAAAACCAGATCTATGTCGAG GTTGAGCAGAGCG	Amplification of Narf promoter by infusion
MK103	AACAGATCTGCGGCCGCGCTTGG CTCACTGCACTAAA	Amplification of GFP by infusion
MK104	CCTCGAGCCGCGGCCGCACCTCG CCGGAGCCGGCG	Amplification of GFP by infusion
MK105	GCGGCCGCGCTCGAGTCGAGGTT GAGCAGAGCGC	Amplification of Narf 5'UTR
MK106	TAGAGGTACCCTCGAGTTTTTTTT TTTTTTTCTATTTTAT	Amplification of Narf 5'UTR
MK107	TTATGCTAGCGGATCCGGGAATTG GGAATTCGTTAACAC	
MK108	GAGCCAAGCGCGGCCGCTATCGT CAAAACATAGCGGTAATTG	
ZY22	CTGACCCTGAAGTTCATC	Sequencing primer for GFP
ZY78	TTGGATTTCACTGGAACTAGG	Sequencing primer (3'white)
ZY101	CGGCGCGGGTCTTGTAGTTG	Sequencing primer for GFP

6.1.9 Fly stocks

Name	Genotype	Source/Lab stocks number
OrR	+/+	Großhans/Wieschau

		's lab
E-Cad-GFP (K-in)	w; DE-Cadherin-GFP[k-in]; +/+; +/+	Huang et al., 2009
xit; E-Cad-GFP	w; *xit* [X-330], Frt [9-2, 18E] Flp122 {ry+}/FM7c;	Deqing Kong
Ovo 2R	yw hs-Flp[122]; ovoD Frt2R[G13] /Cyo, hs-hid;	J. Großhans
shg-α-catenin-GFP	yw; Frt G13 shg-alpha-cat-GFP	Yang Hong, Pittsburgh
Mat 67, 15	w; tub-Gal4-VP16{w+}[67]; tub-Gal4-VP16 {w+}[15]; +/+	St.Johnston/Cambridge
PhiX86Fb	P{ry [+t7.2]=hsp70-flp}1, y[1] w[*]; +/+; M{3xP3-RFP.attP}ZH-86Fb; M{vas-int.B}ZH-102D; +/+	Bloom. 23648 (Bischof et al., 2007)
PhiX51D	yw M{eGFP.vas-int.Dm}ZH-2A; M{RFP.attP}ZH-51D	Basler, Zürich
Src 42A CA	L447 w; Sp/CyO Dfd-GMR-nvYFP; P{w[+mC]=UAS-Src42A.CA}5	Tateno et al., Science. 2000 Förster and Luschnig.,2012
Src 42A DN	L458w?; UAS-Src42A.DN (K295M)/TM6b Dfd-GMR-nvYFP	Shindo et al., 2008
Rho1 CA	UAS::Rho1-V14 (CA)	7330 Greig, J.et al., 2020
Rho1 DN	UAS::Rho1-N19 (DN)	7328 Greig, J.et al., 2020
Rho GEF2	w; Frt[2R,G13]{w+} RhoGEF2[1.1]/CyO, hs-hid{w+}	Barrett et al., 1997
Rho GEF2 uni-E-cad GFP	w; Frt[2R,G13] RhoGEF2[04291]{ry+},	

ubi-E-CadGFP{w+}/CyO	
E-Cad-GFPF[112]	Deqing
E-Cad-GFPF[221]	Deqing
E-Cad-GFPF[122]	Deqing
E-Cad-GFPF[323]	Deqing
E-Cad-GFPF[211]	Na + Deqing
E-Cad-GFPF[330]	Na + Deqing
E-Cad-GFPF[010]	Na + Deqing
E-Cad-GFPF[003]	Na + Deqing
UASt-GFP-Narf WT(68A4)	Na
UASt-GFP-Narf H/R (68A4)	Na
UASt-mCherry-Narf WT (68A4)	Na
UASt-mCherry-Narf H/R (68A4)	Na
Genomic GFP-Narf (ectopic) (68A4, 86Fb, 51D)	Na
Genomic GFP-Narf knock-in (locus)	Na + Maria

6.2 Methods

6.2.1 DNA methods

Molecular cloning

All the molecular cloning methods were carried out following Sambrook and Russell's (2001) guidelines as well as the Grosshans' laboratory protocols unless otherwise stated.

Single-fly DNA preparation

Method 1: DNA purification by phenol/chloroform

(1) One single fly was ground in 30 μl of buffer A and centrifuged at 14,000 g for one minute.

(2) Removing the supernatant which contains RNA. Suspend the pellet (with nuclei) in

200 µl buffer A, centrifuge and discard the supernatant, and then resuspend the pellet in 18 µl buffer B with proteinase K (200 µg/ml).

(3) Incubate the sample at 37°C for 1 hour after adding 2 µl of 10% SDS.

(4) Add 3 µl of 3 M sodium chloride and 10 µl of phenol/chloroform, mix and centrifuge at 14,000 g for 1min.

(5) Transfer 20 µl of the upper phase to a new tube and mix it with 50 µl of 100% ethanol.

(6) Spin for 5 minutes and wash with 70% ethanol, then collect the pellet.

(7) Dry the DNA sample by speed-vac.

(8) Dissolve the pellet in 20 µl of ddH$_2$O.

add 1 µl proteinase K (20 mg/ml) to 100 µl buffer B (Add just before use)

Method 2: Single fly DNA prep for PCR

(1) Put one fly in a 0.5 ml tube and mash the fly for 5-10 seconds with a pipette tip containing 50 µl of SB.

(2) Incubate for 20-30 minutes at 25-37°C (or room temp).

(3) Inactivate the Proteinase K by heating it to 95°C for 1-2 minutes.

Note: 85° C heat inactivation allows longer fragments to be amplified-up to more than 9 kb with long PCR.

This DNA can be stored at 4°C for months.

Squishing Buffer:

Tris-HCl 10 mM (pH=8.2), EDTA 1 mM, NaCl 25 mM, Proteinase K 200 µg/mL.

This protocol can be found at:

http://francois.schweisguth.free.fr/protocols/Single_fly_DNA_prep.pdf.

Polymerase chain reaction (PCR)

Taq-polymerase and Pfus-polymerase were used to produce PCR reactions. The following chemicals were used in the following standard PCR procedures, each at a particular concentration.

Taq-polymerase was used for general reactions like colony PCR.

Forward primer (0.5 µM)	2.5 µl
Reverse primer (0.5 µM)	2.5 µl
dNTP mix (10 mM)	1 µl
Green Taq buffer 10x	5 µl
Taq-polymerase	0.5 µl (0.3 U/µl)
DNA template	50–200 ng
ad 50 ul	

Pfus-polymerase was used for high-fidelity PCR with high-proof reading activity.

Forward primer(0.5 µM)	2.5 µl
Reverse primer(0.5 µM)	2.5 µl
dNTP mix(10 mM)	1 µl
Plusion buffer 5x	10 µl
pfus-polymerase	0.15 µl
DNA template	50–200 ng
ad 50ul	

The following PCR program was used for general DNA amplification.

Initial denaturation	95°C	2 min
Denaturation	95°C	30 s
Annealing	55-60°C (Oligo specific) 1 min	
Extension	72°C	1 kb/min (Taq) 1kb/15-30s (Pfus)
	Repeat 2-4 for 25-35 cycles	
Final extension	72°C	10 min
Hold	4°C	∞

Site-directed mutagenesis

In-fusion cloning

Infusion cloning was performed following the Takara protocol.

DNA sequencing

DNA sequencing was carried out by Microsynth Seqlab.

6.2.2 RNA methods

Total RNA isolation by TRIzol reagent (Invitrogen)

(1) Frozen *Drosophila* embryos with liquid nitrogen.

(2) Add 800 µl of TRIzol reagent drop by drop and homogenize with a pestle in the Eppendorf tube.

(3) Incubate for 5 min at room temperature.

(4) Add 160 µl of chloroform, shake and incubate for 2-3 minutes at RT, and centrifuge at maximum speed for 15 minutes at 4°C.

(5) Transfer the upper aqueous phase to a clean tube and add 400 µl of isopropanol to precipitate the RNA.

(6) Mix well and incubate for 10 minutes at RT. Centrifuge at maximum speed for 10 minutes at 4°C.

(7) Wash the pellet with 75% Ethanol and nuclease-free water, and then centrifuge at maximum speed for 10 min at 4°C.

(8) Resuspend the pellet in nuclease-free water.

Reverse Transcription PCR (RT-PCR)

1 µl of oligo (dT) was added to 1 µg of RNA sample, which was then incubated for 10 minutes at 65°C. Add the remaining material after cooling quickly. Keep the samples at 55°C for 30 minutes after that, followed by 5 minutes at 85°C. The cDNA is ready for qRT-PCR analysis and can be stored at -20°C.

5x RT buffer	4 µl
Ribonucleotide inhibitor	0.5 µl
dNTP mix (10mM)	2 µl
Reverse Transcriptase (Roche)	0.5 µl

Quantitative real-time PCR (qRT-PCR)

The qPCR master mix was produced with the following ingredients. All qPCR reactions were carried out in the Bio-Rad 96-well plates.

SYBR green qPCR mix	12.5 µl
Forward primer	1.25 µl
Reverse primer	1.25 µl
nuclease-free water	8 µl
cDNA	2 µl

The following program was used to detect the E-cadherin mRNA.

Initial denaturation	95°C	3 min
Denaturation	95°C	10 s
Annealing	55-60°C (Oligo specific)	15 min
Extension	72°C	30 s
	Repeat 2-4 for 40 cycles	
Melting curve	55°C to 95°C (increment of 0.5°C) 10 s + plate read	

6.2.3 Biochemical methods

Zipper antibody production

Expression of the recombination protein GST-myosin II.

pGEX-Zip-6P1(Zipper, nonmuscle myosin II heavy chain, amino acids 959–1361) fusion plasmid (a gift from Jeffrey H. Thomas).

(1) pGEX-Zip-6P1 was transformed into the BL21DE (rosetta) E.coli expression strain.

(2) Select a single colony and incubate it in 100 ml of LB + ampicillin medium overnight at 37°C The culture usually reaches an OD600 = 3-5.

(3) Incubate 50 ml of LB + Amp (pre-warmed) with 5 ml (ratio = 1:100) of the fresh overnight culture and add 1 mM IPTG to induce protein expression, then shake for 1-4 hours, check OD, and take one sample per hour.

(4) Centrifuge at 5000 rpm for 1 min at RT. Suspend the cells in the Lämmli buffer.

(5) Cells are collected after 4 h by centrifugation. Suspend the cells with 5 ml of lysis buffer.

(6) Incubate on ice for 30 min. with lysozyme at 1 mg/ml and DNase. Sonicate 6 times for 10 seconds on ice until suspension becomes transparent (max power, 100% pulse).

(7) Then, spin for 20 min at 5000 rpm at 4°C, until the supernatant is a soluble component. Suspend the pellets with 5 ml of lysis buffer.

(8) Repeat the sonication, spin for 20 minutes at 4°C, discard the supernatant, suspend the pellet in 1 mL of Lämmli buffer, and store the samples at -20°C.

(9) Perform an SDS page to analyze the fraction.
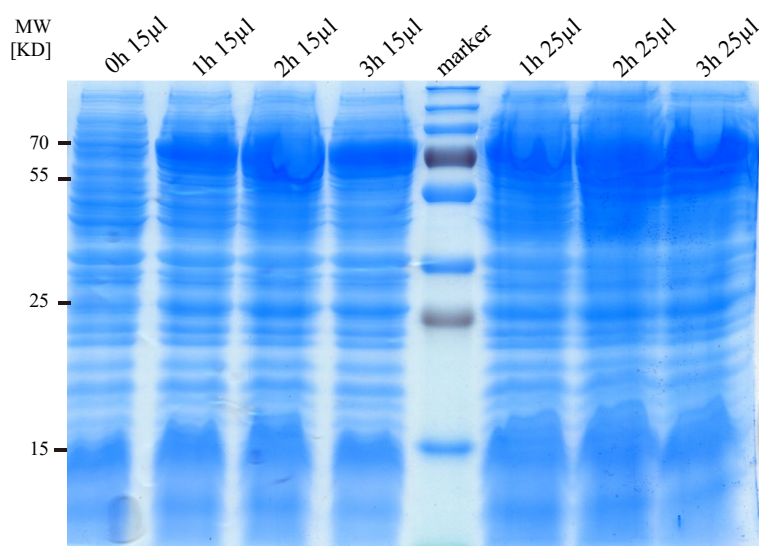
Figure 6.1: Zipper protein expression. Roti-blue quick staining of 0 to 3 hours cultured PGEX-Zip-6P1 with IPTG.

After the confirmation of the better purification conditions, a large-scale expression of PGEX-Zip-6P1 was further performed. (3 hours at 37°C, 1 mM IPTG, DNase, Lysozyme)

Purification of Recombinant proteins

All buffers were sterile-filtered before being chilled to 4°C. Before the purification, the Äkta was cleaned with sterile water, and the columns were adjusted using the lysis buffer.

(1) Load the samples (PGEX-Zip-6P1supernatant) into the super loop and connect them to the Äkta and get rid of air bubbles. Load the samples onto the GST column at a flow rate of 1 ml/min.

(2) Collect flow-through with 10 ml of centrifuge tubes (1-2 ml per tube).

(3) Then wash the column with washing buffer at a flow rate of 1 ml/min till the A280 does not change anymore.

(4) Elute using an elution at a flow rate of 1 ml/min and collect the fraction and put it on ice immediately.

(5) Wash the system with lysis buffer, ddH2O, and 20% ethanol. Put all the tubes into the buffer with 20% ethanol.
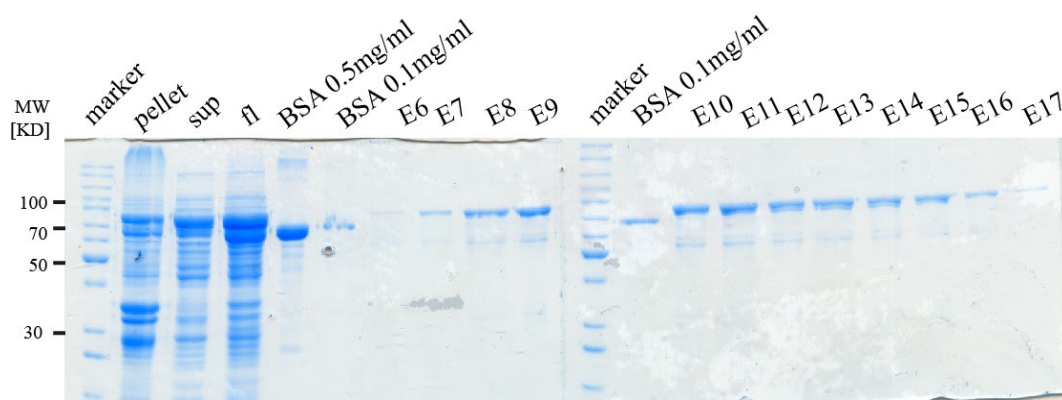
Figure 6.2: Zipper protein purification. Eluted pGEX-Zip-6P1 stained with Roti-blue.

Note: Prepare the Elution buffer just before use.

Buffer exchange and concentration

The eluted protein from the lysis buffer was transferred to PBS by a PD-10 column and concentrated at 1 mg/ml. This process is done at 4°C.

(1) Preparation of the PD-10 desalting column.

(2) Column equilibration with equilibration buffer, discard the flow-through.

(3) Add a maximum of 2.5 ml of samples to the column.

(4) Elute with PBS. The concentration of GST-Zipper protein is 1.05 mg/ml.

Antibody preparation

The GST-Zipper fusion protein was then sent to BioScience (Goettingen,

Germany) to produce polyclonal antibodies. I got rabbit anti-Zipper and guinea pig anti-Zipper final sera. Afterward, I did immunostaining to test the sera with heat-fixed overnight embryos.

Western blot

Sample preparation

(1) Staged embryos were collected and dechorionated with 50% Klorix for 90 seconds. And then frozen with liquid nitrogen quickly.

(2) Homogenize samples with a pestle. Add 2x Lämmli buffer and heat samples for 5 min at 95°C. And stored the samples at -20°C.

SDS-PAGE and transfer

(1) Load the samples (usually 30 embryos per 10 µl) together with a pre-stained protein marker onto an SDS-PAGE gel.

(2) Run the gel at 12 mA/gel until all samples go to the end of the stacking gel. Later, run the gel at 16 mA/gel until the target protein is nicely separated.

(3) Transfer the protein to an NC membrane by wet transfer at 4°C, overnight, 100 mA/membrane for E-cadherin protein.

(4) Block the membrane with 5% nonfat milk powder at RT for 1 h.

(5) Incubate with primary antibody for either 2 h at RT or overnight at 4°C, rinse and wash with PBT for 10 min, and repeat 4 times.

(6) Incubate with the second antibody at RT for 1 h, rinse and wash with PBT for 10 min, and repeat 4 times.

(7) Detect the signals with the Licor Odyssey Fc/DLx imaging system.

Co-immunoprecipitation (Co-IP) assay

(1) Generate a germline clone of *xit*, E-cadherinGFP flies.

(2) Collect 3-6 h embryos, dechorionated and weigh (1mg≈100 embryos), and store at -80°C after being spun and frozen in liquid nitrogen.

(3) Perform the following steps on the ice.

(4) Add one tablet of Roche protease inhibitor to 10 ml of lysis buffer.

(5) Homogenize embryos in lysis buffer with protease inhibitor using several (20-30) strokes in a Dounce homogenizer. (1 mL lysis buffer/10-100 mg embryos)

(6) Spin at 14,000rpm for 15 min at 4°C. Remove the lipids and place the supernatant in a fresh tube.

(7) At the same time, wash the GFP-Trap Agarose beads three times with lysis buffer for 1 min at 2,000 rpm at 4°C.

(8) Add the clear supernatant to the beads and incubate at 4°C for 1 h, rotating on a wheel.

(9) Centrifuge the beads at 2,000 rpm for 1 minute at 4°C, save the unbound material, and wash them five times with lysis buffer.

(10) Elute protein with 2x Lämmli buffer and boil it for 5 minutes at 95°C. Stored the samples at -20°C.

(11) Perform an SDS-PAGE and analyze the protein-protein interaction.

Extraction buffer

50 mM Tris/HCl (pH=7.6), 100 mM NaCl, 1% NP-40, 1% Triton X-100

The buffer was from (Oda et al., 1994).

PNGase F treatment

The experiment was performed according to the NEB PNGase protocol.

PNGase F can remove almost all *N*-linked oligosaccharides from glycoproteins.

(1) Collect staged and dechorionated embryos or homogenized Co-IP samples into lysis buffer.

 (120 µl glycoprotein + 13ul 10x glycoprotein denaturing buffer)

(2) Denatured glycoprotein by heating at 100°C for 10 minutes, Cooldown denatured glycoprotein on ice.

(3) Make a reaction as follows.

10X GlycoBuffer 2	20 µl
10% NP-40	20 µl
sample	133 µl
ddh$_2$O	27 µl

Divide the sample into two parts, one with PNGase F and the other as a control.

(4) Add 1 μl of PNGase F, and mix gently.

(5) Incubate at 37°C for one hour.

(6) Analyzed by SDS-PAGE.

For the Co-IP sample, I first did the Co-IP experiment with GFP-Trap Agarose beads, then I separated them into two samples, one of which was treated with PNGase, and the other was the control.

Mass spectrum (MS) analysis

The MS analysis was carried out by the core facility for mass spectrometry and elemental analysis, chemistry department, Marburg University.

6.2.4 Fly methods

Formaldehyde fixation of embryos

(1) Collect staged embryos, dechorionated with 100% of bleach for 90 s, rinse with tap water, and get rid of water by dipping the net onto a piece of paper.

(2) Transfer embryos to a scintillation vial containing 5 ml heptanes, 4.5 ml PBS, and 0.5 ml of 37% formaldehyde. Shake vigorously for 20 minutes.

(3) Remove the lower layer and add 5 ml of methanol. Shake constantly for 30 seconds.

(4) Collect sinking embryos and transfer them into a new tube.

(5) The samples were washed three times with methanol and stored at -20°C.

Heat fixation of embryos

(1) Heat 3 ml of the salt buffer in a dry bath in advance.

(2) Transfer embryos to a scintillation vial and boil the sample for 10 s.

(3) Add some ice pieces immediately and put the vial on the ice.

(4) Gently discard the salt buffer, add 5 ml of heptane and 5 ml of methanol, and shake constantly.

(5) Harvest the embryos and wash them with methanol several times.

(6) Store the embryos at -20°C.

Salt buffer: 0.4% NaCl, 0.03% Triton X-100

Collect specific early-staged embryos.

Fix the embryos in the first three steps of the heat fixation method. Transfer the embryos onto a piece of apple juice agar and pick the specific stage embryos separately (stage 5, 6, 8 OrR embryos).

Staining

(1) Wash the samples with 0.1% PBT.

(2) Blocking. Incubate with 5% BSA for 1 h.

(3) First antibody incubation. A specific concentration of the first antibody should be incubated for 2 hours at RT, or 4°C overnight.

(4) Rinse with PBT and wash three times.

(5) Second antibody incubation. Incubate for 1 hour at RT.

(6) Rinse with PBT and wash three times.

(7) DAPI staining for 7 minutes at room temperature.

(8) Rinse with PBT and wash three times.

(9) Mount with one drop of aqua-poly-mount or Mowiol medium.

For F-actin staining, hand peeling needs to be done. Afterward, the embryos were covered in PBT and adhered to the double-sided tape. With the aid of a needle, the vitelline membrane was removed. Then the embryos were ready for staining and could be kept in PBT at 4°C for a short time.

LysoTracker^{TM}DND-99 staining

(1) Collect imaginal disks of 3rd larvae in 190 µl of PBS on ice.

(2) Incubate with 10 µl of LysoTracker^{TM}DND-99 (final concentration 50 µM) on ice for 5 minutes in the dark.

(3) Rinse samples three times with PBS.

(4) Fix the wing discs with 4% PFA.

(5) Continue with the normal staining procedure.

Note: all buffers should be in PBS (not with TritonX-100!)

Cuticle preparation

(1) Keep overnight embryos of E-cadherin with 5 *N*-glycosylation mutants and E-cadherin GFP knock-in flies, and let them develop for another day.

(2) Collect the embryos of each and perform dechlorination.

(3) Transfer the embryos to a slide with one drop of Hoyer's mountant (with 1:1 Hoyer's and lactic acid).

(4) Cover the slide with a clean coverslip and incubate the slide overnight at 60°C.

Generation of transgenic flies

Site-specific insertion of transgenes was generated using the attB/phi-C31 system. This method has high integration efficiency. It is better to cross out the phi-C31 integrase after selecting the transgenes.

(1) Generate the target plasmid and dilute it to 0.1-0.2 μg/μl.

(2) Amplify the Pattb fly line (Pattb-86Fb) and prepare a big cage with newly hatched adults. Afterward, feed the flies with yeast and put the cage into the 25°C incubators. Change the apple juice plate frequently to synchronize embryos.

(3) Collect staged pre-blastoderm embryos, dechorionated with 50% of bleach for 90 s, and remove the bleach completely.

(4) Line up the embryos on a piece of apple juice agar. Do not roll the embryos.

(5) Glue the embryos to a covered slide with glue with heptane.

(6) Dry for 10 minutes in a desiccation chamber and cover the embryos with 10S voltalef oil.

(7) Load the plasmid into an opened needle and inject the plasmid with 10 x objective.

(8) Put the slide into an 18°C incubator and cover it with some wet paper. Collect the hatched flies.

(9) Cross the flies with w⁻ flies and collect the hatched flies with red eyes.

(10) Cross the single F1 fly with the red eye with the selected balancer. Females need one more cross to remove the phi-C31 integrase.

Fly genetics and generating germline clones

Germline clones were generated based on Chou and Perrimon, 1992. Heat shocks

were applied to the 1st and 2nd larval at 37°C for an hour to activate Flippase.

To generate the maternal mutation, *xit*, E-Cad GFP FRT or Rho GEF FRT, F323/Cyo twist GFP flies were crossed with ovoD E-Cad GFP and ovoD FRT2R separately. These flies carry a flippase that can be activated by heat shock, and the flippase induces mitotic recombination which leads to a homozygous mutation in the female germline cells (Chou and Perrimon, 1992). Female sterility is caused by the ovoD mutation (Chou et al., 1993).

6.2.5 Microscope methods

Imaging of fixed embryos

Fixed embryos were stained with different antibodies and dyes (phalloidin) and imaged by an LSM980 microscope with a 63x oil objective. E-cadherin clusters were recorded by the Airyscan joint deconvolution system with Z stacks (0.17 μm) and have a size of 1024x1024 pixels. Images were segmented by a tissue-analysis plugin and measured the intensity and plot profile of each junction of E-cadherin in WT and mutants. The variance of each junction was measured in different mutants.

Live imaging

Live imaging of E-cad GFP embryos and other *N*-glycosylated E-cadherin mutants was recorded by an LSM980 confocal microscope with a Zeiss 63x oil-immersion objective (NA = 1.4). Images were captured with a frame size of 512x512 pixels (or 1024x1024) and a 1 μm interval of Z-stacks. Images were segmented with Ilastik /EDGE (Gelbart et al., 2012; Sommer et al., 2011) or maximum intensity projection was performed by Fiji.

Fluorescence recovery after photobleaching (FRAP)

FRAP experiments were performed with an LSM980 confocal microscope with a Zeiss 63x oil-immersion objective (NA=1.4) at room temperature. E-cad GFP WT and F112, F221, F112, F323, *xit* (E-cad GFP knock-in with some glycosylation mutants) embryos were bleaching with 50% of 488 laser intensity with 20 iterations at the 1-second interval at a scan speed of 5. Narrow rectangular ROIs were drawn across the

center of single junctions and this region was ablated. Imaging was started 2 pictures before bleaching and images were captured with a frame size of 512x512 pixels for 2 minutes periods. To measure fluorescence intensities, fluorescence recovery after photobleaching data without focus drift was selected. The fluorescence intensity of the bleaching region of interest (ROI) was measured by Fiji/Image J manually (line width = 6) and normalized. (Normalized intensity: $I = (It - Imin)/(Imax - Imin)$, it represents the intensity at time t, Imin represents the intensity at time 0 and Imax represents the intensity before bleaching.) Afterward, a fitting was performed by nonlinear regression and one phase decay analysis by GraphPad Prism, the mobile fraction was calculated, and half time is the time where the half-maximum intensity was recovered.

Laser ablation

Junctional recoil can be measured by nano-ablation of single junctions. The *Drosophila* embryonic epidermis is especially suited for *in vivo* research on tissue compression. (Greig and Bulgakova, 2020). E-cad GFP, F112, F122, F221, F323, and *xit* staged embryos were collected and dechorionated as mentioned above. Embryos were lined with the following orientation on the apple juice plate and transferred to a 22 mmx22 mm coverslip. The coverslip was attached to a metal slide, and the embryos were immersed in 10s oil before imaging. Laser ablation experiments were performed with an LSM980 confocal microscope with a Zeiss 63x oil-immersion objective (NA = 1.4) and REO-SysCon-Zen system at room temperature. An image of 512x512 pixels resolution with 2x averaging was used. The vertex displacement was measured by Fiji/Image J manually by the distance between the vertices at the ends of ablated junctions and pre-ablation length. And the fitting was done by GraphPad Prism according to (Liang et al., 2016).

6.3 Software

Adobe Illustrator CS6	Adobe, San Jose, USA.
Adobe Photoshop CS6	Adobe, San Jose, USA.
Affinity designer 2020	Serif Europe, West Bridgford, UK

Affinity photo2020	Serif Europe, West Bridgford, UK
Excel	Microsoft, Redmond, USA
Fiji-Image J	NIH, Bethesda, USA
GraphPad Prism 8	GraphPad Software, Inc
Image Studio	LI-COR Biosciences
Powerpoint	Microsoft, Redmond, USA
REO-SysCon-Zen	Rapp OptoElectronic, Wedel, Germany
SeqBuilder	DNASTAR, Madison, USA
SnapGene	GSL Biotech LLC, Chicago, USA
word	Microsoft, Redmond, USA
Zen- blue	Carl Zeiss, Jena, Germany

6.4 Microscopes

LSM780/ LSM980		Carl Zeiss, Jena, Germany.
	Detectors	PMT
		AiryScan
Microinjection microscope		Carl Zeiss, Jena, Germany
ROS-SysCon-Zen (Rapp OptoElectonic)		Carl Zeiss, Jena, Germany

6.5 Equipment

Akta pure	GE healthcare
Centrifuges	Eppendorf
NanoDrop 2000c	Thermo Scientific
Odyssey DLx imaging system	LI-COR Biosciences
Odyssey XF imaging system	LI-COR Biosciences

qPCR machine	Bio-Rad Laboratories
Trans-Blot® SD Semi-Dry Transfer	Bio-Rad Laboratories
Cell	Bio-Rad Laboratories
Mini Trans-Blot® Cell	Bio-Rad Laboratories

7. Reference

Abe, K., and Takeichi, M. (2008). EPLIN mediates linkage of the cadherin–catenin complex to F-actin and stabilizes the circumferential actin belt. Proceedings of the National Academy of Sciences 105, 13-19.

Aberle, H., Butz, S., Stappert, J., Weissig, H., Kemler, R., and Hoschuetzky, H. (1994). Assembly of the cadherin-catenin complex in vitro with recombinant proteins. Journal of cell science 107, 3655-3663.

Adams, B.M., Oster, M.E., and Hebert, D.N. (2019). Protein quality control in the endoplasmic reticulum. The protein journal 38, 317-329.

Angst, B.D., Marcozzi, C., and Magee, A.I. (2001). The cadherin superfamily: diversity in form and function. Journal of cell science 114, 629-641.

Araki, K., and Nagata, K. (2011). Protein folding and quality control in the ER. Cold Spring Harbor perspectives in biology 3, a007526.

Arboleda-Estudillo, Y., Krieg, M., Stühmer, J., Licata, N.A., Muller, D.J., and Heisenberg, C.-P. (2010). Movement directionality in collective migration of germ layer progenitors. Current Biology 20, 161-169.

Avizienyte, E., Fincham, V.J., Brunton, V.G., and Frame, M.C. (2004). Src SH3/2 domain-mediated peripheral accumulation of Src and phospho-myosin is linked to deregulation of E-cadherin and the epithelial-mesenchymal transition. Molecular biology of the cell 15, 2794-2803.

Bertet, C., Sulak, L., and Lecuit, T. (2004). Myosin-dependent junction remodelling controls planar cell intercalation and axis elongation. Nature 429, 667-671.

Biswas, K.H. (2020). Molecular mobility-mediated regulation of E-cadherin adhesion. Trends in biochemical sciences 45, 163-173.

Blankenship, J.T., Backovic, S.T., Sanny, J.S., Weitz, O., and Zallen, J.A. (2006). Multicellular rosette formation links planar cell polarity to tissue morphogenesis. Developmental cell 11, 459-470.

Boller, K., Vestweber, D., and Kemler, R. (1985). Cell-adhesion molecule uvomorulin is localized in the intermediate junctions of adult intestinal epithelial cells. The Journal of cell biology 100, 327-332.

Bosveld, F., Bonnet, I., Guirao, B., Tlili, S., Wang, Z., Petitalot, A., Marchand, R., Bardet, P.-L., Marcq, P., and Graner, F. (2012). Mechanical control of morphogenesis by Fat/Dachsous/Four-jointed planar cell polarity pathway. Science (New York, NY) 336, 724-727.

Brockhausen, I., Narasimhan, S., and Schachter, H. (1988). The biosynthesis of highly branched N-glycans: studies on the sequential pathway and functional role of N-actylglucosaminyltransferases I, II, III, IV, V and VI. Biochimie 70, 1521-1533.

Burda, P., and Aebi, M. (1998). The ALG10 locus of Saccharomyces cerevisiae encodes the α-1, 2 glucosyltransferase of the endoplasmic reticulum: the terminal glucose of the lipid-linked oligosaccharide is required for efficient N-linked glycosylation. Glycobiology 8, 455-462.

Butler, L.C., Blanchard, G.B., Kabla, A.J., Lawrence, N.J., Welchman, D.P., Mahadevan, L., Adams, R.J., and Sanson, B. (2009). Cell shape changes indicate a role for extrinsic tensile forces in Drosophila germ-band extension. Nature cell biology 11, 859-864.

Carvalho, S., Catarino, T., Dias, A., Kato, M., Almeida, A., Hessling, B., Figueiredo, J., Gärtner, F., Sanches, J., and Ruppert, T. (2016). Preventing E-cadherin aberrant N-glycosylation at Asn-554 improves its critical function in gastric cancer. Oncogene 35, 1619-1631.

Cavey, M., and Lecuit, T. (2009). Molecular bases of cell–cell junctions stability and dynamics. Cold Spring Harbor perspectives in biology 1, a002998.

Cavey, M., Rauzi, M., Lenne, P.-F., and Lecuit, T. (2008). A two-tiered mechanism for stabilization and immobilization of E-cadherin. Nature 453, 751-756.

Chen, C.-L., Wang, S.-H., Chan, P.-C., Shen, M.-R., and Chen, H.-C. (2016). Phosphorylation of E-cadherin at threonine 790 by protein kinase Cδ reduces β-catenin binding and suppresses the function of E-cadherin. Oncotarget 7, 37260.

Chihara, D., and Nance, J. (2012). An E-cadherin-mediated hitchhiking mechanism for C. elegans germ cell internalization during gastrulation. Development (Cambridge, England) 139, 2547-2556.

Choi, C.K., Vicente-Manzanares, M., Zareno, J., Whitmore, L.A., Mogilner, A., and Horwitz, A.R. (2008). Actin and α-actinin orchestrate the assembly and maturation of nascent adhesions in a myosin II motor-independent manner. Nature cell biology 10, 1039-1050.

Chou, T.-B., Noll, E., and Perrimon, N. (1993). Autosomal P [ovoD1] dominant female-sterile insertions in Drosophila and their use in generating germ-line chimeras. Development (Cambridge, England) 119, 1359-1369.

Chou, T.-B., and Perrimon, N. (1992). Use of a yeast site-specific recombinase to produce female germline chimeras in Drosophila. Genetics 131, 643-653.

Collinet, C., and Lecuit, T. (2013). Stability and dynamics of cell–cell junctions. Progress in molecular biology and translational science 116, 25-47.

Cremo, C.R., and Geeves, M.A. (1998). Interaction of actin and ADP with the head domain of smooth muscle myosin: implications for strain-dependent ADP release in smooth muscle. Biochemistry 37, 1969-1978.

da Silva, S.M., and Vincent, J.-P. (2007). Oriented cell divisions in the extending germband of Drosophila.

Datta, S., Modak, D., Sarkar, S., Saha, B., and Mukhopadhyay, S. (2015). Identification and glycobiological characterization of circulating immune complexes in patients with visceral leishmaniasis and post kala azar dermal leishmaniasis.

de Beco, S., Gueudry, C., Amblard, F., and Coscoy, S. (2009). Endocytosis is required for E-cadherin redistribution at mature adherens junctions. Proceedings of the National Academy of Sciences 106, 7010-7015.

dos Santos, G., Schroeder, A.J., Goodman, J.L., Strelets, V.B., Crosby, M.A., Thurmond, J., Emmert, D.B., Gelbart, W.M., and Consortium, F. (2015). FlyBase: introduction of the Drosophila melanogaster Release 6 reference genome assembly and large-scale migration of genome annotations. Nucleic acids research 43, D690-D697.

Drees, F., Pokutta, S., Yamada, S., Nelson, W.J., and Weis, W.I. (2005). α-catenin is a molecular switch that binds E-cadherin-β-catenin and regulates actin-filament assembly. Cell 123, 903-915.

Ellgaard, L., and Helenius, A. (2003). Quality control in the endoplasmic reticulum. Nature reviews Molecular cell biology 4, 181-191.

Engl, W., Arasi, B., Yap, L., Thiery, J., and Viasnoff, V. (2014). Actin dynamics modulate mechanosensitive immobilization of E-cadherin at adherens junctions. Nature cell biology 16, 584-591.

Etienne-Manneville, S., and Hall, A. (2002). Rho GTPases in cell biology. Nature 420, 629-635.

Förster, D., and Luschnig, S. (2012). Src42A-dependent polarized cell shape changes mediate epithelial tube elongation in Drosophila. Nature cell biology 14, 526-534.

Foty, R.A., and Steinberg, M.S. (2005). The differential adhesion hypothesis: a direct evaluation. Developmental biology 278, 255-263.

Galbraith, C.G., Yamada, K.M., and Galbraith, J.A. (2007). Polymerizing actin fibers position integrins

primed to probe for adhesion sites. Science (New York, NY) 315, 992-995.

Galbraith, C.G., Yamada, K.M., and Sheetz, M.P. (2002). The relationship between force and focal complex development. The Journal of cell biology 159, 695-705.

Gayrard, C., and Borghi, N. (2016). FRET-based molecular tension microscopy. Methods 94, 33-42.

Gelbart, W.M., Ben-Shaul, A., and Roux, D. (2012). Micelles, membranes, microemulsions, and monolayers (Springer Science & Business Media).

Gheisari, E., Aakhte, M., and Müller, H.-A.J. (2020). Gastrulation in Drosophila melanogaster: Genetic control, cellular basis and biomechanics. Mechanisms of development 163, 103629.

Godt, D., and Tepass, U. (1998). Drosophila oocyte localization is mediated by differential cadherin-based adhesion. Nature 395, 387-391.

Gomez, G.A., McLachlan, R.W., Wu, S.K., Caldwell, B.J., Moussa, E., Verma, S., Bastiani, M., Priya, R., Parton, R.G., and Gaus, K. (2015). An RPTPα/Src family kinase/Rap1 signaling module recruits myosin IIB to support contractile tension at apical E-cadherin junctions. Molecular biology of the cell 26, 1249-1262.

Grashoff, C., Hoffman, B.D., Brenner, M.D., Zhou, R., Parsons, M., Yang, M.T., McLean, M.A., Sligar, S.G., Chen, C.S., and Ha, T. (2010). Measuring mechanical tension across vinculin reveals regulation of focal adhesion dynamics. Nature 466, 263-266.

Greig, J., and Bulgakova, N.A. (2020). Interplay between actomyosin and E-cadherin dynamics regulates cell shape in the Drosophila embryonic epidermis. Journal of cell science 133, jcs242321.

Großhans, J.r., Wenzl, C., Herz, H.-M., Bartoszewski, S., Schnorrer, F., Vogt, N., Schwarz, H., and Müller, H.-A. (2005). RhoGEF2 and the formin Dia control the formation of the furrow canal by directed actin assembly during Drosophila cellularisation.

Guillot, C., and Lecuit, T. (2013a). Adhesion disengagement uncouples intrinsic and extrinsic forces to drive cytokinesis in epithelial tissues. Developmental cell 24, 227-241.

Guillot, C., and Lecuit, T. (2013b). Mechanics of epithelial tissue homeostasis and morphogenesis. Science (New York, NY) 340, 1185-1189.

Gumbiner, B.M. (2005). Regulation of cadherin-mediated adhesion in morphogenesis. Nature reviews Molecular cell biology 6, 622-634.

Halbleib, J.M., and Nelson, W.J. (2006). Cadherins in development: cell adhesion, sorting, and tissue morphogenesis. Genes & development 20, 3199-3214.

Hanna, S., and El-Sibai, M. (2013). Signaling networks of Rho GTPases in cell motility. Cellular signalling 25, 1955-1961.

Harris, T.J., and Peifer, M. (2004). Adherens junction-dependent and-independent steps in the establishment of epithelial cell polarity in Drosophila. The Journal of cell biology 167, 135-147.

Harrison, O.J., Jin, X., Hong, S., Bahna, F., Ahlsen, G., Brasch, J., Wu, Y., Vendome, J., Felsovalyi, K., and Hampton, C.M. (2011). The extracellular architecture of adherens junctions revealed by crystal structures of type I cadherins. Structure 19, 244-256.

Hartenstein, V., and Campos-Ortega, J.A. (1985). Fate-mapping in wild-typeDrosophila melanogaster. Wilhelm Roux's archives of developmental biology 194, 181-195.

Hayashi, T., and Carthew, R.W. (2004). Surface mechanics mediate pattern formation in the developing retina. Nature 431, 647-652.

Hazan, R.B., Kang, L., Roe, S., Borgen, P.I., and Rimm, D.L. (1997). Vinculin is associated with the E-cadherin adhesion complex. Journal of Biological Chemistry 272, 32448-32453.

Heisenberg, C.-P., and Bellaïche, Y. (2013). Forces in tissue morphogenesis and patterning. Cell 153,

948-962.

Helenius, A., and Aebi, M. (2004). Roles of N-linked glycans in the endoplasmic reticulum. Annual review of biochemistry 73, 1019-1049.

Hoffman, B.D., and Yap, A.S. (2015). Towards a dynamic understanding of cadherin-based mechanobiology. Trends in cell biology 25, 803-814.

Hong, S., Troyanovsky, R.B., and Troyanovsky, S.M. (2010). Spontaneous assembly and active disassembly balance adherens junction homeostasis. Proceedings of the National Academy of Sciences 107, 3528-3533.

Huang, J., Zhou, W., Dong, W., Watson, A.M., and Hong, Y. (2009). Directed, efficient, and versatile modifications of the Drosophila genome by genomic engineering. Proceedings of the National Academy of Sciences 106, 8284-8289.

Hulpiau, P., and Van Roy, F. (2009). Molecular evolution of the cadherin superfamily. The international journal of biochemistry & cell biology 41, 349-369.

Hyafil, F., Babinet, C., and Jacob, F. (1981). Cell-cell interactions in early embryogenesis: a molecular approach to the role of calcium. Cell 26, 447-454.

Hyafil, F., Morello, D., Babinet, C., and Jacob, F. (1980). A cell surface glycoprotein involved in the compaction of embryonal carcinoma cells and cleavage stage embryos. Cell 21, 927-934.

Imamura, Y., Itoh, M., Maeno, Y., Tsukita, S., and Nagafuchi, A. (1999). Functional domains of α-catenin required for the strong state of cadherin-based cell adhesion. The Journal of cell biology 144, 1311-1322.

Indra, I., Choi, J., Chen, C.-S., Troyanovsky, R.B., Shapiro, L., Honig, B., and Troyanovsky, S.M. (2018). Spatial and temporal organization of cadherin in punctate adherens junctions. Proceedings of the National Academy of Sciences 115, E4406-E4415.

Ioffe, E., and Stanley, P. (1994). Mice lacking N-acetylglucosaminyltransferase I activity die at mid-gestation, revealing an essential role for complex or hybrid N-linked carbohydrates. Proceedings of the National Academy of Sciences 91, 728-732.

Irvine, K.D., and Wieschaus, E. (1994). Cell intercalation during Drosophila germband extension and its regulation by pair-rule segmentation genes. Development (Cambridge, England) 120, 827-841.

Jamal, B.T., Nita-Lazar, M., Gao, Z., Amin, B., Walker, J., and Kukuruzinska, M.A. (2009). N-glycosylation status of E-cadherin controls cytoskeletal dynamics through the organization of distinct β-catenin-and γ-catenin-containing AJs. Cell health and cytoskeleton 2009, 67.

Jamora, C., and Fuchs, E. (2002). Intercellular adhesion, signalling and the cytoskeleton. Nature cell biology 4, E101-E108.

Kale, G.R., Yang, X., Philippe, J.-M., Mani, M., Lenne, P.-F., and Lecuit, T. (2018). Distinct contributions of tensile and shear stress on E-cadherin levels during morphogenesis. Nature communications 9, 1-16.

Kametani, Y., and Takeichi, M. (2007). Basal-to-apical cadherin flow at cell junctions. Nature cell biology 9, 92-98.

Kardash, E., Reichman-Fried, M., Maître, J.-L., Boldajipour, B., Papusheva, E., Messerschmidt, E.-M., Heisenberg, C.-P., and Raz, E. (2010). A role for Rho GTPases and cell–cell adhesion in single-cell motility in vivo. Nature cell biology 12, 47-53.

Katsumi, A., Milanini, J., Kiosses, W.B., del Pozo, M.A., Kaunas, R., Chien, S., Hahn, K.M., and Schwartz, M.A. (2002). Effects of cell tension on the small GTPase Rac. The Journal of cell biology 158, 153-164.

Keller, R. (2006). Mechanisms of elongation in embryogenesis.

Kerridge, S., Munjal, A., Philippe, J.-M., Jha, A., De Las Bayonas, A.G., Saurin, A.J., and Lecuit, T. (2016). Modular activation of Rho1 by GPCR signalling imparts polarized myosin II activation during morphogenesis. Nature cell biology 18, 261-270.

Kiehart, D.P., Galbraith, C.G., Edwards, K.A., Rickoll, W.L., and Montague, R.A. (2000). Multiple forces contribute to cell sheet morphogenesis for dorsal closure in Drosophila. The Journal of cell biology 149, 471-490.

Kong, D., and Großhans, J. (2020). Planar Cell Polarity and E-Cadherin in Tissue-Scale Shape Changes in Drosophila Embryos. Frontiers in Cell and Developmental Biology, 1710.

Kong, D., Wolf, F., and Großhans, J. (2017). Forces directing germ-band extension in Drosophila embryos. Mechanisms of development 144, 11-22.

Kornfeld, R., and Kornfeld, S. (1985). Assembly of asparagine-linked oligosaccharides. Annual review of biochemistry 54, 631-664.

Kovács, M., Thirumurugan, K., Knight, P.J., and Sellers, J.R. (2007). Load-dependent mechanism of nonmuscle myosin 2. Proceedings of the National Academy of Sciences 104, 9994-9999.

Krzic, U., Gunther, S., Saunders, T.E., Streichan, S.J., and Hufnagel, L. (2012). Multiview light-sheet microscope for rapid in toto imaging. Nature methods 9, 730-733.

Kuribara, T., and Totani, K. (2021). Structural insights into N-linked glycan-mediated protein folding from chemical and biological perspectives. Current opinion in structural biology 68, 41-47.

Larue, L., Ohsugi, M., Hirchenhain, J., and Kemler, R. (1994). E-cadherin null mutant embryos fail to form a trophectoderm epithelium. Proceedings of the National Academy of Sciences 91, 8263-8267.

Lecuit, T., Lenne, P.-F., and Munro, E. (2011). Force generation, transmission, and integration during cell and tissue morphogenesis. Annual review of cell and developmental biology 27, 157-184.

Lecuit, T., and Yap, A.S. (2015). E-cadherin junctions as active mechanical integrators in tissue dynamics. Nature cell biology 17, 533-539.

Leptin, M. (1999). Gastrulation in Drosophila: the logic and the cellular mechanisms. The EMBO journal 18, 3187-3192.

Levayer, R., Pelissier-Monier, A., and Lecuit, T. (2011). Spatial regulation of Dia and Myosin-II by RhoGEF2 controls initiation of E-cadherin endocytosis during epithelial morphogenesis. Nature cell biology 13, 529-540.

Liang, X., and Gomez, G.A. (2015). Current perspectives on cadherin-cytoskeleton interactions and dynamics. Cell Health and Cytoskeleton 7, 11-24.

Liang, X., Michael, M., and Gomez, G.A. (2016). Measurement of mechanical tension at cell-cell junctions using two-photon laser ablation. Bio-protocol 6, e2068-e2068.

Lien, W.-H., Klezovitch, O., and Vasioukhin, V. (2006). Cadherin–catenin proteins in vertebrate development. Current opinion in cell biology 18, 499-506.

Liu, W., Kovacevic, Z., Peng, Z., Jin, R., Wang, P., Yue, F., Zheng, M., Huang, M.L., Jansson, P.J., and Richardson, V. (2015). The molecular effect of metastasis suppressors on Src signaling and tumorigenesis: new therapeutic targets. Oncotarget 6, 35522.

Liu, Z., Tan, J.L., Cohen, D.M., Yang, M.T., Sniadecki, N.J., Ruiz, S.A., Nelson, C.M., and Chen, C.S. (2010). Mechanical tugging force regulates the size of cell–cell junctions. Proceedings of the National Academy of Sciences 107, 9944-9949.

Liwosz, A., Lei, T., and Kukuruzinska, M.A. (2006). N-glycosylation affects the molecular organization and stability of E-cadherin junctions. Journal of Biological Chemistry 281, 23138-23149.

Müller, H., and Wieschaus, E. (1996). armadillo, bazooka, and stardust are critical for early stages in formation of the zonula adherens and maintenance of the polarized blastoderm epithelium in Drosophila. The Journal of cell biology 134, 149-163.

Maître, J.-L., and Heisenberg, C.-P. (2013). Three functions of cadherins in cell adhesion. Current Biology 23, R626-R633.

Marinari, E., Mehonic, A., Curran, S., Gale, J., Duke, T., and Baum, B. (2012). Live-cell delamination counterbalances epithelial growth to limit tissue overcrowding. Nature 484, 542-545.

Martin, A.C., Gelbart, M., Fernandez-Gonzalez, R., Kaschube, M., and Wieschaus, E.F. (2010). Integration of contractile forces during tissue invagination. Journal of Cell Biology 188, 735-749.

Mateja, A., Szlachcic, A., Downing, M.E., Dobosz, M., Mariappan, M., Hegde, R.S., and Keenan, R.J. (2009). The structural basis of tail-anchored membrane protein recognition by Get3. Nature 461, 361-366.

Matsuyoshi, N., Hamaguchi, M., Taniguchi, S.i., Nagafuchi, A., Tsukita, S., and Takeichi, M. (1992). Cadherin-mediated cell-cell adhesion is perturbed by v-src tyrosine phosphorylation in metastatic fibroblasts. The Journal of cell biology 118, 703-714.

Mazuel, F., Reffay, M., Du, V., Bacri, J.-C., Rieu, J.-P., and Wilhelm, C. (2015). Magnetic flattening of stem-cell spheroids indicates a size-dependent elastocapillary transition. Physical review letters 114, 098105.

McCaffrey, K., and Braakman, I. (2016). Protein quality control at the endoplasmic reticulum. Essays in biochemistry 60, 227-235.

McLachlan, R.W., Kraemer, A., Helwani, F.M., Kovacs, E.M., and Yap, A.S. (2007). E-cadherin adhesion activates c-Src signaling at cell–cell contacts. Molecular biology of the cell 18, 3214-3223.

Meng, W., and Takeichi, M. (2009). Adherens junction: molecular architecture and regulation. Cold Spring Harbor perspectives in biology 1, a002899.

Mogilner, A., and Oster, G. (2003). Force generation by actin polymerization II: the elastic ratchet and tethered filaments. Biophysical journal 84, 1591-1605.

Morelli, L.G., Uriu, K., Ares, S., and Oates, A.C. (2012). Computational approaches to developmental patterning. Science (New York, NY) 336, 187-191.

Nagafuchi, A., Shirayoshi, Y., Okazaki, K., Yasuda, K., and Takeichi, M. (1987). Transformation of cell adhesion properties by exogenously introduced E-cadherin cDNA. Nature 329, 341-343.

Nagathihalli, N.S., and Merchant, N.B. (2012). Src-mediated regulation of E-cadherin and EMT in pancreatic cancer. Front Biosci (Landmark Ed) 17, 2059-2069.

Narasimhan, S. (1982). Control of glycoprotein synthesis. UDP-GlcNAc: glycopeptide beta 4-N-acetylglucosaminyltransferase III, an enzyme in hen oviduct which adds GlcNAc in beta 1-4 linkage to the beta-linked mannose of the trimannosyl core of N-glycosyl oligosaccharides. Journal of Biological Chemistry 257, 10235-10242.

Nollet, F., Kools, P., and Van Roy, F. (2000). Phylogenetic analysis of the cadherin superfamily allows identification of six major subfamilies besides several solitary members. Journal of molecular biology 299, 551-572.

Nose, A., Nagafuchi, A., and Takeichi, M. (1988). Expressed recombinant cadherins mediate cell sorting in model systems. Cell 54, 993-1001.

Oda, H., and Takeichi, M. (2011). Structural and functional diversity of cadherin at the adherens junction. Journal of Cell Biology 193, 1137-1146.

Oda, H., and Tsukita, S. (1999). Nonchordate classic cadherins have a structurally and functionally

unique domain that is absent from chordate classic cadherins. Developmental biology 216, 406-422.

Oda, H., Tsukita, S., and Takeichi, M. (1998). Dynamic behavior of the cadherin-based cell–cell adhesion system duringdrosophilagastrulation. Developmental biology 203, 435-450.

Oda, H., Uemura, T., Harada, Y., Iwai, Y., and Takeichi, M. (1994). A Drosophila homolog of cadherin associated with armadillo and essential for embryonic cell-cell adhesion. Developmental biology 165, 716-726.

Ozawa, M., Baribault, H., and Kemler, R. (1989). The cytoplasmic domain of the cell adhesion molecule uvomorulin associates with three independent proteins structurally related in different species. The EMBO journal 8, 1711-1717.

Palovuori, R., and Eskelinen, S. (2000). Role of vinculin in the maintenance of cell-cell contacts in kidney epithelial MDBK cells. European Journal of Cell Biology 79, 961-974.

Patel, S.D., Ciatto, C., Chen, C.P., Bahna, F., Rajebhosale, M., Arkus, N., Schieren, I., Jessell, T.M., Honig, B., and Price, S.R. (2006). Type II cadherin ectodomain structures: implications for classical cadherin specificity. Cell 124, 1255-1268.

Peifer, M., and Wleschaus, E. (1990). The segment polarity gene armadillo encodes a functionally modular protein that is the Drosophila homolog of human plakoglobin. Cell 63, 1167-1178.

Peifer, M., and Yap, A.S. (2003). Traffic control: p120-catenin acts as a gatekeeper to control the fate of classical cadherins in mammalian cells. The Journal of cell biology 163, 437-440.

Pinho, S.S., Osório, H., Nita-Lazar, M., Gomes, J., Lopes, C., Gärtner, F., and Reis, C.A. (2009). Role of E-cadherin N-glycosylation profile in a mammary tumor model. Biochemical and biophysical research communications 379, 1091-1096.

Pinho, S.S., Seruca, R., Gärtner, F., Yamaguchi, Y., Gu, J., Taniguchi, N., and Reis, C.A. (2011). Modulation of E-cadherin function and dysfunction by N-glycosylation. Cellular and molecular life sciences 68, 1011-1020.

Quang, B.-A.T., Mani, M., Markova, O., Lecuit, T., and Lenne, P.-F. (2013). Principles of E-cadherin supramolecular organization in vivo. Current Biology 23, 2197-2207.

Ratheesh, A., and Yap, A.S. (2012). A bigger picture: classical cadherins and the dynamic actin cytoskeleton. Nature reviews Molecular cell biology 13, 673-679.

Rauzi, M., and Lenne, P.-F. (2011). Cortical forces in cell shape changes and tissue morphogenesis. Current topics in developmental biology 95, 93-144.

Reiss, G., Heesen, S.t., Zimmerman, J., Robbins, P., and Aebi, M. (1996). Isolation of the ALG6 locus of Saccharomyces cerevisiae required for glucosylation in the N-linked glycosylation pathway. Glycobiology 6, 493-498.

Reuter, R., Grunewald, B., and Leptin, M. (1993). A role for the mesoderm in endodermal migration and morphogenesis in Drosophila. Development (Cambridge, England) 119, 1135-1145.

Rice, T.B., and Garen, A. (1975). Localized defects of blastoderm formation in maternal effect mutants of Drosophila. Developmental biology 43, 277-286.

Rickoll, W.L., and Counce, S. (1980). Morphogenesis in the embryo ofDrosophila melanogaster—Germ band extension. Wilhelm Roux's archives of developmental biology 188, 163-177.

Riveline, D., Zamir, E., Balaban, N.Q., Schwarz, U.S., Ishizaki, T., Narumiya, S., Kam, Z., Geiger, B., and Bershadsky, A.D. (2001). Focal contacts as mechanosensors: externally applied local mechanical force induces growth of focal contacts by an mDia1-dependent and ROCK-independent mechanism. The Journal of cell biology 153, 1175-1186.

Rozbicki, E., Chuai, M., Karjalainen, A.I., Song, F., Sang, H.M., Martin, R., Knölker, H.-J., MacDonald,

M.P., and Weijer, C.J. (2015). Myosin-II-mediated cell shape changes and cell intercalation contribute to primitive streak formation. Nature cell biology 17, 397-408.

Schmidt, A., and Grosshans, J. (2018). Dynamics of cortical domains in early Drosophila development. Journal of cell science 131, jcs212795.

Schuh, R., Vestweber, D., Riede, I., Ringwald, M., Rosenberg, U.B., Jäckle, H., and Kemler, R. (1986). Molecular cloning of the mouse cell adhesion molecule uvomorulin: cDNA contains a B1-related sequence. Proceedings of the National Academy of Sciences 83, 1364-1368.

Shaevitz, J.W., and Fletcher, D.A. (2007). Load fluctuations drive actin network growth. Proceedings of the National Academy of Sciences 104, 15688-15692.

Shewan, A.M., Maddugoda, M., Kraemer, A., Stehbens, S.J., Verma, S., Kovacs, E.M., and Yap, A.S. (2005). Myosin 2 is a key Rho kinase target necessary for the local concentration of E-cadherin at cell–cell contacts. Molecular biology of the cell 16, 4531-4542.

Shi, Q., Maruthamuthu, V., Li, F., and Leckband, D. (2010). Allosteric cross talk between cadherin extracellular domains. Biophysical Journal 99, 95-104.

Skropeta, D. (2009). The effect of individual N-glycans on enzyme activity. Bioorganic & medicinal chemistry 17, 2645-2653.

Smutny, M., Cox, H.L., Leerberg, J.M., Kovacs, E.M., Conti, M.A., Ferguson, C., Hamilton, N.A., Parton, R.G., Adelstein, R.S., and Yap, A.S. (2010). Myosin II isoforms identify distinct functional modules that support integrity of the epithelial zonula adherens. Nature cell biology 12, 696-702.

Sommer, C., Straehle, C., Koethe, U., and Hamprecht, F.A. (2011). Ilastik: Interactive learning and segmentation toolkit. Paper presented at: 2011 IEEE international symposium on biomedical imaging: From nano to macro (IEEE).

Song, S., Eckerle, S., Onichtchouk, D., Marrs, J.A., Nitschke, R., and Driever, W. (2013). Pou5f1-dependent EGF expression controls E-cadherin endocytosis, cell adhesion, and zebrafish epiboly movements. Developmental cell 24, 486-501.

Stagljar, I., Te Heesen, S., and Aebi, M. (1994). New phenotype of mutations deficient in glucosylation of the lipid-linked oligosaccharide: cloning of the ALG8 locus. Proceedings of the National Academy of Sciences 91, 5977-5981.

Sugimura, K., Lenne, P.-F., and Graner, F. (2016). Measuring forces and stresses in situ in living tissues. Development (Cambridge, England) 143, 186-196.

Takeichi, M. (1991). Cadherin cell adhesion receptors as a morphogenetic regulator. Science (New York, NY) 251, 1451-1455.

Tamada, M., Shi, J., Bourdot, K.S., Supriyatno, S., Palmquist, K.H., Gutierrez-Ruiz, O.L., and Zallen, J.A. (2021). Toll receptors remodel epithelia by directing planar-polarized Src and PI3K activity. Developmental Cell 56, 1589-1602. e1589.

Tepass, U., Gruszynski-DeFeo, E., Haag, T.A., Omatyar, L., Török, T., and Hartenstein, V. (1996). shotgun encodes Drosophila E-cadherin and is preferentially required during cell rearrangement in the neurectoderm and other morphogenetically active epithelia. Genes & development 10, 672-685.

Tepass, U., and Hartenstein, V. (1994a). The development of cellular junctions in the Drosophila embryo. Developmental biology 161, 563-596.

Tepass, U., and Hartenstein, V. (1994b). Epithelium formation in the Drosophila midgut depends on the interaction of endoderm and mesoderm. Development (Cambridge, England) 120, 579-590.

Thompson, C.J., Vu, V.H., Leckband, D.E., and Schwartz, D.K. (2021). Cadherin cis and trans interactions are mutually cooperative. Proceedings of the National Academy of Sciences 118.

Uemura, T., Oda, H., Kraut, R., Hayashi, S., Kotaoka, Y., and Takeichi, M. (1996). Zygotic Drosophila E-cadherin expression is required for processes of dynamic epithelial cell rearrangement in the Drosophila embryo. Genes & development 10, 659-671.

Uozumi, N., Yanagidani, S., Miyoshi, E., Ihara, Y., Sakuma, T., Gao, C.-X., Teshima, T., Fujii, S., Shiba, T., and Taniguchi, N. (1996). Purification and cDNA cloning of porcine brain GDP-L-Fuc: N-acetyl-β-D-glucosaminide α1→ 6fucosyltransferase. Journal of Biological Chemistry 271, 27810-27817.

Van Roy, F., and Berx, G. (2008). The cell-cell adhesion molecule E-cadherin. Cellular and molecular life sciences 65, 3756-3788.

Vicente-Manzanares, M., and Horwitz, A.R. (2011). Adhesion dynamics at a glance. Journal of cell science 124, 3923-3927.

Vleminckx, K., Vakaet Jr, L., Mareel, M., Fiers, W., and Van Roy, F. (1991). Genetic manipulation of E-cadherin expression by epithelial tumor cells reveals an invasion suppressor role. Cell 66, 107-119.

Vogt, N., Koch, I., Schwarz, H., Schnorrer, F., and Nüsslein-Volhard, C. (2006). The γTuRC components Grip75 and Grip128 have an essential microtubule-anchoring function in the Drosophila germline.

Vu, V., Light, T., Sullivan, B., Greiner, D., Hristova, K., and Leckband, D. (2021). P120 catenin potentiates constitutive E-cadherin dimerization at the plasma membrane and regulates trans binding. Current Biology 31, 3017-3027. e3017.

Walck-Shannon, E., and Hardin, J. (2014). Cell intercalation from top to bottom. Nature reviews Molecular cell biology 15, 34-48.

Wang, B., Heath-Engel, H., Zhang, D., Nguyen, N., Thomas, D.Y., Hanrahan, J.W., and Shore, G.C. (2008). BAP31 interacts with Sec61 translocons and promotes retrotranslocation of CFTRΔF508 via the derlin-1 complex. Cell 133, 1080-1092.

Wang, Y.-C., Khan, Z., Kaschube, M., and Wieschaus, E.F. (2012). Differential positioning of adherens junctions is associated with initiation of epithelial folding. Nature 484, 390-393.

Webb, D.J., Donais, K., Whitmore, L.A., Thomas, S.M., Turner, C.E., Parsons, J.T., and Horwitz, A.F. (2004). FAK–Src signalling through paxillin, ERK and MLCK regulates adhesion disassembly. Nature cell biology 6, 154-161.

Wheelock, M.J., Shintani, Y., Maeda, M., Fukumoto, Y., and Johnson, K.R. (2008). Cadherin switching. Journal of cell science 121, 727-735.

Wood, W. (2012). Wound healing: calcium flashes illuminate early events. Current Biology 22, R14-R16.

Wu, Y., Jin, X., Harrison, O., Shapiro, L., Honig, B.H., and Ben-Shaul, A. (2010). Cooperativity between trans and cis interactions in cadherin-mediated junction formation. Proceedings of the National Academy of Sciences 107, 17592-17597.

Wu, Y., Kanchanawong, P., and Zaidel-Bar, R. (2015). Actin-delimited adhesion-independent clustering of E-cadherin forms the nanoscale building blocks of adherens junctions. Developmental cell 32, 139-154.

Wu, Y., Vendome, J., Shapiro, L., Ben-Shaul, A., and Honig, B. (2011). Transforming binding affinities from three dimensions to two with application to cadherin clustering. Nature 475, 510-513.

Yap, A.S., Brieher, W.M., Pruschy, M., and Gumbiner, B.M. (1997). Lateral clustering of the adhesive ectodomain: a fundamental determinant of cadherin function. Current Biology 7, 308-315.

Yap, A.S., Gomez, G.A., and Parton, R.G. (2015). Adherens junctions revisualized: organizing cadherins as nanoassemblies. Developmental cell 35, 12-20.

Yonemura, S. (2011). Cadherin–actin interactions at adherens junctions. Current opinion in cell biology 23, 515-522.

Yoshida-Noro, C., Suzuki, N., and Takeichi, M. (1984). Molecular nature of the calcium-dependent cell-cell adhesion system in mouse teratocarcinoma and embryonic cells studied with a monoclonal antibody. Developmental biology 101, 19-27.

Zallen, J.A., and Wieschaus, E. (2004). Patterned gene expression directs bipolar planar polarity in Drosophila. Developmental cell 6, 343-355.

Zhang, Y., Kong, D., Reichl, L., Vogt, N., Wolf, F., and Großhans, J. (2014). The glucosyltransferase Xiantuan of the endoplasmic reticulum specifically affects E-Cadherin expression and is required for gastrulation movements in Drosophila. Developmental biology 390, 208-220.

Zhang, Y., Sivasankar, S., Nelson, W.J., and Chu, S. (2009). Resolving cadherin interactions and binding cooperativity at the single-molecule level. Proceedings of the National Academy of Sciences 106, 109-114.

Zhao, H., Liang, Y., Xu, Z., Wang, L., Zhou, F., Li, Z., Jin, J., Yang, Y., Fang, Z., and Hu, Y. (2008). N-Glycosylation affects the adhesive function of E-Cadherin through modifying the composition of adherens junctions (AJs) in human breast carcinoma cell line MDA-MB-435. Journal of cellular biochemistry 104, 162-175.

Zhou, F., Su, J., Fu, L., Yang, Y., Zhang, L., Wang, L., Zhao, H., Zhang, D., Li, Z., and Zha, X. (2008). Unglycosylation at Asn-633 made extracellular domain of E-cadherin folded incorrectly and arrested in endoplasmic reticulum, then sequentially degraded by ERAD. Glycoconjugate journal 25, 727-740.

Zhu, B., Chappuis-Flament, S., Wong, E., Jensen, I.E., Gumbiner, B.M., and Leckband, D. (2003). Functional analysis of the structural basis of homophilic cadherin adhesion. Biophysical Journal 84, 4033-4042.

Zielinska, D.F., Gnad, F., Schropp, K., Wiśniewski, J.R., and Mann, M. (2012). Mapping N-glycosylation sites across seven evolutionarily distant species reveals a divergent substrate proteome despite a common core machinery. Molecular cell 46, 542-548.

8. Abbreviations

abbreviation	Explanation
%	percent
°C	degree Celsius
aa	amino acid
Ab	antibody
Amp	ampicillin
anterior-posterior	A-P
a.u.	arbitrary unit
asparagine	Asn
bp	base pairs
BSA	bovine serum albumin
cDNA	complementary DNA
CNX	calnexin
Co-IP	Co-immunoprecipitation
CP	cytoplasmic
CRT	calreticulin
d	day(s)
DAPI	4', 6'-Diamidino-2-phenylindole
ddH2O	double distilled water
Dia	diaphanous
Dlg	discs-large
DNA	deoxyribonucleic acid
DTT	1,4-dithiothreitol
EC	extracellular
E-cad	E-cadherin
E.coil	*Escherichia coli*

EDTA	ethylenediaminetetraacetic acid
ER	endoplasmic reticulum
ERAD	ER-associated degradation
ERQC	ER quality control
et al.	The Latin phrase for "and others"
F-actin	filamentous actin
F-PALM	fluorescence photoactivated localization microscopy
FRAP	fluorescence recovery after photobleaching
FRT	flippase recognition target
FTase	farnesyltransferase
GFP	green fluorescent protein
GlcNAc	N-acetylglucosamine
gny	garnystan
gp	guinea pig
gp80	glycoprotein
h	hour(s)
I	intensity
IPTG	Isopropyl-ß-D-thiogalactopyranoside
LB	luria-Bertani medium
LG	laminin globular domain
M	mol/l
max	maximize
min	minute(s)
mm	millimeter
mRNA	messenger RNA
MW	molecular weight
NA	numerical aperture
OD	optical density

PBS	phosphate-buffered saline
PCR	polymerase chain reaction
PFA	Perfluoroalkoxy polymers
pH	potential of hydrogen
PMSF	phenylmethylsulfonyl fluoride
PTM	post-translational modification
qPCR	quantitative real-time PCR
RNA	ribonucleic acid
ROI	region of interest
rpm	revolutions per minute
RT	room temperature
s	second(s)
shg	shotgun
SDS	sodium dodecyl sulfate
SDS-PAGE	SDS-polyacrylamide gel electrophoresis
Shi	Shibire
STORM	stochastic optical reconstruction microscopy
TA	tail-anchored
TM	transmembrane
Tris	Tris(hydroxymethyl) aminomethane
U	Unit (s)
μm	micrometer
μl	microliter
VH	Vinculin homology
WB	Western blot
wol	*wollknäuel*
wt	wild type
xit	*xiantuan*

9. Curriculum vitae

Personal data

Name	Zhang, Na
Date of birth	01.03.1991
Place of birth	Shanxi, China
E-mail	nazhangluck@126.com

Education

11/2018-now	Ph.D. student
	Department of Developmental Biochemistry
	University of Göttingen, Medical school, Germany
09/2015-06/2018	Master student
	Nanjing Medical University, China
09/2010-06/2015	Bachelor student
	Harbin Medical University, China

Publications

1. Lv, Z., Zhang, N., Zhang, X., Großhans, J., & Kong, D. (2022). The Lateral Epidermis Actively Counteracts Pulling by the Amnioserosa During Dorsal Closure. Frontiers in cell and developmental biology, 10, 865397.

Manuscript in preparation

1. *N*-glycosylation dependent mechanosensitive immobilization and clustering of E-cadherin during tissue morphogenesis.

10. List of Figures